

POLITECNICO DI TORINO



Master's degree course in Mechanical Engineering

MASTER'S DEGREE THESIS

CFD analysis on NO_x emission reduction of a diffusive flame gas turbine combustor through water injection

Supervisors

Prof.ssa Daniela Anna Misul

Prof. Mirko Baratta

Prof. Simone Salvadori

Dott. Ing. Prashant Goel

Candidate

Carlo Lo Faro

ACADEMIC YEAR 2020/2021

Index

ABSTRACT	4
1. Introduction.....	5
1.1. Gas turbine.....	5
1.2. Purpose of the study.....	10
1.3. Thesis overview	12
2. Basic theoretical elements.....	13
2.1. Conservation equations.....	13
2.2. Thermal and caloric equation of state.....	18
2.3. Transport models	20
2.4. Chemistry of combustion.....	24
2.5. Turbulence modelling.....	26
2.5.1. Large Eddy Simulation (LES).....	28
2.5.2. RANS Model	30
2.5.3. Eddy viscosity models.....	33
3. Gas turbine combustor design.....	36
3.1. Introduction.....	36
3.2. Combustion fundamentals	38
3.2.1. Flame classification	38
3.2.2. Stability limits	39
3.3. Combustor types	40
3.3.1. Tubular.....	41
3.3.2. Turboannular.....	42
3.3.3. Annular	43
3.4. Diffusive flame combustor design.....	44
3.4.1. Industrial combustion chambers.....	48
4. NO _x emission control solutions in gas turbines	50
4.1. Introduction.....	50
4.2. Environmental legislation.....	51
4.3. Mechanism for pollutants formation in gas turbines	53

4.3.1.	Carbon monoxide	54
4.3.2.	Unburned hydrocarbons	55
4.3.3.	Smoke	55
4.3.4.	Oxides of nitrogen	56
4.4.	NO _x reduction in conventional combustors	60
4.4.1.	Water or steam injection.....	60
4.4.2.	Dry low-NO _x systems	63
5.	The 0D model.....	65
5.1.	Introduction.....	65
5.2.	Model description	66
5.3.	Results.....	71
6.	TG-20 combustor CFD simulation and results	75
6.1.	Converge CFD Software.....	75
6.1.1.	Finite Volume method.....	77
6.1.2.	Mesh generation	80
6.2.	Introduction to CFD TG-20 combustor model.....	83
6.3.	Dry case	87
6.4.	Wet case.....	99
7.	Conclusion and future developments.....	113
8.	Bibliography.....	114

ABSTRACT

The present thesis object is to evaluate the reduction of nitrogen oxides (NO_x) emissions through water injection in a gas turbine made by EthosEnergy Italia, using Computational Fluid Dynamic (CFD) analysis.

The results will be used to improve the current way water injection is performed in the company gas turbines.

The purpose is firstly to improve an already existing CFD combustor model in order to get better agreement on NO_x emissions, on temperature and on velocity profiles between real measurements and computed ones. Then, the CFD combustor model is modified by a water injection implementation which allow to study the effect of water for NO_x emission reduction.

Since the computational effort on describing the water injection spray using Volume of Fluid (VOF) approach is very computationally demanding, a simple approach which consider water injection like a simple heat sink is proposed. In this way the effect of heat extraction made by water evaporation, which is the major responsible of NO_x emission reduction, is the same as the real one.

Nowadays environmental legislation on the emission of nitrogen oxides for gas turbines became harsher all over the world, so a study to reduce NO_x emissions became of crucial importance for the company.

CFD simulation are done using Converge CFD software, which is an innovative software for simulating three-dimensional fluid flow. Converge software features truly autonomous meshing, which allows to save time because it is needed just the geometry model implementation.

As a conclusion, the CFD model accuracy need to improve in order to better meet and describe the NO_x emission.

1. Introduction

1.1. Gas turbine

Gas turbine is a motor machine which is used in many industries that require power [1]. The power may be used to generate electricity or to drive other operating machines such as pumps or process compressors. Another important application for gas turbines is the naval one, where the machine is used for naval propulsion. History of gas turbines goes back in the early 1900s where many trials were made to build an operational gas turbine. The first gas turbine using a rotary compressor and turbine which produced an excess power of about 8 kW (11 HP) was built in Norway by Aegidius Elling in 1903 [1]. By 1904 Elling improved its machine, which is now capable of producing about 33 kW (44 HP), rotating at about 20.000 rpm and achieving exhaust gas temperatures of 500 °C [1].

For industrial electric power generation, the most used and simple layout for gas turbines is the one showed in Figure 1.1. There is one rotating shaft which links compressor, turbine and the electric generator (load). While the compressor is an operating machine which absorbs mechanical power and transfers it to the air flow, the turbine is a motor machine which extract power from the exhausted gases and then transforms it into available mechanical power. A multistage compressor sucks air from the environment, compresses it and then delivers it to a combustion chamber. Here fuel is added in order to get a combustion which increase gas temperature. The hot gas flow is then expanded into a turbine which lowers the gas pressure and delivers it back to the environment. Part of the power produced by the turbine is absorbed by the

compressor while the remaining one is provided to the electrical generator to produce electrical power. A conspicuous thermal power is present in the hot gas flow leaving the turbine.

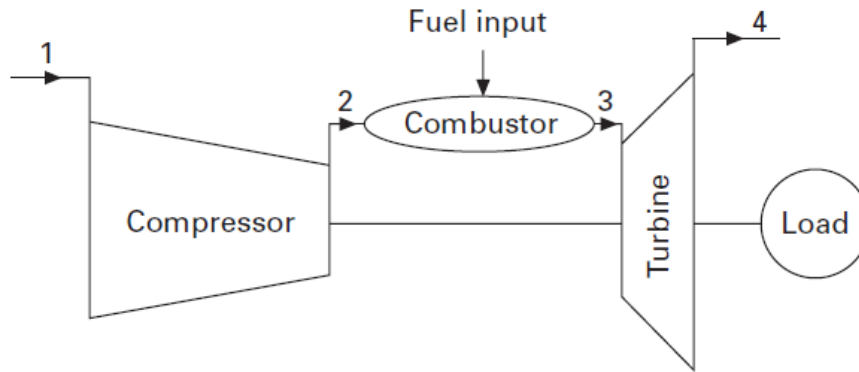


Figure 1.1 - Basic layout of a single shaft gas turbine

Bryton (or Joule) cycle is the process involved in the ideal gas turbine cycle which can be summarized as:

1. Compression (isentropic);
2. Heat addition (constant pressure);
3. Expansion (isentropic);
4. Heat rejection (constant pressure).

The gas turbine cycle can be represented in a clear way in the temperature-entropy diagram, shown in Figure 1.2.

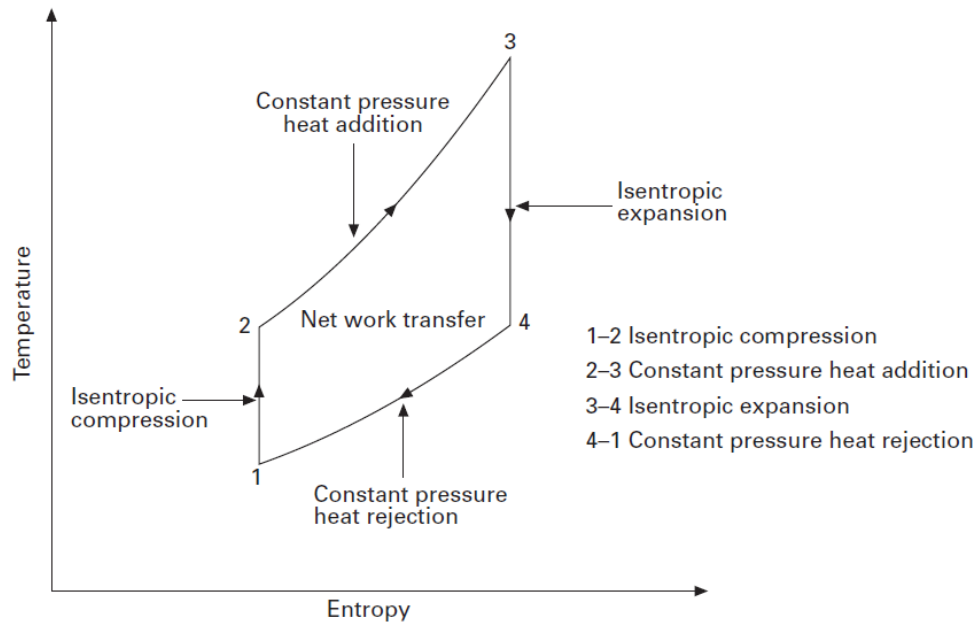


Figure 1.2 - Representation of gas turbine ideal cycle on temperature-entropy diagram

In order to consider such cycle as ideal cycle, it is necessary that all the adiabatic transformations must be isentropic and that isobars transformation must be without any pressure losses inside all devices which provide heat exchanges. Also, the fluid has to be considered ideal, which means it doesn't undergo any state and composition transformations [1]. Ideal gas has constant and independent from temperature specific heat c_p and obey to the well-known state equation:

$$pv = RT \quad (1.1)$$

Where:

- P is the pressure [Pa];
- v is the volume occupied by one kilogram of fluid [m^3/kg];
- R is the universal gas constant divided by the mass per mole of the gas [$\text{J}/(\text{kg}\cdot\text{K})$];
- T is the gas temperature [K].

The adiabatic compression work, the adiabatic expansion work and heat input are given, respectively, by:

$$W_{12} = c_p(T_2 - T_1) \quad (1.2)$$

$$W_{34} = c_p(T_3 - T_4) \quad (1.3)$$

$$Q_{23} = c_p(T_3 - T_2) \quad (1.4)$$

Where:

- c_p is the specific heat at constant pressure [J/(kg*K)];
- T is the fluid temperature [K].

The net work done by the cycle per unit of mass [J/kg] (the specific work, W_{net}) is the difference between the expansion and compression work:

$$W_{\text{net}} = c_p(T_3 - T_4) - c_p(T_2 - T_1) \quad (1.5)$$

Equation (1.5) shows that the net specific work output depends on the maximum cycle temperature T_3 . The cycle thermal efficiency η_{th} , is defined as the ratio between the net work done and the heat input:

$$\begin{aligned} \eta_{\text{th}} &= \frac{W_{\text{net}}}{Q_{23}} = \frac{c_p(T_3 - T_4) - c_p(T_2 - T_1)}{c_p(T_3 - T_2)} = \frac{(T_3 - T_4) - (T_2 - T_1)}{(T_3 - T_2)} \\ &= 1 - \frac{T_4 - T_1}{T_3 - T_2} \end{aligned} \quad (1.6)$$

In the adiabatic transformations (1-2) and (3-4) showed in Figure 1.2, the following equations holds:

$$\frac{T_4}{T_3} = \left(\frac{p_4}{p_3}\right)^{\frac{k-1}{k}} \quad \frac{T_1}{T_2} = \left(\frac{p_1}{p_2}\right)^{\frac{k-1}{k}} \quad (1.7)$$

Where k is the ratio between the specific heat at constant pressure c_p and the specific heat at constant volume c_v (both measured in $J/(kg \cdot K)$).

Defining the variables β and φ in the following way:

$$\beta = \frac{p_2}{p_1} = \frac{p_3}{p_4} \quad \varphi = \frac{k-1}{k} \quad (1.8)$$

It is possible to write:

$$\beta^\varphi = \frac{T_2}{T_1} = \frac{T_3}{T_4} \quad \rightarrow \quad T_2 T_4 = T_1 T_3 \quad \rightarrow \quad \frac{T_4}{T_1} = \frac{T_3}{T_2} \quad (1.9)$$

Now it is possible to express the thermal efficiency in this way:

$$\eta_{th} = 1 - \frac{T_1}{T_2} = 1 - \frac{1}{\beta^\varphi} \quad (1.10)$$

Equation (1.10) shows a very important result: the thermal efficiency of the ideal cycle depends only on the pressure ratio β and on the nature of the gas through φ . If the compression ratio β increases, the thermal efficiency η_{th} increases, tending to 1 for β tending to ∞ (Figure 1.3).

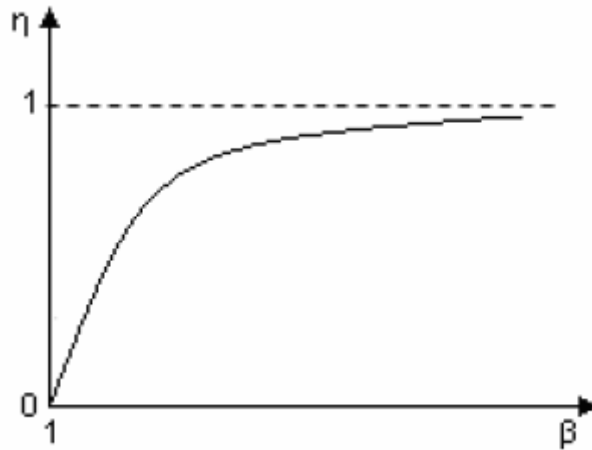


Figure 1.3 - Thermal efficiency η_{th} tends to 1 when compression ratio β tends to ∞

1.2.Purpose of the study

This thesis come from a collaboration between Politecnico di Torino and EthosEnergy Group, which is a company making steam turbines, heavy duty gas turbines, compressors, generators and other rotating equipment for power generation, industrial and Oil & Gas sector. EthosEnergy operates in more than one hundred countries and offers many services for energy sector's components like new build, commercial operation and maintenance, as well as machinery life extension and decommissioning. As a result of this partnership, students are contributing for developing new technological solutions for many company's products. This work is focused on investigating the effectiveness of water injection in order to lowers the NOx emission of the TG20B7/8 gas turbine (Figure 1.4). This 48 MW machine is from Fiat turbo gas division and was developed starting from Westinghouse W251 project. The TG20 turbine has experienced many technical revision and update from its initial project (1959), like compressor redesign and new coating surfaces.

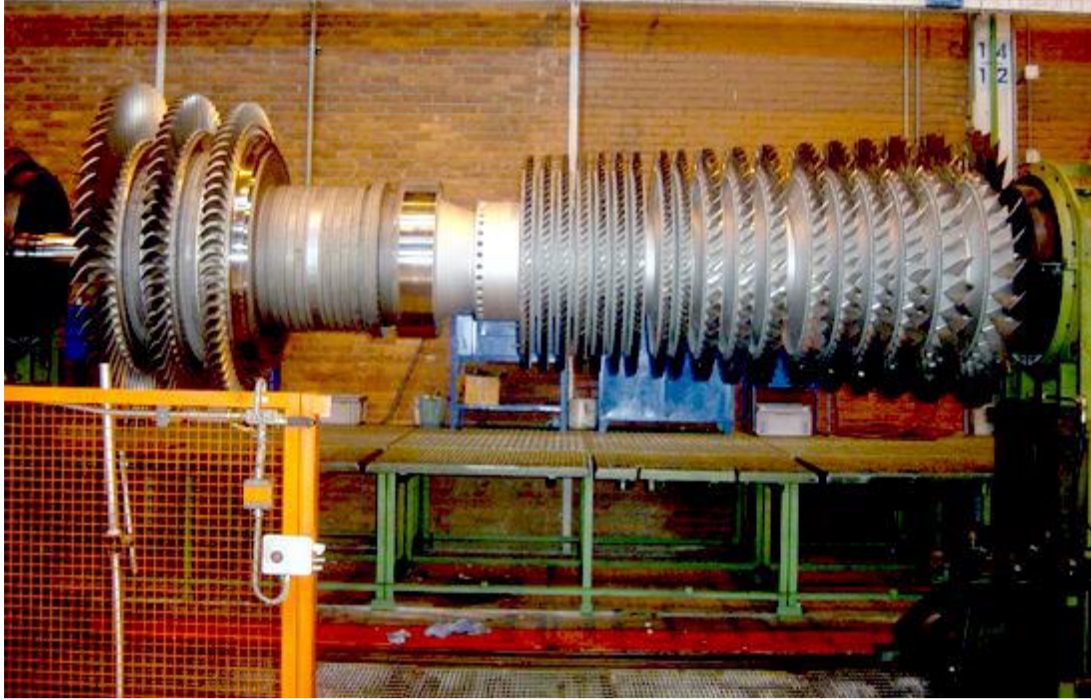


Figure 1.4 - TG20B7/8 turbine, courtesy of EthosEnergy group

1.3.Thesis overview

This thesis is divided into seven chapters:

- In the first chapter an introduction is presented and the goal of the study is explained;
- In the second chapter the theoretical background of the thesis is presented. It is very important to highlight the effect of turbulence on the combustion process;
- Third chapter is dedicated to the description of gas turbine combustors. In particular the design of diffusive flame combustor is considered;
- Fourth chapter deals with the problem of emission reduction for gas turbines. This is a crucial topic for gas turbine makers because the problem of environmental pollution dictates the design criteria for any new gas turbine combustor;
- The fifth chapter is dedicated to the 0D model. It is described the reasons for its development, the purpose, the description and its functioning;
- In the sixth chapter the CFD model of the TG20 combustor is presented, both the dry case and wet case (which means considering water as a mean to reduce NOx emissions). A brief presentation CFD software Converge is proposed. The software is described in terms of solution methods, mesh generation and grid size variation tools;
- Last chapter contains the conclusion and future developments.

2. Basic theoretical elements

In order to deal with the large variety of phenomena in engineering, it is necessary to have equations which can describe isothermal and non-isothermal fluid flow [2]. These equations are often called conservation laws since they derive from physical principles that express the conservation of mass, momentum, and energy. While isothermal flows are fully described by means of the continuity equation (mass balance) and momentum equation, non-isothermal problems also require the energy equation to be considered. The problem formulation is completed by introducing the auxiliary equations that express the initial conditions, the boundary conditions and the constitutive laws.

2.1. Conservation equations

Mass conservation is described by the continuity equation, which is here expressed in its differential form:

$$\frac{\partial \rho}{\partial t} + \nabla \cdot (\rho \mathbf{u}) = 0 \quad (2.1)$$

Where:

- ρ is the mixture density [kg/m³];
- \mathbf{u} is the fluid flow velocity vector field [m/s];
- t is the time [s].

The vector $(\rho\mathbf{u})$ is the mass flux vector and its divergence, which is $\nabla \cdot (\rho\mathbf{u})$, represents the net mass flux rate per unit volume. This equation states that the mass rate entering in a system is equal to the rate at which mass leaves the system plus the accumulation of mass within the system.

If the fluid is incompressible, continuity equation became the much simpler equation

$$\nabla \cdot \mathbf{u} = 0 \quad (2.2)$$

The momentum equation provides a mathematical expression of Newton's second law applied to fluids. It states that the rate of change of momentum of a fluid particle equals the sum of forces on the fluid particle. It is possible to describe it by means of the Navier-Stokes equation [2]:

$$\frac{\partial(\rho\mathbf{u})}{\partial t} + \nabla \cdot (\rho\mathbf{u}\mathbf{u}) + \nabla \cdot \boldsymbol{\tau} + \nabla p - \rho\mathbf{g} = 0 \quad (2.3)$$

Where:

- \mathbf{g} is the gravitational acceleration vector field [m/s²];
- $\boldsymbol{\tau}$ is the stress tensor;
- p is the pressure [Pa].

The quantity $(\rho\mathbf{u}\mathbf{u})$ is the convective momentum-flux tensor and its divergence, namely $\nabla \cdot (\rho\mathbf{u}\mathbf{u})$, is the net rate of momentum due to convection. All the remaining terms of the equation represent the external forces applied to the fluid particle, which include viscous, pressure and gravitational forces. The momentum equation and continuity equation govern the velocity and pressure fields of an isothermal fluid flow. In order

to obtain these two fields, it is necessary to set the boundary conditions, the initial conditions and the constitutive equations.

Regarding the energy conservation equation, it is necessary to first define the total energy e , which is the sum of the internal energy e_i and the kinetic energy e_k , that is:

$$e = e_i + e_k = e_i + \frac{1}{2} \mathbf{u} \cdot \mathbf{u} \quad (2.4)$$

Where each term is expressed per unit of mass. Indeed, the unit of e is (J/kg). The energy equation is

$$\frac{\partial(\rho e)}{\partial t} = -\nabla \cdot ((\rho e)\mathbf{u}) - \nabla \cdot \mathbf{q} - \nabla \cdot (p\mathbf{u}) - \nabla \cdot (\boldsymbol{\tau} \cdot \mathbf{u}) + \rho \mathbf{g} \cdot \mathbf{u} \quad (2.5)$$

Where \mathbf{q} is the heat flux vector. The term on left side of the equation (2.5) is the rate of change of the total energy. Regarding the terms on the right side of the equation, the first term is the net convective flow rate of the total energy, the second one is the net heat flux, third one is the rate of work done by pressure, fourth one is the rate of work done by the viscous stresses and the last one is the rate of work done by gravity.

For the sake of convenience, it is chosen to show the energy conservation equation written in terms of specific enthalpy h (J/kg). In the specific case there is absence of volumetric heat sources, it becomes

$$\frac{\partial(\rho h)}{\partial t} + \nabla \cdot (\rho \mathbf{u} h) + \nabla \cdot \mathbf{q} + \boldsymbol{\tau} : (\nabla \mathbf{u}) - \frac{Dp}{Dt} = 0 \quad (2.6)$$

In the equation (2.6) the term $\boldsymbol{\tau} : (\nabla \mathbf{u})$ represents the enthalpy production due to viscous dissipation while the last term on the left hand side of the equation represents the enthalpy production due to pressure variations.

During combustion the compositions of the reaction flow varies in a continuous way, so it is important to take it into account by the conservation of mass of all chemical species

$$\frac{\partial \rho_i}{\partial t} + \nabla \cdot (\rho_i \mathbf{u}_i) = \dot{w}_i, \quad i \in [1, N_s] \quad (2.7)$$

Where:

- ρ_i is the mass density of species i ;
- N_s is the total number of species;
- \mathbf{u}_i the velocity of species i ;
- \dot{w}_i is the chemical source term for species i . It represents the formation or destruction due to chemical reactions.

Chemical reactions don't alter the total amount of mass, so that the following equation holds

$$\sum_{i=1}^{N_s} \dot{w}_i = 0 \quad (2.8)$$

The mass conservation for all the species can be also written according to the following formulation

$$\frac{\partial(\rho Y_i)}{\partial t} + \nabla \cdot (\rho \mathbf{u} Y_i) = -\nabla \cdot (\rho \mathbf{U}_i Y_i) + \dot{w}_i, \quad i \in [1, N_s] \quad (2.9)$$

Where

$$\mathbf{u}_i = \mathbf{u} + \mathbf{U}_i \quad (2.10)$$

And

$$Y_i = \frac{\rho_i}{\rho} \quad (2.11)$$

In the last two equations, \mathbf{U}_i is the diffusion velocity for species i and Y_i represent the mass fraction for species i .

Equation (2.9) is important because it allows to consider the different physical aspects. Indeed, the terms in this equation represent, starting from the first term in the left-hand side, the time-dependency, convection, diffusion and chemical production. The summation of equation (2.9) when referred to all the species together with equations (2.8) leads to the constraint:

$$\sum_{i=1}^{N_s} Y_i \mathbf{u}_i = 0 \quad (2.12)$$

Showing that the sum of the diffusion velocities is zero.

2.2. Thermal and caloric equation of state

The thermal equation of state links the pressure to density, to temperature and to the species mass fractions. In this system of equations, the density, temperature, and species mass fractions are primitive variables, so that the pressure is computed from those quantities. The ideal gas law for the partial pressure p_i is equal to

$$p_i = n_i R^0 T \quad (2.13)$$

Where:

- n_i is the molar concentration for species i ;
- R^0 is the gas constant;
- T is the mixture temperature.

In order to get the thermodynamic pressure p , it is necessary to make the following summation

$$p = \sum_{i=1}^{N_s} p_i = \sum_{i=1}^{N_s} \rho R^0 T \frac{Y_i}{M_i} \quad (2.14)$$

Where it was used that

$$n_i = n X_i = n Y_i \frac{\bar{M}}{M_i} = \rho \frac{Y_i}{M_i} \quad (2.15)$$

Where:

- n is the molar concentration of the total gas mixture;
- X_i is the species mole fraction;
- M_i the molecular mass of species i ;
- \bar{M} is the average molar mass.

The total enthalpy of the mixture h is equal to the summation over the species enthalpies h_i :

$$h = \sum_{i=1}^{N_s} Y_i h_i, \quad \text{with} \quad h_i = h_i^{\text{ref}} + \int_{T^{\text{ref}}}^T c_{p,i}(T) dT \quad (2.16)$$

Where $c_{p,i}$ is the specific heat of species i at constant pressure.

The specific heat at constant pressure of the mixture is the average specific heat of all the species weighted by species mass fractions

$$c_p = \sum_{i=1}^{N_s} Y_i c_{p,i} \quad (2.17)$$

2.3. Transport models

The previous mentioned viscous stress tensor $\boldsymbol{\tau}$ can be modelled using the Stokes' law of friction. In the case of Newtonian fluid, it is possible to write [3]:

$$\boldsymbol{\tau} = \mu \left(\nabla \mathbf{u} + (\nabla \mathbf{u})^T - \frac{2}{3} (\nabla \cdot \mathbf{u}) \mathbf{I} \right) \quad (2.18)$$

Where μ is the mixture dynamic viscosity and \mathbf{I} is the unit tensor.

Solving the equation of Stefan-Maxwell, it is possible to obtain the diffusion velocity field \mathbf{U}_i in the assumption of neglecting the influence of pressure and temperature gradients [4]

$$\nabla X_i = \sum_{j=1}^{N_s} \frac{X_i X_j}{D_{ij}} (\mathbf{U}_j - \mathbf{U}_i) \quad (2.19)$$

Where D_{ij} is the binary mass diffusion coefficient of species i into species j . Since solving the equation (2.19) require very high computational effort, it is preferred to adopt a simplified approach coming from Fick's law

$$\mathbf{U}_i = -\frac{D_i}{X_i} \nabla X_i \quad (2.20)$$

Where D_i is the mixture-averaged diffusion coefficient.

Fourier's law gives the expression for the heat flux

$$\mathbf{q} = -\lambda \nabla T + \rho \sum_{i=1}^{N_s} \mathbf{U}_i Y_i h_i \quad (2.21)$$

Where λ is the thermal conductivity of the mixture. Two different heat transport are present: the one due to conduction and the one due to mass diffusion. Combining equations (2.16), (2.17) and (2.20) it is possible to rewrite the equation for heat flux

$$\mathbf{q} = -\frac{\lambda}{c_p} \nabla h - \frac{\lambda}{c_p} \sum_{i=1}^{N_s} \left(\frac{1}{Le_i} - 1 \right) h_i \nabla Y_i \quad (2.22)$$

Where Le_i is the Lewis number for species i , which is a dimensionless number equal to the ratio between thermal diffusivity (λ/c_p) and the species mass diffusivity (ρD_i).

$$Le_i = \frac{\lambda}{c_p \rho D_i} \quad (2.23)$$

When $Le = 1$ it means that mass and heat diffuse at an equal rate in the flame but when $Le \neq 1$ species and heat locally redistribute. Most turbulent combustion models assume, for fuel like methane, constant Lewis number.

Dynamic viscosity can be modelled in this way [5]:

$$\mu = \sum_{i=1}^{N_s} \frac{Y_i \mu_i}{M_i \left(\sum_{j=1}^{N_s} \frac{Y_j \phi_{ij}}{M_{ij}} \right)} \quad (2.24)$$

Where

$$\phi_{ij} = \frac{1}{\sqrt{8}} \left(1 + \frac{M_i}{M_j} \right)^{-\frac{1}{2}} \left[1 + \left(\frac{\mu_i}{\mu_j} \right)^{\frac{1}{2}} \left(\frac{M_j}{M_i} \right)^{\frac{1}{4}} \right]^2 \quad (2.25)$$

Mixture thermal conductivity λ and the mixture-averaged diffusion coefficient D_i for species are equal to [6]:

$$\lambda = \frac{1}{2} \left[M \sum_{i=1}^{N_s} \frac{Y_i \lambda_i}{M_i} + \left(M \sum_{i=1}^{N_s} \frac{Y_i}{M_i \lambda_i} \right)^{-1} \right] \quad (2.26)$$

and

$$D_i = \frac{1 - Y_i}{\bar{M} \left(\sum_{j \neq i}^{N_s} \frac{Y_j}{M_j D_{ij}} \right)} \quad (2.27)$$

Pressure and temperature gradient dependence has been neglected because of their high complex modelling. In this way it is possible to reduce the computational cost of the CFD analysis.

Finally, inserting the equation (2.22) into the conservation equations for enthalpy and species yields

$$\begin{aligned} & \frac{\partial(\rho h)}{\partial t} + \nabla \cdot (\rho \mathbf{u} h) \\ &= \nabla \cdot \left(\frac{\lambda}{c_p} \nabla h \right) + \nabla \cdot \left(\frac{\lambda}{c_p} \sum_{i=1}^{N_s} \left(\frac{1}{Le_i} - 1 \right) h_i \nabla Y_i \right) + \rho \mathbf{u} \cdot \mathbf{g} + \tau : (\nabla \mathbf{u}) \\ &+ \frac{dp}{dt} \quad (2.28) \end{aligned}$$

And

$$\frac{\partial(\rho Y_i)}{\partial t} + \nabla \cdot (\rho \mathbf{u} Y_i) = \nabla \cdot \left(\frac{\lambda}{Le_i c_p} \nabla Y_i \right) + \dot{w}_i \quad (2.29)$$

Now it is convenient to show the definition of elemental mass fraction Z_j of element j :

$$Z_j = \sum_{i=1}^{N_s} \left(\frac{a_{ji} M_j}{M_i} \right) Y_i = \sum_{i=1}^{N_s} w_{ji} Y_i, \quad \text{with } j \in [1, N_s] \quad (2.30)$$

Where:

- a_{ji} denotes the number of atoms of j in species i ;
- M_j is the molar mass of element j ;
- M_i the molar mass of species i ;
- N_s the number of elements;
- w_{ji} the relative mass fraction of element j in species i .

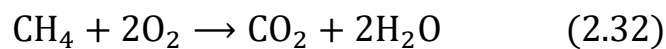
Thanks to this definition is now possible to rewrite the equation (2.29) into the conservation of elements equation

$$\frac{\partial(\rho Z_j)}{\partial t} + \nabla \cdot (\rho \mathbf{u} Z_j) = \nabla \cdot \left(\frac{\lambda}{c_p} \nabla Z_j \right) + \nabla \cdot \left(\frac{\lambda}{c_p} \sum_{i=1}^{N_s} \left(\frac{1}{Le_i} - 1 \right) w_{ji} \nabla Y_i \right) \quad (2.31)$$

Where the last term of the left-hand side is the preferential diffusion.

2.4. Chemistry of combustion

Combustion process is an exothermic chemical reaction where some reactant is oxidized into products. Rather than a single step, combustion is characterized by a large sequence of elementary chemical steps, in which intermediate radical elements participate. Since this subject is very large and complex, here is proposed a simple example of a global reaction of combustion of methane with air:



In equation (2.32) the chemical reaction appears as single step reaction, however it involves a large number of elementary reactions. A general reversible chemical reaction can be written in the following way

$$\sum_{i=1}^{N_r} v'_{ij} \mathcal{A}_i \rightleftharpoons \sum_{i=1}^{N_r} v''_{ij} \mathcal{A}_i \quad \text{for } j \in [1, N_r] \quad (2.33)$$

Where:

- v'_{ij} and v''_{ij} are the forward and backward molar stoichiometric coefficients of species i in reaction j ;
- N_r the number of elementary reactions;
- \mathcal{A}_i represents species i .

The chemical source term for species i depends on all chemical reactions where species i is involved

$$\dot{w}_i = M_i \sum_{j=1}^{N_r} (v''_{ij} - v'_{ij}) r_j, \quad i \in [1, N_r] \quad (2.34)$$

Where r_j is the reaction rate of elementary reaction j , which can be expressed by

$$r_j = k_j^f \prod_{i=1}^{N_r} \left[\frac{\rho Y_i}{M_i} \right]^{v'_{ij}} - k_j^b \prod_{i=1}^{N_r} \left[\frac{\rho Y_i}{M_i} \right]^{v''_{ij}} \quad j \in [1, N_r] \quad (2.35)$$

Where:

- k is the reaction rate coefficient;
- Superscript f refers to forward (going from left to right in equation (2.33));
- Superscript b refers to backward (going from right to left in equation (2.33));

The rate of formation and consumption depends on reaction rate constants, molar concentrations and stoichiometric coefficients. The reaction rate for reaction j , expressed by k_j , is defined by a modified Arrhenius expression [7]:

$$k_j = A_j T^{\beta_j} \left(\frac{-E_{a,j}}{R^0 T} \right) \quad j \in [1, N_r] \quad (2.36)$$

Where:

- A_j is the pre-exponential constant;
- β_j is the temperature exponent;
- $E_{a,j}$ is the activation energy;
- R^0 is the universal gas constant.

2.5. Turbulence modelling

Combusting fluid flow are turbulent [8], so it is necessary to face turbulence as an important aspect of this thesis. Since turbulent flows are highly unsteady, for most of the observer the fluid speed as a function of time would appear random. They would say that the fluid flow is chaotic, but there is another word that describes it better, which is stochastic flow. The velocity fluid flow field is three-dimensional. This means that the time-averaged velocity may be a function of only two coordinates, but for sure the instantaneous field fluctuates rapidly in all three spatial coordinates. Vorticity is also present, which means that vortex stretching is one of the principal mechanisms by which the intensity of turbulence is increased. Turbulence is also the major way to increase the rate at which observed quantities are stirred. Indeed, stirring is a process by which parcels of fluid with different concentrations are brought into contact. So even if the actual mixing is accomplished by diffusion, the mixing process due to turbulence is often called turbulent diffusion. Turbulence is the responsible for the mixing of fluid volume which has different momentum content: the reduction of the velocity gradient due to the action of viscosity reduces the kinetic energy of the flow. So, it is possible to say that mixing is a dissipative process. Since turbulent flow fluctuate on a broad range of length and time scales, it is difficult to make direct numerical simulation of turbulent flow. The effect due to turbulence are not good or bad a priori. Indeed, in some application turbulence effect may be desirable while for other supplication the same effect may be undesirable. For example, turbulence effects are good for chemical mixing or heat transfer problem because turbulence can increase the order of magnitude of those two elements. On the other hand, increase mixing of momentum results in increased frictional forces, which in turn increase the power needed to pump a fluid or to propels a vehicle. It is very important to understand and predict those effect in order to properly carry out the design process of a machine. Sometimes it is possible to control the turbulence, at least in part. While in the past the approach towards turbulence was experimental, which means that the quantities of interest were measured. Some parameters, such as the time-averaged drag or heat transfer, are relatively easy to measure. But as the sophistication of engineering devices increases, the levels of detail and accuracy required also increase so that it is now difficult, costly and time demanding to perform measurements. Some types of measurements are impossible to make at the present time. As a result, numerical methods have an important role in this field.

There are several schemes to predict turbulent flows. According to Bardina et al. (1980) [9] there are six categories:

1. The first involves the use of correlations such as ones that give the friction factor as a function of the Reynolds number or the Nusselt number of heat transfer as a function of the Reynolds and Prandtl numbers. This method, although very useful, is limited to simple types of flows, the ones that can be characterized by just a few parameters.
2. The second one uses the integral equations which can be derived from the equations of motion by integrating over one or more coordinates. This reduces the problem to one or more ordinary differential equations which are easily solved.
3. The third is based on equation obtained by averaging the equation of motion over time. This approach is called one-point closure and leads to a set of partial differential equation called the Reynolds-averaged Navier-Stokes (RANS) equations. This method does not form a closed set so it is necessary to introduce some approximations (turbulence models).
4. The fourth method is called two-point closure. It uses equations for the correlation of the velocity components at two spatial points or, more frequently, the Fourier transform of these equations.
5. The fifth is large eddy simulation (LES) and solves for the largest scale motions of the flow while approximating or modelling only the small-scale motions. It can be regarded as a kind of compromise between one-point closure methods and direct numerical simulation.
6. The last method is the direct numerical simulation (DNS), where the Navier-Stokes equations are solved for all of the motions in a turbulent flow.

All the six methods exposed require the solution of some form of the conservation equations for mass, momentum, energy or chemical species. The major difficulty is that turbulent flows contain variations on a much wider range of length and time scales than laminar flows. So, even though they are similar to the laminar flow equations, the equations describing turbulent flows are usually much more difficult and expensive to solve.

2.5.1. Large Eddy Simulation (LES)

Figure 2.1 shows, on the left-hand side, the range of eddy sizes that might be found in a flow while the right-hand side of this figure shows the time history of a typical velocity component at a point in the flow

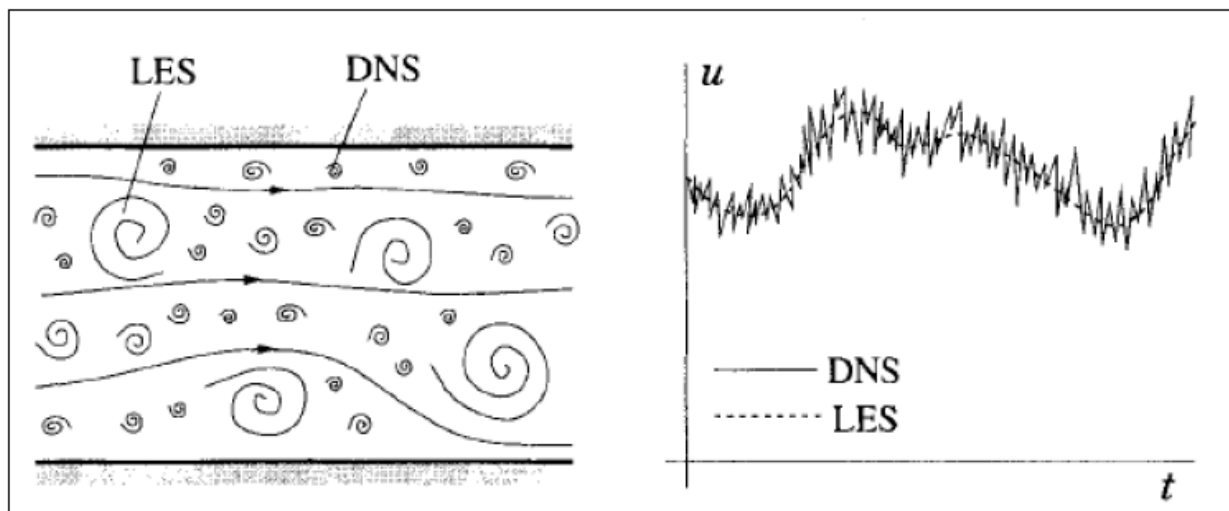


Figure 2.1 - Schematic representation of turbulent motion (left) and the time dependence of a velocity component at a point (right).

The large-scale motions are generally much more energetic than the small-scale ones; their size and strength make them by far the most effective transporters of the conserved properties. The small-scales are usually much weaker and provide little transport of these properties. The consequence is that a simulation that treats the large eddies more exactly than the small ones may have sense and large eddy simulation is just such an approach. Since DNS is more accurate, it is preferred to use this method whenever is feasible. LES is the preferred method for flows in which the Reynolds number is too high or the geometry is too complex to allow application of DNS.

The velocity field must contain only the large-scale components of the total field. For the sake of simplicity, it is possible to use the one-dimensional notation considering that it is always possible to extend the treatment to the three dimensions. The filtered velocity is defined by (and introduced by [10]):

$$\bar{u}_i(x) = \int G(x, x') u_i(x') dx' \quad (2.37)$$

Where $G(x, x')$ is the filtered kernel, which is a localized function. This function, which have been applied in LES, include a Gaussian, a box filter, and a cut-off. When the Navier-Stokes equations with constant density (incompressible flow) are filtered, it possible to obtain a set of equations very similar to the RANS equations:

$$\frac{\partial(\rho \bar{u}_i)}{\partial t} + \frac{\partial(\rho \overline{u_i u_j})}{\partial x_j} = -\frac{\partial \bar{p}}{\partial x_i} + \frac{\partial}{\partial x_j} \left[\mu \left(\frac{\partial \bar{u}_i}{\partial x_j} + \frac{\partial \bar{u}_j}{\partial x_i} \right) \right] \quad (2.38)$$

Continuity equation is linear, so filtering does not change it

$$\frac{\partial(\rho \bar{u}_i)}{\partial t} = 0 \quad (2.39)$$

Since

$$\overline{u_i u_j} \neq \bar{u}_i \bar{u}_j \quad (2.40)$$

And the quantity on the left side of this inequality is not easily computed, a modelling approximation for the difference between the two sides of this inequality must be introduced:

$$\tau_{ij}^s = -\rho(\overline{u_i u_j} - \overline{u_i} \overline{u_j}) \quad (2.41)$$

Where the quantity τ_{ij}^s is called the sub grid-scale Reynolds stress. The name stress comes from the way in which it is treated rather than its physical nature. Also, the name sub grid scale is misleading. The width of the filter, Δ , need not have nothing to do with the grid size, h , other than the obvious condition that $\Delta > h$. Some authors do make such a connection and their nomenclature has stuck.

2.5.2. RANS Model

In a statically steady flow, every variable can be written as the sun of a time-averaged value and a fluctuation value about that value:

$$\phi(x_i, t) = \overline{\phi}(x_i) + \phi'(x_i, t) \quad (2.42)$$

Where

$$\overline{\phi}(x_i) = \lim_{T \rightarrow \infty} \frac{1}{T} \int_0^T \phi(x_i, t) dt \quad (2.43)$$

Here, t is the time and T is the averaging interval, which has to be large compared to the typical time scale of the fluctuations. The interest is on the limit for $T \rightarrow \infty$, see Figure 2.2. If T is large enough, $\overline{\phi}$ does not depend on the time at which the averaging is started.

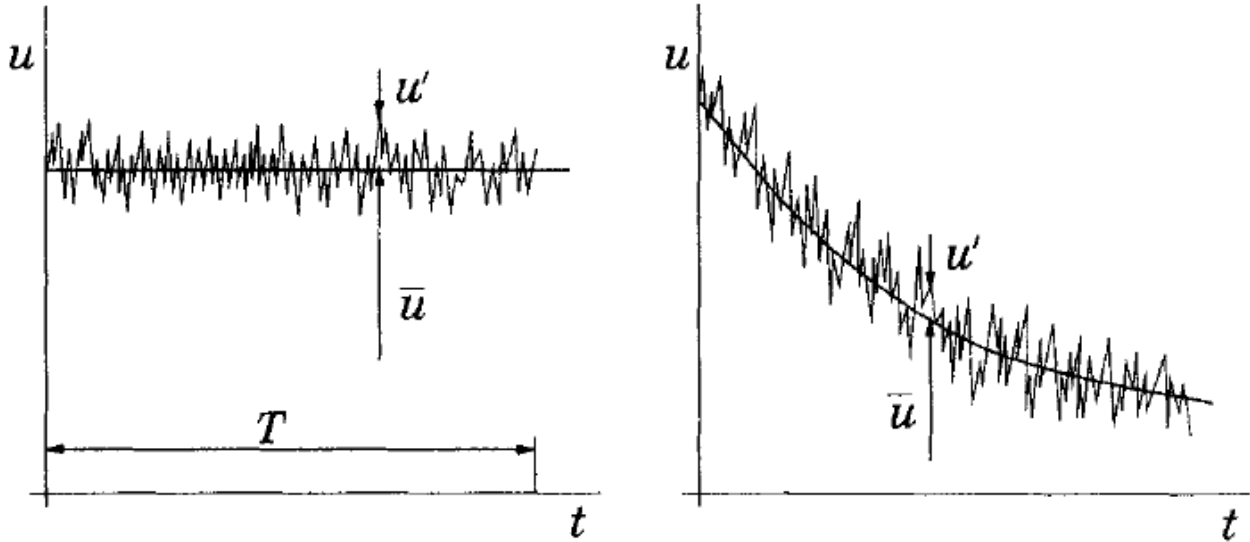


Figure 2.2 - Time averaging for a statistically steady flow (left) and ensemble averaging for an unsteady flow (right).

If the flow is unsteady, time averaging can't be used and it must be replaced by ensemble averaging (see Figure 2.2):

$$\bar{\phi}(x_i, t) = \lim_{N \rightarrow \infty} \frac{1}{N} \sum_{n=1}^N \phi(x_i, t) \quad (2.44)$$

Where N is the number of members of the ensemble and must be large enough to eliminate the effects of the fluctuations. The term Reynolds averaging is used to refer to any of these averaging processes. If it is applied to the Navier-Stokes equations it

yields the Reynolds-averaged Navier-Stokes (RANS) equations. From equation (2.42), it follows that $\overline{\phi'} = 0$. So, averaging any linear term in the conservation equations simply gives the identical term for the averaged quantity. From a quadratic nonlinear term, we get two terms, the product of the average and a covariance:

$$\overline{u_1 \phi} = \overline{(\bar{u}_1 + u'_1)(\bar{\phi} + \phi')} = \bar{u}_1 \bar{\phi} + \overline{u'_1 \phi'} \quad (2.45)$$

The last term is zero only if the two quantities are uncorrelated but, since this happens rarely in the case of turbulent flows, the conservation equations contain terms called Reynolds stresses and turbulent scalar flux among others.

The averaged continuity and momentum equations can, for incompressible flows without body forces, be written in tensor notation and Cartesian coordinates as:

$$\frac{\partial(\rho \bar{u}_i)}{\partial x_i} = 0 \quad (2.46)$$

$$\frac{\partial(\rho \bar{u}_i)}{\partial t} + \frac{\partial}{\partial x_j} (\rho \bar{u}_i \bar{u}_j + \overline{\rho u'_i u'_j}) = -\frac{\partial \bar{p}}{\partial x_i} + \frac{\partial \bar{\tau}_{ij}}{\partial x_j} \quad (2.47)$$

Where the $\bar{\tau}_{ij}$ are the mean viscous stress tensor components:

$$\bar{\tau}_{ij} = \rho \left(\frac{\partial \bar{u}_i}{\partial x_j} + \frac{\partial \bar{u}_j}{\partial x_i} \right) \quad (2.48)$$

Finally, the equation for the mean of a scalar quantity can be written:

$$\frac{\partial(\rho \bar{\phi})}{\partial t} + \frac{\partial}{\partial x_j} (\rho \bar{u}_j \bar{\phi} + \overline{\rho u'_j \phi'}) = \frac{\partial}{\partial x_j} \left(\Gamma \frac{\partial \bar{\phi}}{\partial x_j} \right) \quad (2.49)$$

The presence of the Reynolds stresses and turbulent scalar flux in the conservation equations means that the latter are not closed because they contain more variables than there are equations. Closure require use of some approximations, which usually take the form of prescribing the Reynolds stress tensor and turbulent scalar fluxes in terms of the mean quantities. It is possible to derive equations for the higher order correlations, but these contain still more unknown correlations that require modelling approximations. These equations will be introduced later but the important point is that is impossible to derive a closed set of exact equations. The approximations introduced are called turbulence models in engineering or parametrization in the geosciences.

2.5.3. Eddy viscosity models

In order to close the equations, it is necessary to introduce a turbulence model. In this case, the eddy-viscosity model suits for the Reynolds stress:

$$-\overline{\rho u'_i u'_j} = \mu_t \left(\frac{\partial \bar{u}_i}{\partial x_j} + \frac{\partial \bar{u}_j}{\partial x_i} \right) - \frac{2}{3} \rho \delta_{ij} k \quad (2.50)$$

And the eddy-diffusion model for a scalar:

$$-\overline{\rho u'_j \phi'} = \Gamma_t \frac{\partial \bar{\phi}}{\partial x_j} \quad (2.51)$$

In equation (2.50), k is the turbulent kinetic energy:

$$k = \frac{1}{2} \overline{u'_i u'_i} = \frac{1}{2} (\overline{u'_x u'_x} + \overline{u'_y u'_y} + \overline{u'_z u'_z}) \quad (2.52)$$

Although the eddy-viscosity hypothesis is not correct in detail, it is easy to implement and, with careful application, can provide reasonably good results for many flows. In

a very simple way, turbulence can be characterized by two parameters: its kinetic energy k , or a velocity $q=\sqrt{2k}$ and a length scale L . Dimensional analysis shows that:

$$\mu_t = C_\mu \rho q L \quad (2.53)$$

Where C_μ is a dimensionless constant whose value will be given later.

The equation required to determine the length scale of turbulence is chosen between the most popular ones. The most popular one is based on the observations that the dissipation is needed in the energy equation and, in so-called equilibrium turbulent flows. The dissipation ε , k and L are related by:

$$\varepsilon = \frac{k^{3/2}}{L} \quad (2.54)$$

The equation for dissipation can be derived from a commonly used one:

$$\frac{\partial(\rho\varepsilon)}{\partial t} + \frac{\partial(\rho u_j \varepsilon)}{\partial x_j} = C_{\varepsilon 1} P_k \frac{\varepsilon}{k} - \rho C_{\varepsilon 2} \frac{\varepsilon^2}{k} + \frac{\partial}{\partial x_j} \left(\frac{\mu_t}{\sigma_\varepsilon} \frac{\partial \varepsilon}{\partial x_j} \right) \quad (2.55)$$

Where the eddy viscosity is expressed in the following way:

$$\mu_t = \rho C_\mu \sqrt{k} L = \rho C_\mu \frac{k^2}{\varepsilon} \quad (2.56)$$

The model based on equation (2.56) is called the k - ε model and has been widely used. This model contains five parameters. The most commonly used values for them are:

$$C_\mu = 0.09; \quad C_{\varepsilon 1} = 1.44; \quad C_{\varepsilon 2} = 1.92; \quad \sigma_k = 1.0; \quad \sigma_\varepsilon = 1.3 \quad (2.57)$$

The implementation of this model on a computer is very easy. The RANS equations have the same form as the laminar equations provided the molecular viscosity is replaced by the effective viscosity. The most important difference is that two new partial differential equations need to be solved. This would cause no problem but, because the time scales associated with the turbulence are much shorter than those connected with the mean flow, the equations with the k- ε model are much stiffer than the laminar equations. A more in-depth description of these models is given in [8].

3. Gas turbine combustor design

3.1. Introduction

The design process of a combustion system is a complex duty because it involves so many aspects such as fluid dynamic, combustion and mechanical design. In the past the design process of a gas turbine combustor relied in theoretical treatment but much more on trial and error approach. This means that a considerable amount of time and economic resources was required. The rapidly use and propagation of computational fluid dynamics (CFD) in recent years has had significant impact on the design process, leading to a better understanding the complex flow and reducing the amount of trial and error [11].

As for many others design processes in engineering, also for gas turbine combustor the problem of design is the one of reaching a good compromise between a number of conflicting requirements, which depends on the specific application. Gas turbine combustion system for ground application has different requirement from gas turbine combustors used for aircraft application. Also, the different type of fuel used, which goes from liquid petroleum distillates to natural gas, affects the design process. While in the past the goal for gas turbine combustor design was to reach high combustion efficiency and flame stability nowadays, that the awareness for the environment impact are raised, there are others aspect to be considered such as the production of NO_x emissions. Indeed, the factors required for high thermal efficiency, which are high pressure ratio and high turbine inlet temperature, both lead to increase the NO_x emission level.

It is clear that while in the past the design process didn't even consider the emission problem, nowadays, on modern combustors, the design is totally dominated by the need for low emissions of NO_x, CO and unburned hydrocarbons (UHC). Early combustors didn't mix the air and fuel upstream the combustion process resulting in a diffusion flame, which is very stable but produces high amount of emission. Modern combustors use lean pre-mix systems, where the fuel is pre-mixed with air before ignition. This leads to a greatly reduced emissions but at the expense of flame stability, flame-out, aerodynamic or acoustic vibration and mechanical stresses which lowers the durability. Even if in the recent years some factors influencing the design of gas turbine combustor has evolved, there are some of them that remains constant and can be considered as the main and basic requirement that a gas turbine combustor should fulfil. Key issues can be summarized as follow [11]:

- Gas temperature after combustion must be below a certain threshold in order to meet the highly stressed turbine materials requirements. Material development and improved blade cooling technique has led to a temperature rise from about 1100 K to about 1850 K for aircraft application;
- At turbine inlet, gas temperature distribution must be of desired form in order to meet the turbine blade requirement. Indeed, from root to tip, the centrifugal stress decrease and so temperature can increase;
- Formation of carbon deposits must be avoided because even small particles carried in the high velocity gas stream can erode the blades and block cooling passages;
- Even if gas turbine combustion systems have reached very high level of efficiency, they still produce pollutants such as NO_x, carbon monoxide (CO) and unburned hydrocarbons (UHC). These emissions must be controlled to very low levels. In the last decades, gas turbine has enhanced their performance mainly by increasing the compressor pressure ratio and by increasing turbine inlet temperature (TIT). These two actions result in increased production of NO_x. Since more stringent emission legislations have been produced by the government, it is now necessary to make heavy changes in combustor design in order to fulfil the emission problem.
- Since the compressor delivery air density is strictly dependent on the air mass flow rate, it is possible to consider quite constant the air velocity at entry of combustor. This aspect eases the combustor designer's problem [11].

3.2. Combustion fundamentals

In a very simple and essential way, combustion can be described like an exothermic reaction of a fuel and an oxidant [12]. In gas turbine application, the fuel can be gaseous or liquid but the oxidant is always air because of its wide availability. It is possible to distinguish between two important regimes of combustion: deflagration and detonation [13].

Deflagration is the combustion regime that happens in all gas turbine combustors. It is characterized by a fast process that requires less than 1 millisecond for 80% of the completion and by a flame which propagates through the unburned mixture.

Detonation is a phenomenon characterized by a shock wave which is produced by a zone of chemical reaction. These waves travel at supersonic speed (from 1 up to 4 km/s). It is very rare that detonation happens in gas turbine combustors. For combustors which use oxygen injection there are some possibilities that detonation develops.

3.2.1. Flame classification

Even if a flame can propagate through a static gas mixture, it is preferable, for study purposes, to stabilize the flame at a fixed point and supply it with a continuous flow of combustible mixture so that flames can be distinguished into two main categories: premixed flames and diffusion flames [12]. While in the former the fuel and the air are mixed together before combustion, in the latter the fuel and the air are mixed by diffusion directly in the flame zone.

Another classification depends on fluid velocities, so that a flame can be classified as a laminar flame or turbulent flame.

An example of diffusion flame is represented by a burning candle: fuel vapor rises from the wick and can burn in the neighbourhood of the wick only to the extent that it can mix with the oxygen in the air. For diffusion flame, the rate of mixing between the fuel and the oxidant limits the overall rate of combustion. Instead, for laminar premixed gaseous flames the combustion process is predominantly ruled by flame chemistry, local heat and mass transfer.

For premixed gases, combustible mixture is available from the beginning of combustion process and the combustion can start at some point in the mixture (by means of an electric spark, for example), then it will propagate throughout the entire available volume of combustible mixture [12]. Turbulence is of primary importance

because most of flowing fuel-air mixtures are turbulent and turbulence is known to enhance flame speeds considerably.

3.2.2. Stability limits

For each combustion chamber there is both a rich and a weak limit to the air/fuel ratio beyond which the flame is unstable. The chosen air/fuel limit for instability is the one that produces rough running, which indicates poor combustion and generates aerodynamic vibration which reduces the lifespan of combustion chamber and cause vibration problem. The air/fuel limit is also the one that causes a flame blow out, even if the instability often occurs before this limit is reached [12]. If the air flow velocity increases, the range of air/fuel ratio between the rich and weak limits is reduced and, beyond a certain air flow speed, it is not even possible for combustion to take place. It is possible to produce a chart where the stability air/fuel ratio is plotted against the air mass flow rate. Figure 3.1 shows a typical stability loop.

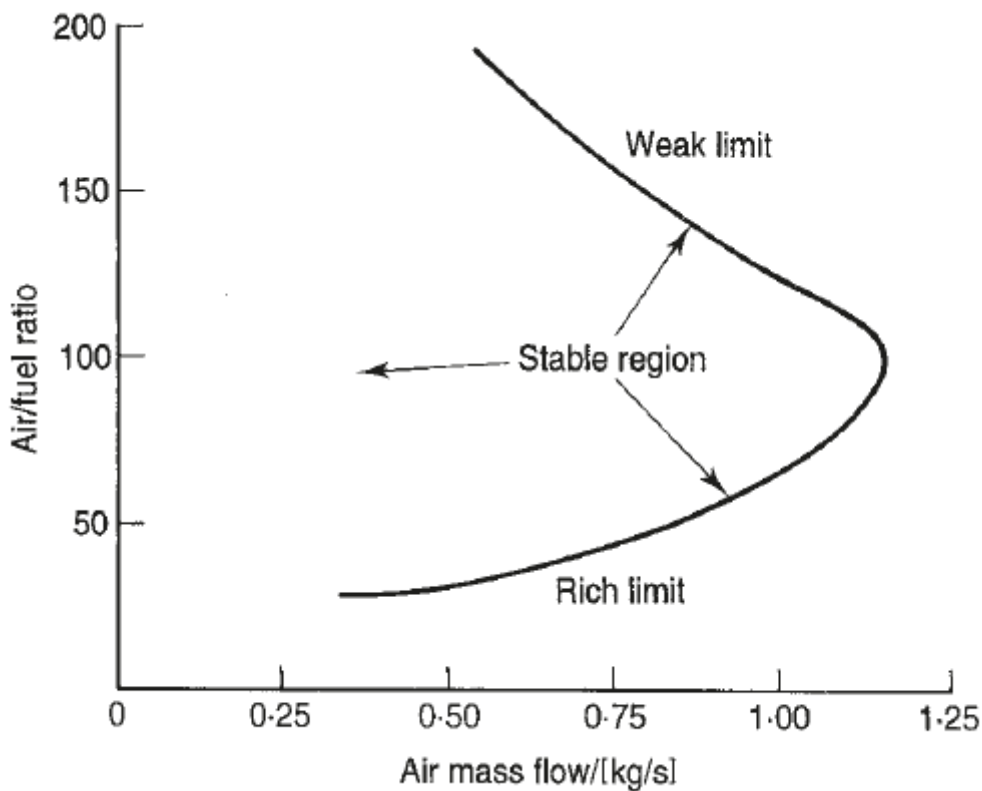


Figure 3.1 - Stability loop

The operating range of a stable gas turbine combustor must be in accordance to the stability loop proposed, not only is steady-state condition but also during transitory operations. During an acceleration there is a rapid increase of the fuel flow while the air flow won't reach its equilibrium value until the engine has reached its new speed. In such situation the combustor will operate at a very low air/fuel ratio but it has to be designed in such a way to guarantee stable operations. Indeed, some combustor has some built-in devices that setups some upper and lower thresholds both for fuel and air in order to not trespass the stability region.

The stability loop is a function of the chamber pressure: a decrease in pressure reduces the rate at which the chemical reactions proceeds and consequently it narrows the stability limits. For engines in aircraft application it is extremely important to verify that the limits are sufficiently wide for a pressure which exists at the highest operating altitude. The combustors that operate at high pressure have less problems in design process with regard to the ones which operates at lower pressure. If the stability limits are too narrow, changes in design must happen in order to improve the recirculation pattern in the primary zone.

3.3. Combustor types

The combustor type and layout are based on two main requirements: the overall engine design and the available space. Two basic types of combustor are present: tubular and annular. A third type, which is a compromise between the two, is the “tuboannular” or “can-annular” combustor where a number of equally spaced tubular liners are placed all around an annular air casing [14]. Figure 3.2 shows the three different combustor types.

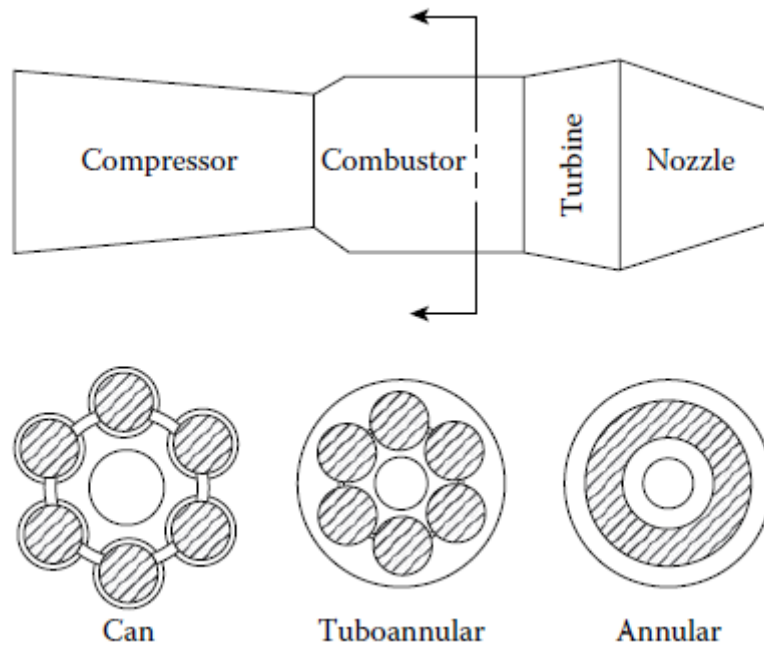


Figure 3.2 - Three different combustor types

3.3.1. Tubular

The tubular (or “can”) combustor is made of a cylindrical liner mounted concentrically inside a cylindrical casing. In Figure 3.3 it is represented a multi-can combustor arrangement. The main advantage of tubular system is represented by the relatively low cost and little time for its development. Unfortunately, the excessive length and weight makes this combustor type not suitable for aircraft application. Instead, they are suitable for industrial application, where the weight and dimension are not a problem.

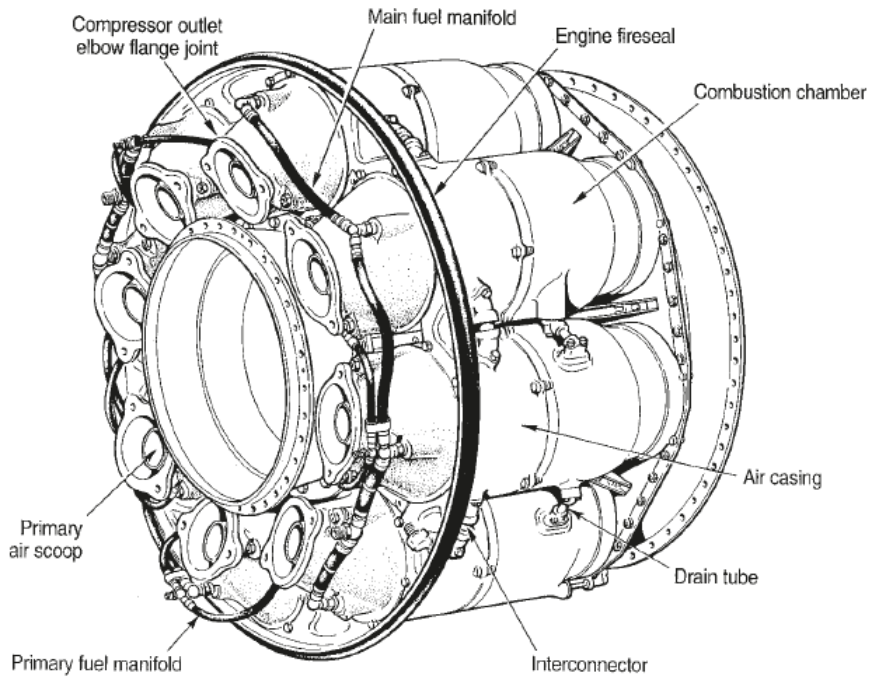


Figure 3.3 – Multi-tubular combustor

3.3.2. Turboannular

The diffusion and utilization of the turboannular (or can-annular) combustor become to increase when the engine pressure ratios started to increase. A group of tubular liners, from 6 to 10, is arranged inside a single annular casing as shown in Figure 3.4.

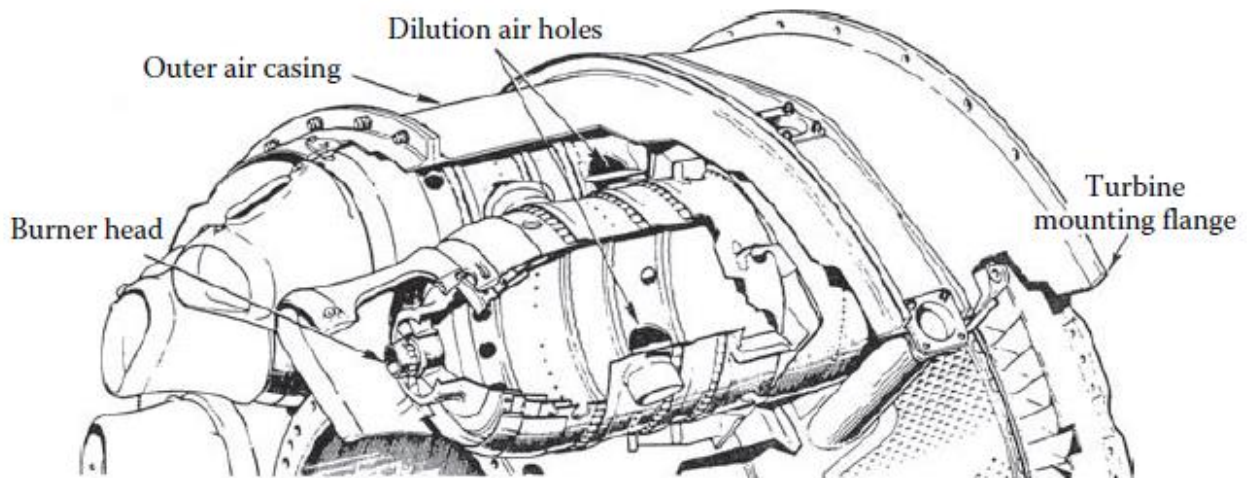


Figure 3.4 - Turboannular combustor

Thanks to its design, the tuboannular combustor combines the compactness of the annular chamber with the mechanical strength of the tubular chamber. One advantage of tuboannular arrangement over the annular one is that, during development and testing phases, it is possible to consider just one segment of the total chamber containing one or more liners instead of considering the whole combustor. In this way it is possible to test the combustor with a relatively low amount of air. Unfortunately, it is difficult to get a satisfactory and consistent airflow pattern. This is in part due to the need of interconnections (cross-fire tubes) between each tubular liner.

3.3.3. Annular

In the annular type combustor, the liner is mounted concentrically inside an annular casing. This shape, which is shown in Figure 3.5, is the ideal shape for a combustion chamber because it allows for lower pressure loss with respect to the other two arrangements.

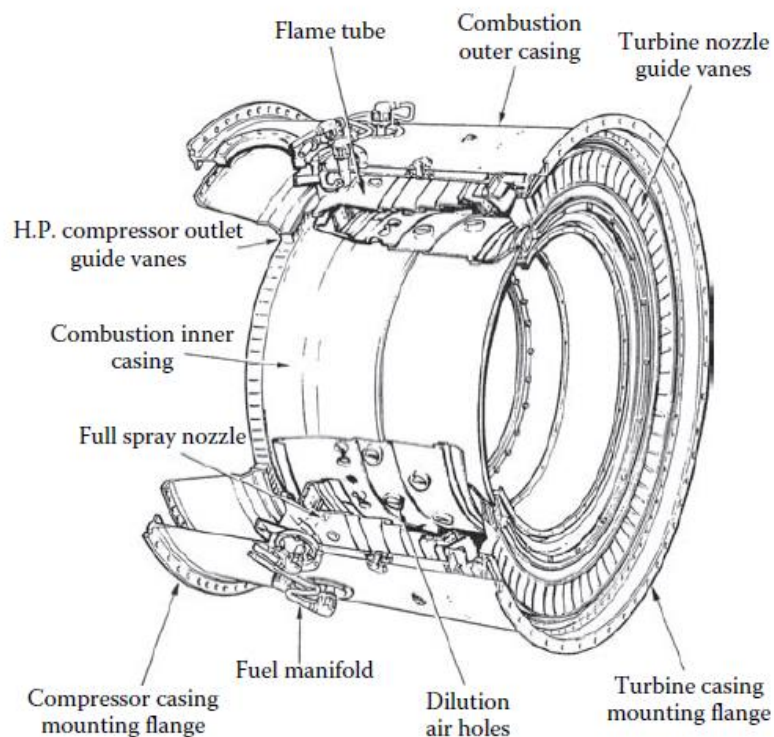


Figure 3.5 - Annular combustor

Since the out liner is subject to a heavy buckling load, in the early days of turbojet development, the use of annular liners was allowed only for low pressure ratio engines. The testing phase is very expensive because it is necessary to provide air at the same pressure, temperature and flow rate of the one present during full-load conditions.

3.4. Diffusive flame combustor design

Figure 3.6 shows a typical layout of a diffusion flame gas turbine combustor, which is made by three different zones: primary zone, intermediate zone and dilution zone. In the figure is possible to notice the snout, which is formed by cowls that project upstream from the dome [12]. The snout function is to provide a high uniform static pressure for feeding the air swirler, which is attached to the dome, the air blast atomizer and the dome cooling airflows.

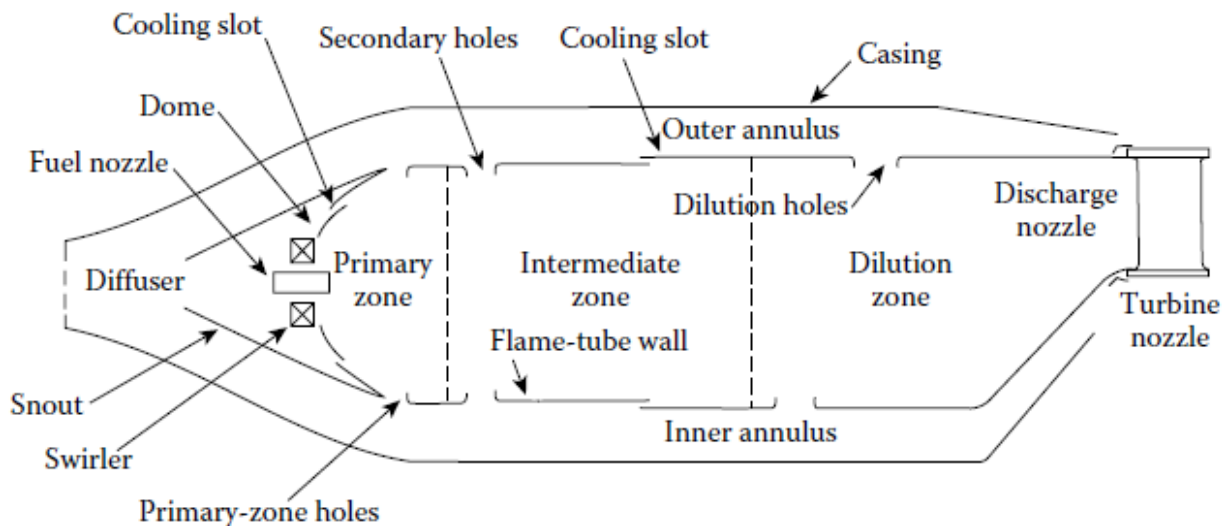


Figure 3.6 – Main components of a diffusive flame combustor

The main function of the primary zone is to anchor the flame and provide sufficient time, temperature and turbulence to reach complete combustion of the incoming air-fuel mixture. The airflow pattern created by the primary zone is of primary interest. Indeed, even if many different patterns are employed, they all have one feature in common: the creation of a toroidal flow reversal that entrains and recirculates a portion of the hot combustion gases to provide continuous ignition to the incoming air and fuel. Some combustor makes use of air swirlers to create the toroidal flow pattern while others have no swirlers, but are still capable of generating flow recirculation thanks to air flowing through holes drilled directly in the liner wall at the upstream end of the liner itself [12]. Figure 3.7 shows a combustor developed by Lucas combustion group.

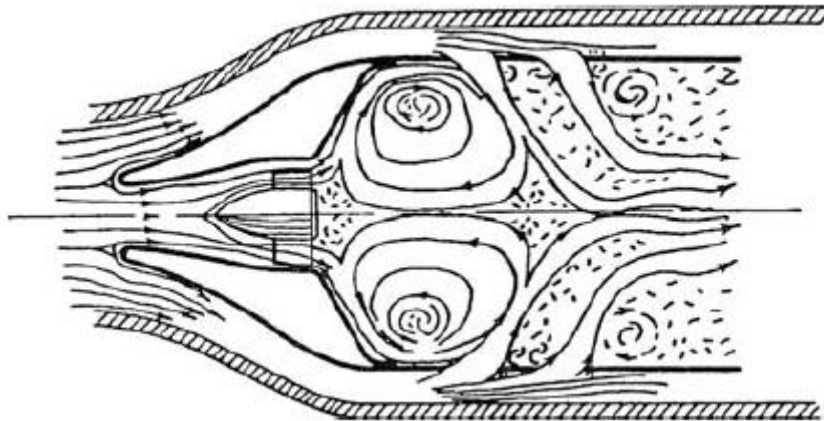


Figure 3.7 - Lucas primary-zone airflow pattern

From that figure it is possible to notice that both swirling air and primary air jets are used to produce the desired flow reversal, in this way a strong and stable primary zone air-flow pattern is produced. This in turn will guarantee wide stability limits, good ignition performance and freedom from the type of flow instabilities that often give rise to combustion pulsation and noise. Lucas company combustor arrangement had a strong influence not only on British combustor design but it is also possible to find the basic aerodynamic features shown in Figure in the combustors design form many other gas turbine combustors.

Since in the primary zone the temperature could reach 2000 K, dissociation will result in the appearance of significant concentrations of carbon monoxide (CO) and hydrogen (H₂) in the efflux gases. These gases pass to the intermediate zone and, if a massive amount of air is added, the gas composition would be “frozen” in the sense that CO will be discharged from the combustor unburned. CO is both a pollutant and a source of combustion inefficiency. For this reason, it is necessary to drop temperature to an intermediate level by the addition of small amounts of air. In this way the burnout of

soot is promoted and combustion of CO can happen as well as other unburned hydrocarbons (UHC) in order to proceed toward combustion completion [12].

The objective of the dilution zone is to admit the remaining air after the combustion and wall-cooling requirements and to provide an outlet stream with a temperature distribution that is acceptable to the turbine. This temperature distribution is usually called “pattern factor” or “temperature traverse quality”. The amount of available air is usually between 20% and 40% of the total combustor airflow and it is introduced into the hot gas stream through one or more rows of holes in the liner walls. The size and shape of these holes are selected to optimize the penetration of the air jets and their subsequent mixing with the main stream. Since it is found that the mixing process initially improves greatly with an increase in mixing length and then at a progressively slower rate. This is the reason why the length/diameter ratios of dilution zones all tend towards to a narrow range between 1.5 and 1.8. For modern high-performance engines, an ideal pattern factor would be the one that gives minimum temperature at the turbine blade root where stresses are highest and at turbine blade tip in order to protect seal materials. Being able to obtain the desired pattern factor is of primary importance, owing to its major impact on the maximum allowable mean turbine entry temperature and hot-section durability. Due to the importance and severity of the problem, a large proportion of the total combustor development effort is devoted to achieving the desired pattern factor.

Liner functions are to contain the combustion process and to facilitate the distribution of air to all the various combustor zones in the prescribed amounts. The liners must be stronger enough to withstand buckling load created by pressure differential across the liner wall. It is required to have also good thermal resistance to withstand continuous and cyclic high-temperature operation. In order to meet those requirements, the use of high-temperature, oxidant-resistant materials combined with the effective use of cooling air are adopted. On many combustors the amount of air used for wall cooling requirement is up to 20% of the total combustor air-mass flow [12]. The liner wall temperature is determined by the balance of two main factors:

- The heat received via radiation and convection from the hot gas;
- The heat transferred from it by convection to the annulus air and by radiation to the air casing.

The problem of liner cooling has become increasingly severe because of the increase of the inlet air temperature. Figure 3.8 shows the historical trend of turbine entry

temperature. It is possible to notice that turbine inlet temperatures have raised over the years in order to maximize fuel economy. Higher inlet air temperature has a two main adverse effect: it raises the flame temperature, which increases the rate of heat transfer to the liner wall and it reduces the effectiveness of the air as a coolant.

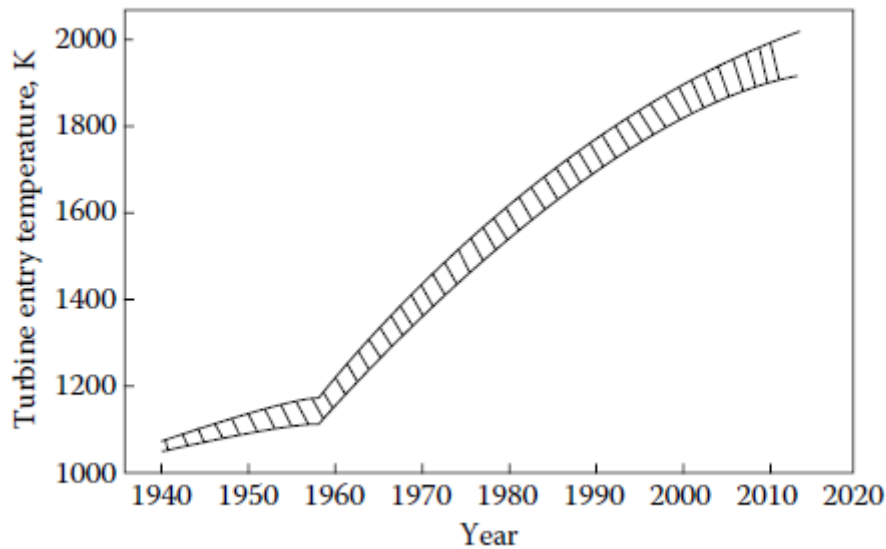


Figure 3.8 - Historical trend of turbine entry temperature

Further increase in the amount of air used for wall cooling (above the high-current values) is not technically acceptable, because this means less air for combustion and dilution. It would also worsen the radial temperature profile at the combustor outlet, and so reducing the life of turbine blades. The only practical alternative is to make more efficient use of the already available cooling air.

3.4.1. Industrial combustion chambers

Industrial gas turbines are required to operate economically and reliably over long periods without attention. With respect to engines used for aircraft operations, the compactness is no longer important and it is considered only if the engine has to fit into an existing building or if delivery is made difficult. Others requirements regard the fuel economy, low pollutant emissions and accessibility for maintenance [15]. In order to fulfil those requirements, combustor for industrial gas turbine tend to be much larger than their aeronautical counterparts. This results in longer residence times, which is an advance when burning poor quality fuels. Air flow velocities are lower, so that pressure losses are smaller. Any industrial unit may come from “industrialized” aero engines, where they usually burn gaseous and/or light to medium distillate fuels, or from systems that are designed to burn gaseous fuels, heavy distillates, and residual oils, and depart fairly radically from aeronautical practice.

One of the most successful industrial unit that fall into the latter category is the 80 ME GE MS7001 gas turbine, which is showed in Figure 3.9. Each machine has ten sets of combustion hardware, and each set is made of a casing, and end cover, a set of fuel nozzles, a flow sleeve, a combustion liner and a transition piece.

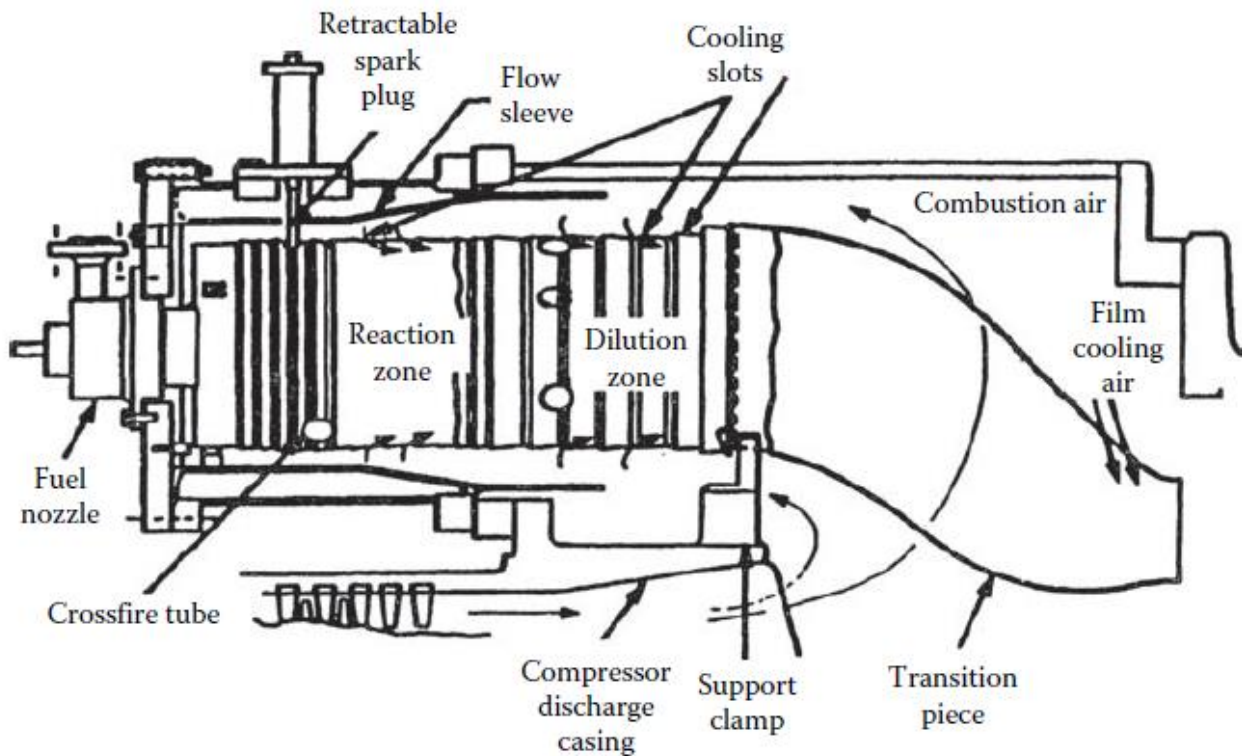


Figure 3.9 - General Electric conventional industrial combustor

Other constructors prefer to build engines using a single, large combustor that is mounted outside the engine, as shown in Figure 3.10. This allows the combustor to be exclusively designed to meet the requirements of good combustion performance. Also, the ease of inspection, maintenance, and repair all of which can be accomplished without removing large casing components [16]. Even with all these aspects in favour of single tubular combustor, multiple fuel injectors (burners) are preferred because they provide a shorter flame and a more uniform distribution of temperature in the gases flowing into the dilution holes.

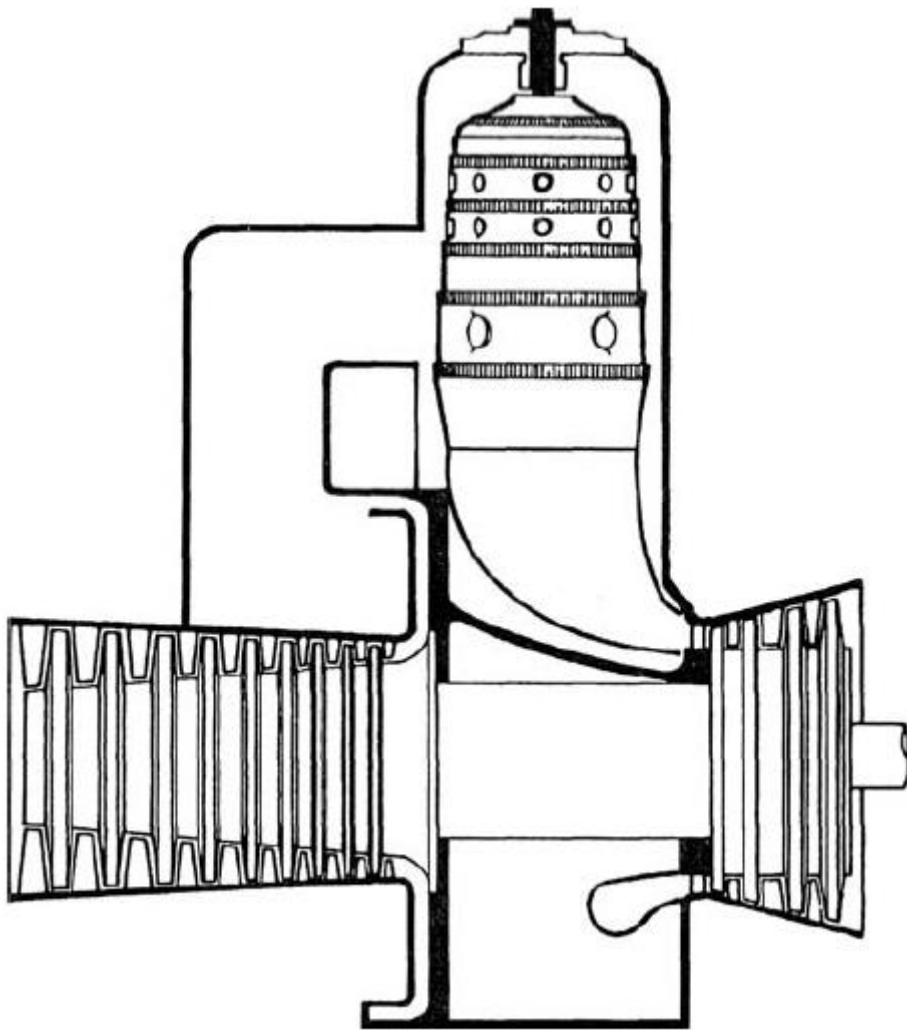


Figure 3.10 - Industrial engine featuring single tubular combustor

4. NO_x emission control solutions in gas turbines

4.1. Introduction

The past decades have witnessed an increase in the awareness for environmental consequences due to human activity. Pollution and environmental protection are now perceived by the society as an inevitable aspect that must always accompany new technologies. All these aspects led to changes both in the regulations for controlling gas turbine emissions and in the technologies used to meet these regulations. During the same period the fuel consumption by civil aviation has raised to the extent that is now perceived as one of the world's fastest growing energy-use sectors. On the other hand, stationary gas turbine has become firmly established as prime movers in the gas and oil industry. All these developments have increased the pressure on combustion engineer to reduce pollutant emissions from all types of gas turbines [12].

The elements present in the exhaust of an aircraft engine is composed of carbon monoxide (CO), carbon dioxide (CO₂), water vapour (H₂O), unburned hydrocarbons (UHC), particulate matter (mainly carbon), nitrogen oxides (NO + NO₂ indicated as NO_x) and excess atmospheric oxygen and nitrogen (N₂). CO₂ and H₂O have not always been regarded as pollutant because they are a natural consequence of a complete combustion of a hydrocarbon fuel. Unfortunately, they both are contributing to the global warming so that it is necessary to reduce those emissions. The only way to reduce emission of those two elements is that of burning less fuel so to increase gas turbine thermal efficiency which will also reduce direct operating costs.

All the other emissions are toxic for human body and contribute to environmental pollution. CO reduces the capacity of the blood to absorb oxygen and, in high concentration, cause asphyxiation and death. UHC are toxic and, in combination with NO_x and sunlight, form photochemical smog. Particulate matter (called soot or smoke) creates problems of exhaust visibility and soiling of the atmosphere. NO_x (made by NO and NO₂), of which the predominant compound is NO, contribute to the production of photochemical smog, cause damage to plant life and promotes acid rain. NO_x emissions are responsible for a problem of particular concern, which is the formation of ozone in the troposphere (the region which extends from ground level to approximately 12 km above the earth's surface). This is the region where stationary gas turbine and subsonic aircraft operate. The relevant reactions are



Sometimes, for stationary engine, fuel of poor quality is used for its cheap price. Unfortunately, this kind of fuel contains some sulfur contamination which, once burned, produce additional pollutant like oxide of sulfur (SO_x), mainly SO_2 and SO_3 . These compounds are toxic for the human body, they are corrosive and lead to the formation of sulfuric acid in the atmosphere. The only way to avoid the formation of oxides of sulfur is to remove sulfur from fuel before combustion.

Since the world energy demand is forecast to grow over the next 30 years at around 1,8% per annum will be met predominantly by the combustion of fossil fuel, the manufactures of both stationary and aircraft engine are asked to cope with the pollutant reduction [12].

4.2.Environmental legislation

The laws for governing the emission of stationary gas turbines are very complex because not only the government legislation varies from one country to another but they depend also by local or site-specific regulations and ordinances governing the size and usage of the plant under consideration and the type of fuel used. If a stationary engine burns natural gas, the emission of UHC, particulate matter, and SO_x are so small that can be neglected. So, most of the regulations are oriented towards the reduction of NO_x . In the United States of America, the Environmental Protection Agency (EPA) has promulgated emission standards which depend on the engine's input energy and the intended usage (which can be utility or industrial). A brief resume of such regulations is here proposed:

- For turbine burning natural gas fuel and intended for producing electricity power, the NO_x limits are: 42 ppmv (parts per million by volume) below 3 MW (4000 HP), 25 ppmv between 3-110 MW (4000-150*10⁶ HP) and 15 ppmv above 110 MW (above 150*10⁶ HP);
- For new electricity-producing turbines which burns other fuel than natural gas, the NO_x limits are: 96 ppmv below 3 MW (4000 HP), 74 ppmv between 3-110 MW and 42 ppmv above 110 MW;

- For new mechanical drive turbines with a power below 3.5 MW, the NO_x limits are: 100 ppmv for those which use natural gas fuel and 150 ppmv for fuels other than natural gas;
- SO₂ emissions are limited to 110 ng/J gross energy output for turbines that are located in continental areas and 780 ng/J gross energy output for turbines located in non-continental areas.

The limits expressed above are referred to parts per million volume (ppmv) and referenced to 15% oxygen on a dry basis. The correction formula is

$$(\text{NO}_x)_{\text{ref15\%oxygen}} = \frac{(5.9)(\text{NO}_{x\text{measured}})}{(20.9 - \text{O}_{2\text{measured}})} \quad (4.2)$$

Where NO_x concentrations are expressed in ppmv in dry conditions and O₂ content is expressed in percentage by volume.

The rest of the world is substantially aligned with the EPA regulations, like Europe and Japan. In some areas, like Southern California and parts of Japan, the regulation are even more stringent because of the production of smog, thus, some local regulations now call for NO_x limits as low as 9 ppmv.

Until the late 1980s, the “best available control technology” (referred as BACT) for reaching levels of NO_x emission of 25 ppmv was by water or steam injection into combustion zone [17]. Nowadays, the technology used to reduce the NO_x emission below 10 ppmv is a combination of water or steam injection or lean premixed combustion, supplemented by exhaust gas treatment using selective catalytic reduction (SCR). This solution although allows for reaching very low level of NO_x emission, has some drawbacks. First of all is a very expensive solution because it requires not only to equip the engine with huge SCR but it needs also fine control strategy. It can also aggravate the pollution problem because of the releasing of ammonia gas and increase CO concentrations into atmosphere.

Even if there are no EPA regulations for CO and UHC emissions, there are some local regulations that impose a limitation for such emissions. For example, typical CO limits range from 10 to 40 ppm.

In the past there was no major difficulties to respect low CO levels because of the user's insistence on high combustion efficiencies to minimize fuel consumption. Nowadays, the increasing pressure to reduce NO_x emissions has resulted in copious amounts of water or steam injection directly into the combustion zone and, recently, on the adoption of lean, premix combustion. Those solution involve the lowering of flame temperature, which in turns leads to promote the formation of CO. The control of CO levels has now become a more difficult problem with respect to the past, when the legislation for stationary engine were formulated and weren't so stringent on NO_x emission levels.

4.3.Mechanism for pollutants formation in gas turbines

Concentration levels for pollutants in gas turbines is linked to temperature, time, and concentration histories of the combustion process. These dependencies vary from one combustor to another and for different operating conditions. The concentration of CO and UHC are highest at low-power conditions, while diminish for a power increase. Concentrations of NO_x and smoke are low at low-power conditions and reach maximum level at highest power conditions. Figure 4.1 show such trend

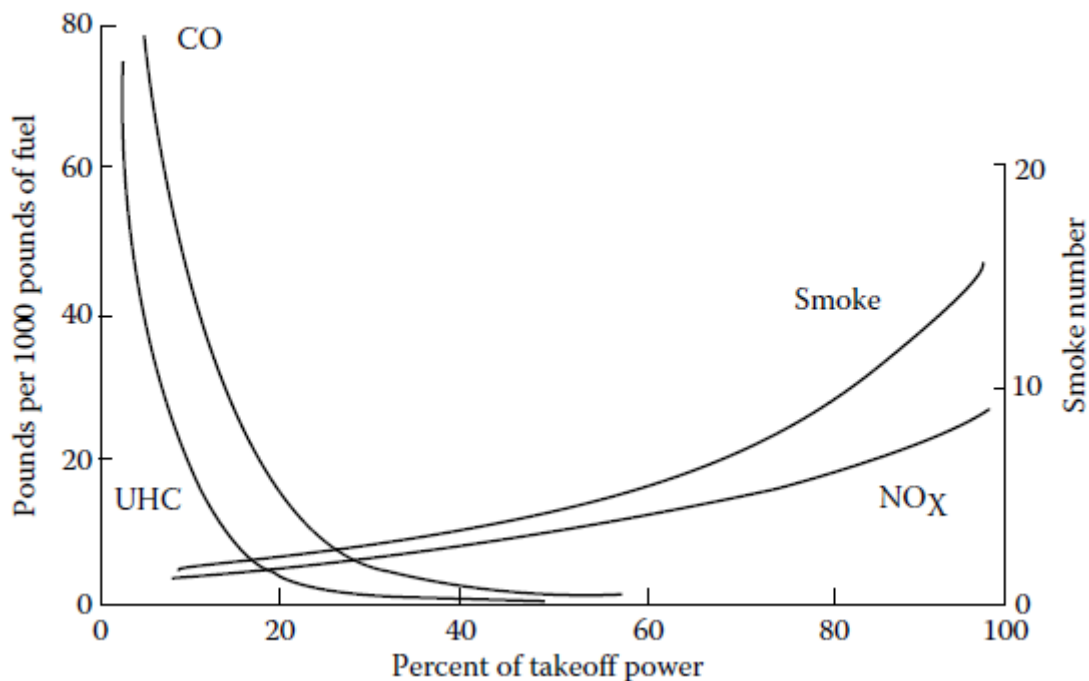


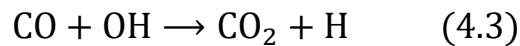
Figure 4.1 - Emission characteristics of gas turbine engines

4.3.1. Carbon monoxide

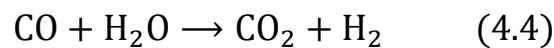
Carbon monoxide (CO) forms inside combustor when a combustion zone is operating at fuel-rich conditions, because there is not sufficient oxygen to complete the reaction to CO_2 . It can also happen that CO is formed in cases the mixture is stoichiometric or fuel-lean because of the dissociation of CO_2 . Much of the CO arises from incomplete combustion of fuel which can be caused by one or more of the following:

- In the primary zone inadequate burning rates occurs due to fuel/air ratio that is too low and insufficient residence time;
- Inadequate mixing of fuel and air producing in some region weak combustion conditions which produces poor combustion processes or other regions where over-rich combustion produces high local concentrations of CO;
- Quenching of the post flame products by entrainment into the liner wall-cooling air, especially in the primary zone.

One may think to reduce CO emission formed in primary zone by providing additional air downstream to achieve a gradual reduction in burned gas temperature. But, once formed, CO is very resistant to oxidation so that it no longer oxidizes to form CO₂. In high temperatures, the major reaction removing CO is



At lower temperatures, the following reaction holds



Which represents an important reaction to remove CO.

4.3.2. Unburned hydrocarbons

Unburned hydrocarbons (UHC) include fuel that leaves the combustor in the form of drops or vapor, or fuel species of lower molecular weight. The causes that produce UHC are poor atomization, inadequate burning rates, chilling effect of film-cooling air, or a combination of these. Even if the reaction kinetics for UHC formation are more complex than for CO formation, it is generally found that those factors influencing CO emissions also influence UHC emissions.

4.3.3. Smoke

Smoke is due to finely divided particles called soot which form in fuel-rich regions of the flame that are always close to the spray. In this region, recirculation burned products move upstream towards the fuel injector and local pockets of fuel vapour become enveloped in oxygen-deficient gases at high temperatures. Unfortunately, in these fuel-rich regions, smoke is produced in large amount. Most of the soot produced

in the primary zone is then consumed in the high-temperature regions downstream from the fuel injector. So, the soot measured at the exhaust port of combustor is due to the difference between the soot produced in the primary zone and the soot consumed in the intermediate zone (in most recent gas turbine combustor also in the last zone of combustor, called dilution zone). Analysis composition of soot shows that the major component is due to carbon (96%) and a mixture of hydrogen, oxygen and other elements. Since soot is not an equilibrium product of combustion, it is impossible to predict its rate of formation or final concentration from kinetic or thermodynamic data. It seems that soot formation is more determined by physical processes rather than fuel air mixing by kinetics.

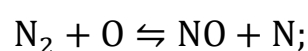
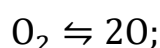
4.3.4. Oxides of nitrogen

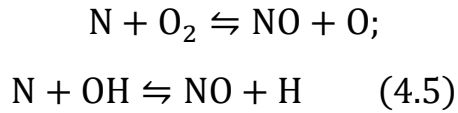
Since most of nitric oxide (NO) formed in combustion than oxidizes in carbon dioxides (NO₂), it is convenient to refer on NO_x to address to both NO and NO₂. The mechanisms of formation are four:

- Thermal NO;
- Nitrous oxide mechanism;
- Prompt NO;
- Fuel NO.

Thermal nitric oxide

Thermal nitric oxide is produced from oxidation of atmospheric nitrogen. Indeed, air composition by volume is made of about 79% of N₂ and 21% of O₂ (if other gases in the atmospheric air are neglected). So, there is abundance of nitrogen in the air. The process which leads to thermal nitric oxide formation is endothermic and it is significant only when high temperature is reached (1850 K). Extended Zeldovic mechanism includes the following reactions





In order to have thermal nitric oxides formation, two aspect must be present: oxygen abundance and high temperature. This is the reason why peak formation of NO_x is found on the fuel-lean side of stoichiometric. In the rich side of the stoichiometric, even if the temperature is higher the oxygen is consumed preferentially by the fuel. The exponential dependence on thermal NO on flame temperature is demonstrated in Figure 4.2. It is possible to notice that the NO production lowers very rapidly as temperature is reduced, in particular for normal combustor residence time of around 5 ms.

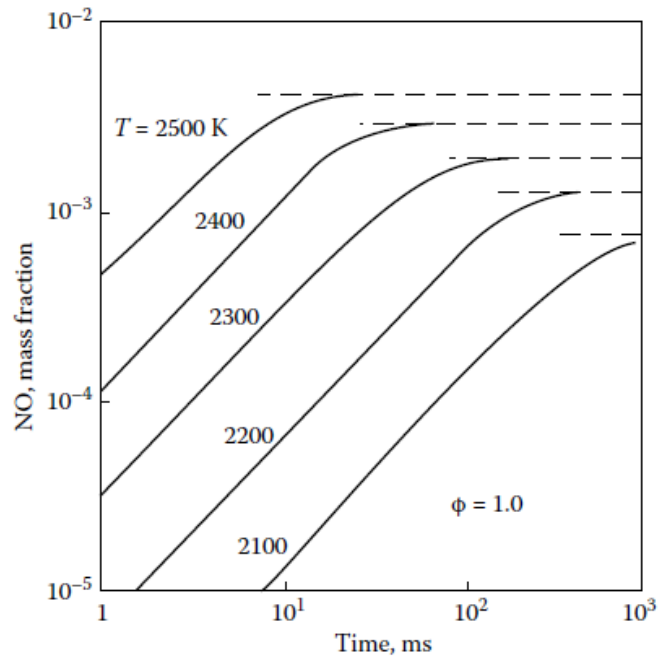


Figure 4.2 - NO_x formation as a function of time and temperature at a pressure of 1 MPa

Another difference lies on the fuel state, which can be in gaseous state or liquid state. As can be seen from Figure 4.3, the difference in NO_x production between liquid fuel and gaseous fuel diminish for very high temperature [18].

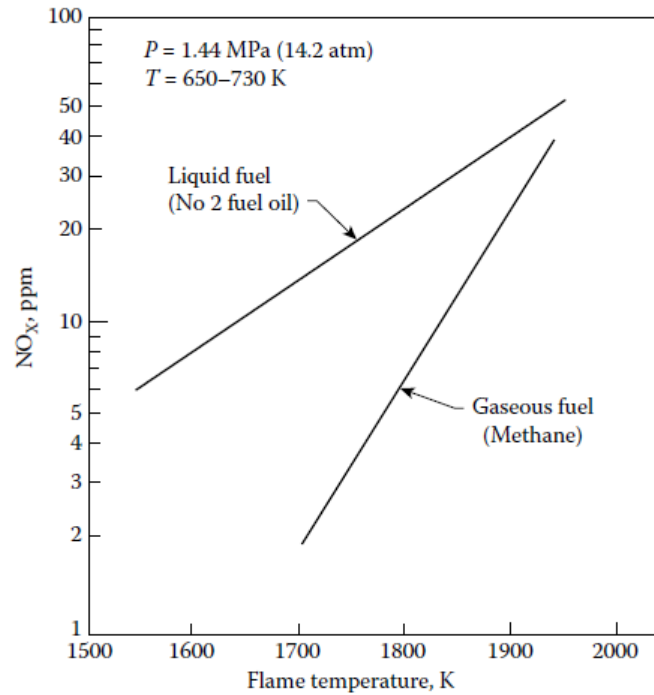


Figure 4.3 - Dependence of NO_x formation on flame temperature for liquid and gaseous fuel

Combustor residence time is also a factor that influences the formation of NO_x. The more the residence time, the more the formation of NO_x emission, except for very lean mixtures ($\phi < 0.5$) for which the rate of formation is so low that that it becomes fairly insensitive to time. Figure 4.4 shows the effect of residence time for different residence times and different equivalence ratios.

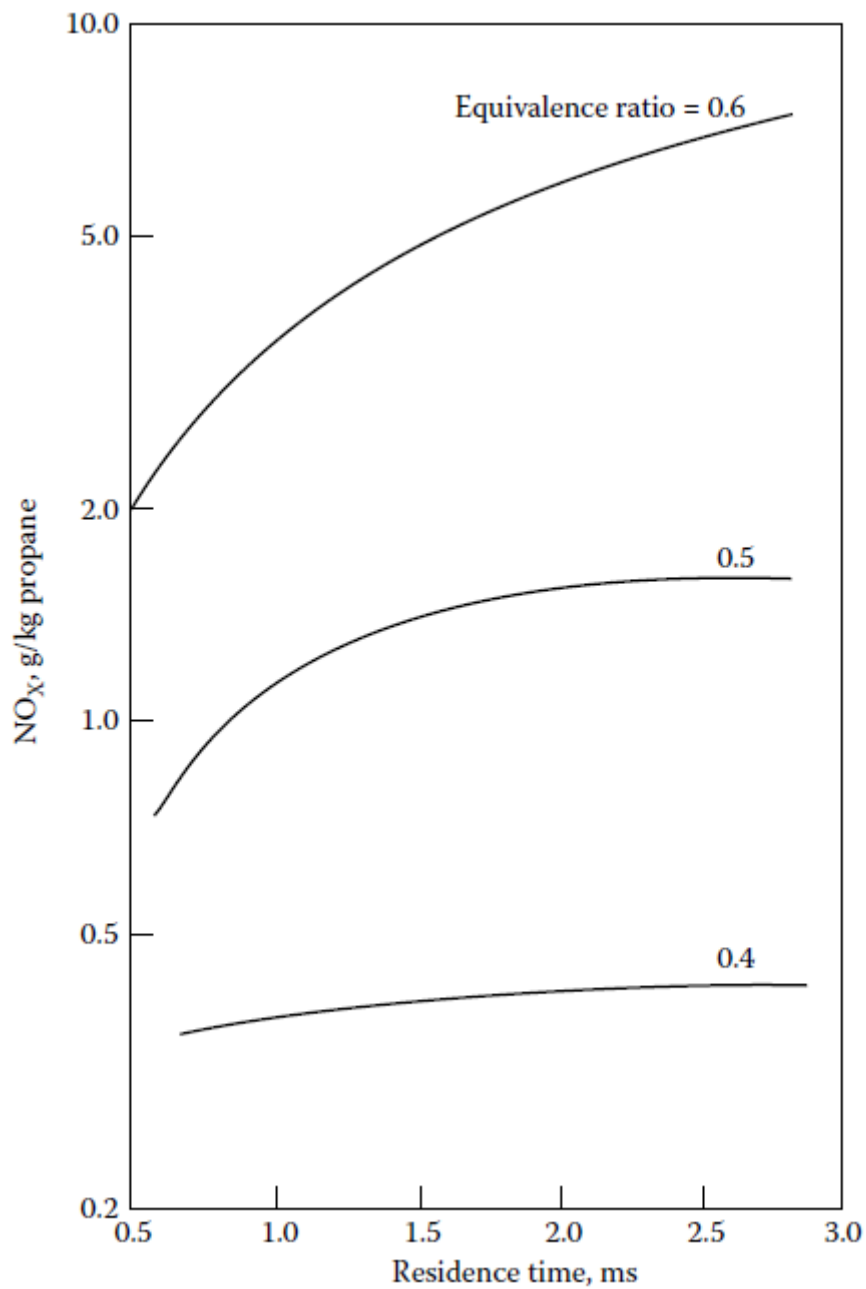


Figure 4.4 - Effect of residence time on NO_x in a premixed fuel-air system for different equivalence ratios

From previous considerations, it is possible to figure out some important considerations on the design of lean-premixed combustors:

- Thermal NO formation is largely affected by flame temperature;
- Little NO emission is formed for temperatures below 1850 K;

- NO emission increase with time for combustors operating at conventional operative conditions;
- For lean-premixed combustors ($\varphi < 0.5$), NO formation is largely independent of residence time.

4.4.NOx reduction in conventional combustors

From the previous considerations, it is clear that every time one tries to reduce NO_x emission from a gas turbine combustor, the first thing to do is to lower the reaction temperature and then to avoid the formation of hot spots from the reaction zone. In real life, in conventional combustor, the adopted solutions include the addition of more air into the primary combustion zone, improved atomization, increase in liner pressure drop to promote better mixing, eliminating hot spot from the combustion zone, and reduction of combustion residence time. The reduction of flame temperature and residence time promotes the formation of CO and UHC, so that any attempt in order to reduce the NO_x formation results in the promotion of CO and UHC so that a trade-off must be reached. Here are proposed two solutions commonly adopted in the vast majority of gas turbine combustor.

4.4.1. Water or steam injection

Since NO_x emission formation depends exponentially on temperature, a good way to reduce such emission is to lower the temperature of the combustion zone. This result can be obtained by increasing the amount of air or introducing a heat sink. Unfortunately, increasing the amount of air has some serious drawbacks like the increasing in the primary-zone gas velocity which, in turn, affects the ignition and stability performance. So, it is preferred to subtract heat through the adoption of a heat sink. Introducing water or steam injection directly into the combustion zone lowers the flame temperature because this injection behaves like a heat sink. This technique is not recommended for aircraft application because of the large amount of water and steam required, but it fits perfectly when a stationary engine is considered. In some cases, the water or steam is injected directly into the flame, through a number of separate nozzles located at the head of the combustor or through holes that are integrated into the fuel nozzle. Another possible solution is to inject water or steam upstream of the combustor liner, into the airstream, which then flows into the combustor zone through the main air swirler. This approach guarantees good atomization because of the smaller droplets are carried by the airflow through the swirler into the combustion zone, whereas the

larger droplets impinge on the swirler vanes and form a liquid film, which is atomized as it flows over the downstream edge of the vane [19].

When only steam is used, this can be injected directly into the combustion zone or into air that subsequently flows into the combustion zone. Sometimes the steam is injected into the compressor discharge air. This method is simple but implies a steam waste because only about 40% of steam actually flows into the combustion zone [20]. The following equations shows the effectiveness of water and steam injection for reducing NO_x emission

$$\frac{\text{wet NO}_x}{\text{dry NO}_x} = \exp -(0.2X^2 + 1.41X) \quad (4.6)$$

Where X denotes the water to fuel ratio (water/fuel).

This relationship holds for both liquid and gaseous fuel and it shows that equal mass flow rates of fuel and water (X=1) produce an 80% reduction of NO_x emission [21]. Water injection is more effective when combustion takes place at high pressures and temperatures where thermal NO_x is higher and less effective at low pressures and temperatures where a larger proportion of NO_x formation is due via prompt mechanism. Of course, water injection always reduces NO_x emission but its effectiveness depends on the combustor operating conditions. Even if water or steam injections are useful for NO_x emission reductions, this solution involves some drawbacks. Between them there are the increase in the capital costs for providing the gas turbine plant of the water injection mechanism and an increase in the fuel consumption in order to heat the water up to the combustion temperature. However, the additional water mass flow rate that flows inside the turbine increases the turbine power output. Before injecting water inside the combustor, water must be of high purity to prevent corrosion and deposits in the combustor. Experience shows that for those plant which uses water injection, the inspection time is reduced as well as maintenance intervals. Water and steam injection involve combustion performance deterioration. It is possible to understand if this deterioration happens from an increase in the level of CO and UHC emissions and by increase in combustor pressure oscillations. It is possible to collect all the drawbacks of water injection technique for NO_x emission reduction [22]:

- Higher capital cost;
- Increase in fuel consumption;
- High cost of water treatment;
- Possible corrosion of hot section components;
- Higher maintenance costs;
- Increase in CO and UHC emissions;
- Increase in combustion pressure pulsations.

All these drawbacks led in the past to an increase in pressure on combustion engineers to find alternative solutions for NO_x emission reduction. Among them, “dry low-NO_x” (DLN) combustors were developed. They are combustors capable of meeting the emissions goals without relying on water or steam injection techniques.

4.4.2. Dry low-NO_x systems

In order to show the dry low-NO_x combustor, the General Electric solution was chosen because it is possible to highlight the basic concepts of this technique. Figure 4.5 shows a schematic view of this type of combustor.

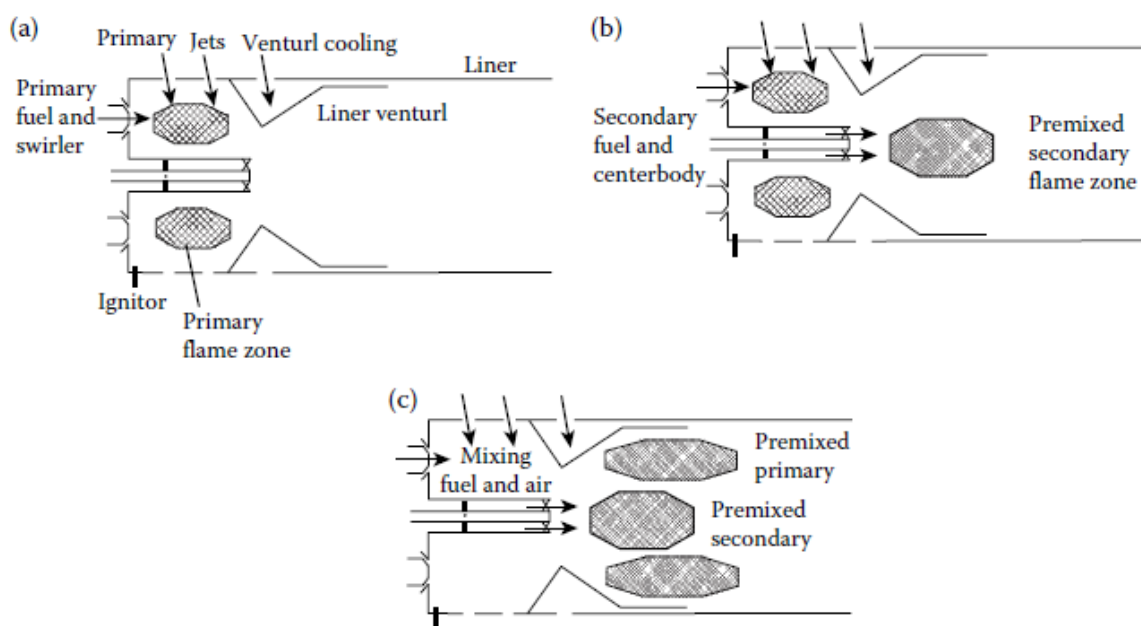


Figure 4.5 - GE DLN combustor in various operational modes: (a) primary; (b) lean-lean; and (c) premix.

The main idea behind this system is the use of a two-stage combustion in order to meet low emission and high operability over the entire load range. This combustion system consists of four main components: primary fuel nozzle, liner, venturi and cap/center-body assembly. It has been described in some detail in a number of publications, including [23], [24], [25] and [26]. All these components are organized in order to provide three zones:

- The primary zone is showed in Figure 4.5a. It extends from the six primary nozzles mounted on the cap face to the end of the center-body;

- The secondary zone is showed in Figure 4.5b. It includes the volume from the centerbody exit to the plane of the dilution holes;
- The third zone is showed in Figure 4.5c. It occupies the space from the dilution holes to the end of the liner.

The combustor operates in four different modes:

- **Primary:** this mode of operation is used to ignite, accelerate and operate for low-power settings up to 40% full load. Primary combustion air enters through swirlers surrounding each nozzle and through the primary air holes.
- **Lean-lean:** When the engine load increase, fuel is supplied to the secondary zone from four radial stub pipes located in the centerbody. Primary and secondary zones both operate at low equivalence ratios, so the name of the mode.
- **Secondary:** This mode is a transition mode between lean-lean and premix mode. While the fuel supply is reduced for the primary zone, the fuel supply is increased for the secondary zone. When transition is over, the primary flame is extinguished and flame is present only in the secondary zone.
- **Premix:** In this operation mode the fuel is re-introduced through the primary nozzles while the primary combustion zone (which is now premixed) is shifted to a region downstream of the liner venturi, where it is ignited by the secondary flame zone. Thanks to the venturi, it is possible to accelerates the flow from the first stage to prevent flashback and to create a toroidal recirculation zone in order to stabilize the primary combustion zone. During this operational mode, the emission levels are at the minimum.

5. The 0D model

5.1.Introduction

The starting point of this thesis simulations is represented by some information which come directly from the EthosEnergy company. This information come from an existing plant sited in Duino, Trieste, Italy. This company is a paper mill and uses a TG20 gas turbine for the generation of both electric power and steam needed for the production of paper, cardboard and derivatives. Indeed, the gas turbine is organized in a cogeneration way. In such plants the heat present in the exhaust gas from turbine can be used to provide the necessary heating load for the steam production.

The dataset is composed of several information which come from four different trial in the Duino plant. These trials were made to make some data acquisition and to prove that emission reductions due to water injection are within the regulations. Some of these data are collected in Figure 5.1.

	T1 [°C]	T2 [°C]	P1 [bar]	P2 [bar]	β	\dot{m}_f [kg/s]	\dot{m}_a [kg/s]	α	\dot{m}_{H2O} [kg/s]	Pu [MW]
1° trial	29,15	360,06	1,02	10,74	10,62	1,86	143,32	77,01	0,39	17,52
2° trial	32,78	378	1,02	11,02	10,91	2,17	139,73	64,49	0,7	23,13
3° trial	29,52	371,41	1,02	10,69	10,57	2,19	139,79	63,70	0,6	23,29
4° trial	27,19	362,13	1,02	10,39	10,27	1,89	140,12	74,18	0,297	18,04

	$\eta_{c, is}$	$\eta_{c, pol}$	T4 [°C]	β_t	T3 [°C]
1° trial	0,87	0,90	413,94	10,27	819,22
2° trial	0,85	0,89	467,84	10,54	921,89
3° trial	0,84	0,88	470,24	10,27	921,76
4° trial	0,84	0,88	423,75	9,99	837,57

Figure 5.5.1 - Duino trials information dataset

Since all the trials were performed in wet condition (water injection is present in all four trials), it was necessary to have a model which is capable of removing the water injection. In this way it is possible to appreciate the effect of water on quantities such as emission and temperature. This model will be useful as a reference data in order to operate a comparison with the CFD 3D model results, in particular with the temperature

reached at the end of the combustion. Since this was a preliminary study, it was necessary to develop a fast and easy-to-modify model, so a 0-D model was chosen.

5.2. Model description

This model has been made in Matlab/Simulink environment for the easy and simple way each component of a gas turbine plant can be modeled. Figure 5.2 shows the blocks that, together, form the system.

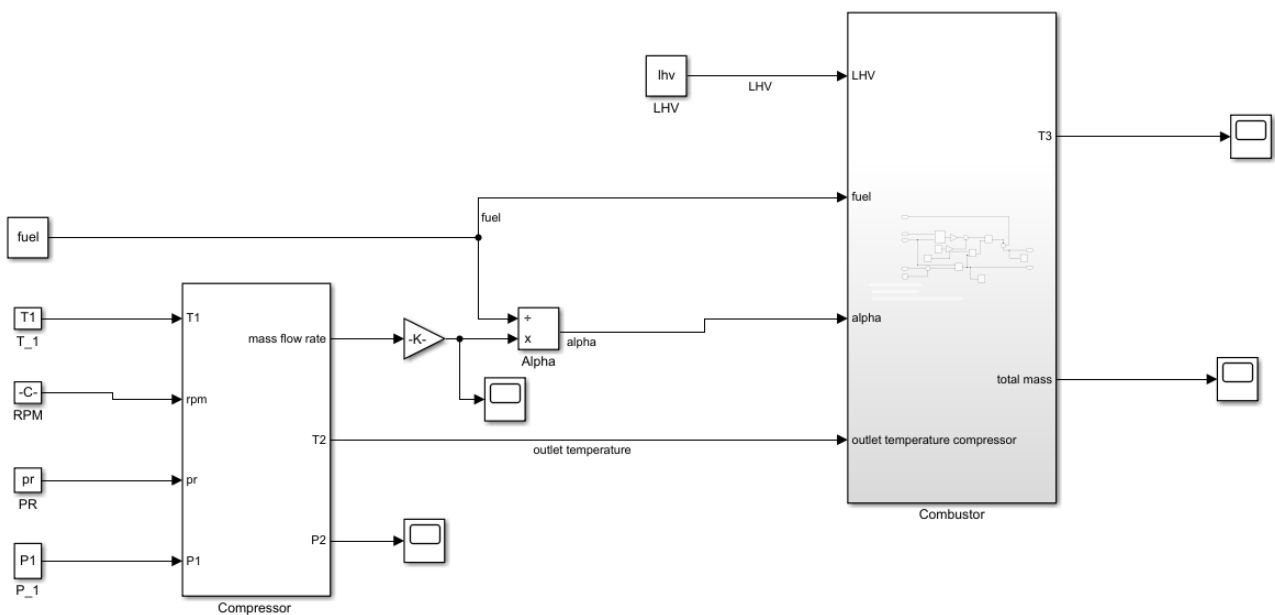


Figure 5.5.2 - Gas turbine modelling on Simulink environment

The model is a static model composed by two subsystems: compressor and combustor. The inputs quantities are the pressure ratio, the compressor shaft speed, the fuel and water mass flow rates. The output are the turbine inlet temperature and the air to fuel ratio. Figure 5.3 show the compressor block

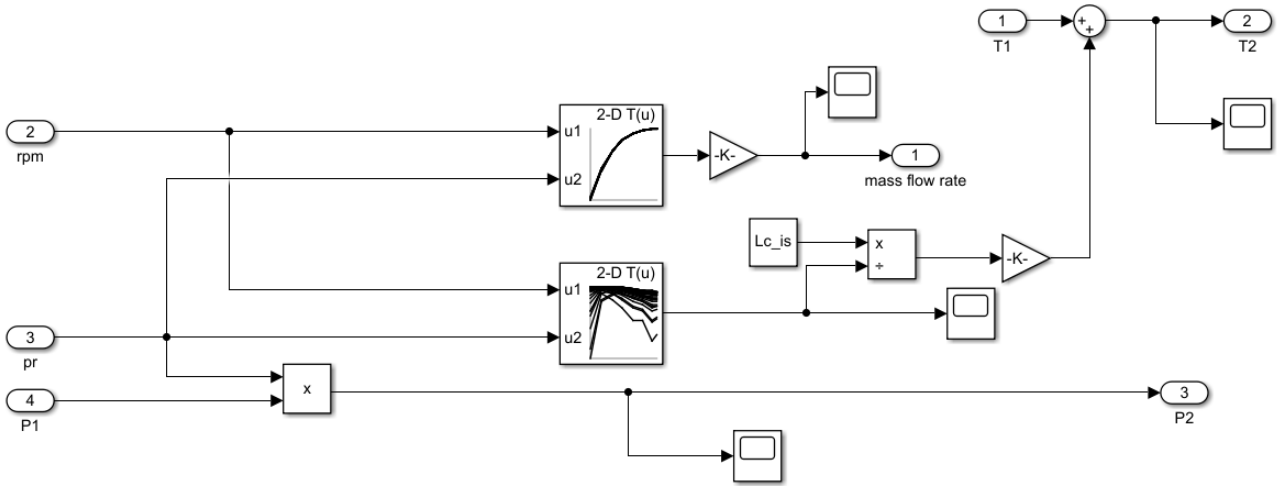


Figure 5.5.3 - Compressor simulink block

The compressor block is based on the compressor map which is provided by EthosEnergy. The map shows the corrected air mass flow rate, the corrected compressor shaft speed, the isentropic efficiency and the pressure ratio. From this information, it is possible to extract the operating point (composed by the air flow rate and the efficiency) starting from the pressure ratio and the corrected shaft speed using a 2-D lookup table strategy. If surge limit is reached, the model gives a “NaN” result. In order to improve the accuracy of this strategy, the map has been extended using the Matlab command “polyfit” and “polyval”. In this way, other operative points different than the ones present in the map are calculated. The output of the compressor block is the pressure P2 and the temperature T2. The pressure P2 is easily computed once the pressure ratio is obtained while for the calculation of T2 temperature the following equation was used:

$$T_2 = T_1 + \frac{L_c}{c_p} \quad (5.1)$$

Where L_c is the compressor work and c_p is the air specific heat at constant pressure, computed according to [27]:

$$c_p = \frac{1000}{Mw_{air}} * (a + b * T_{mean} + c * (T_{mean})^2 + d * (T_{mean})^3) \quad (5.2)$$

Where

- a, b, and c are experimental coefficient;
- $M_{w_{air}}$ is the molar weight of the air;
- T_{mean} is the mean temperature between the inlet and the outlet compressor temperature. The outlet temperature is the one given from the experimental data provided by EthosEnergy.

Water injection in the 0-D model is made considering water enthalpy of vaporization h_w at the same pressure inside the combustor. Water mass flow rate is multiplied to the enthalpy of vaporization in order to get the thermal power:

$$\dot{Q}_{water} = \dot{m}_{water} * h_{water} \quad (5.3)$$

This thermal power is in turn subtracted from the heat generated by the combustor, according to the following formula:

$$\eta_b * H_L * \dot{m}_{fuel} - \dot{Q}_{water} = (\dot{m}_{air} + \dot{m}_{fuel} + \dot{m}_{water}) * c_p' * (T_3 - T_2) \quad (5.4)$$

Where:

- η_b is the combustor efficiency;
- H_L is the fuel lower heating value;
- c_p' is the specific heat at constant pressure for the exhaust gases, computed according to [28].

From equation (6.4) it is possible to extract temperature T3 which will be lower compared to the dry case due to the heat extraction by water evaporation.

Figure 5.4 shows how water injection is performed inside the combustor block

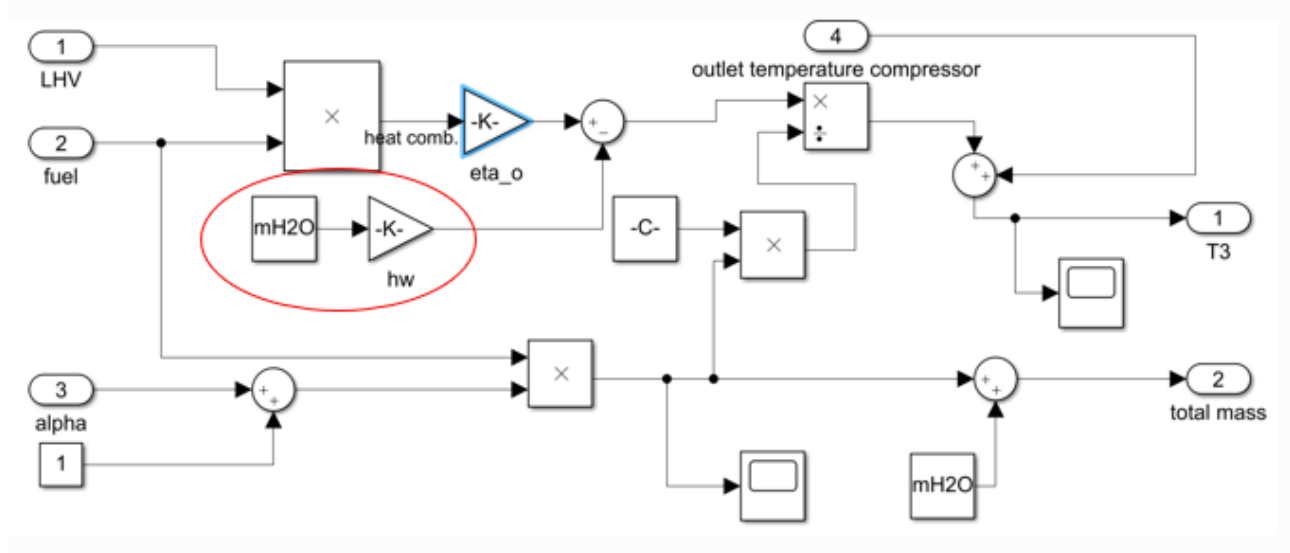


Figure 5.4 - Combustor simulink model. The red circle shows how water injection is performed in the 0D model

The turbine outlet temperature T4 calculation requires a turbine map which can characterize the turbine in term of efficiency. Since there is no availability of such information, turbine is not implemented into the Simulink (like the compressor). So an alternative solution was need in order to compute temperature T4. From Duino trials, the power output measured at the generator terminals are available, so it is possible to compute the turbine work L_t from the following equation:

$$L_t = \frac{\frac{P_u}{\eta_0} + \dot{m}_{air}L_c}{(\dot{m}_{air}\dot{m}_{fuel}\dot{m}_{water})} \quad (5.5)$$

Where η_0 is the organic efficiency

At this point it is possible to compute temperature at the turbine discharge T_4 according to:

$$T_4 = T_3 - \frac{L_t}{c_p'} \quad (5.6)$$

5.3.Results

Results coming from the 0-D model show that the model produces quantities that are aligned with the available experimental information. Two comparison are proposed:

- One considering the variation of T2 temperature (compressor outlet temperature) with the compressor pressure ratio;
- The other one considering the variation of T4 temperature (turbine outlet temperature) with different water to fuel ratios.

Figure 5.5 shows a comparison between outlet compressor temperature. In red the results coming from the numerical 0-D model, in black the experimental data provided by EthosEnergy. It is possible to notice a good agreement between these two results, thus showing a proper functioning of the model itself.

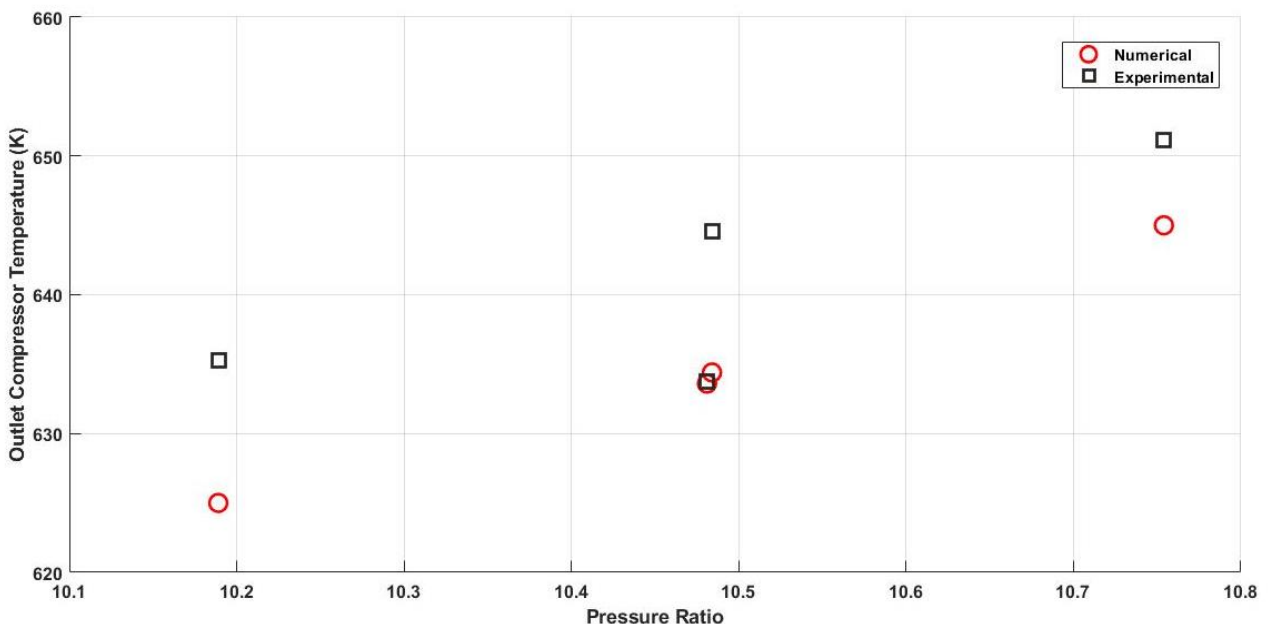


Figure 5.5 - Comparison between the outlet compressor temperature and the experimental data provided by EthosEnergy. Maximum error is about +/- 2%.

Figure 5.6 shows a comparison between turbine outlet temperature and the ratio of water to total mass flow rate. The best agreement between the numerical data (in red) and the experimental results (in black) is at a value of the water to total mass flow rate of 0.5

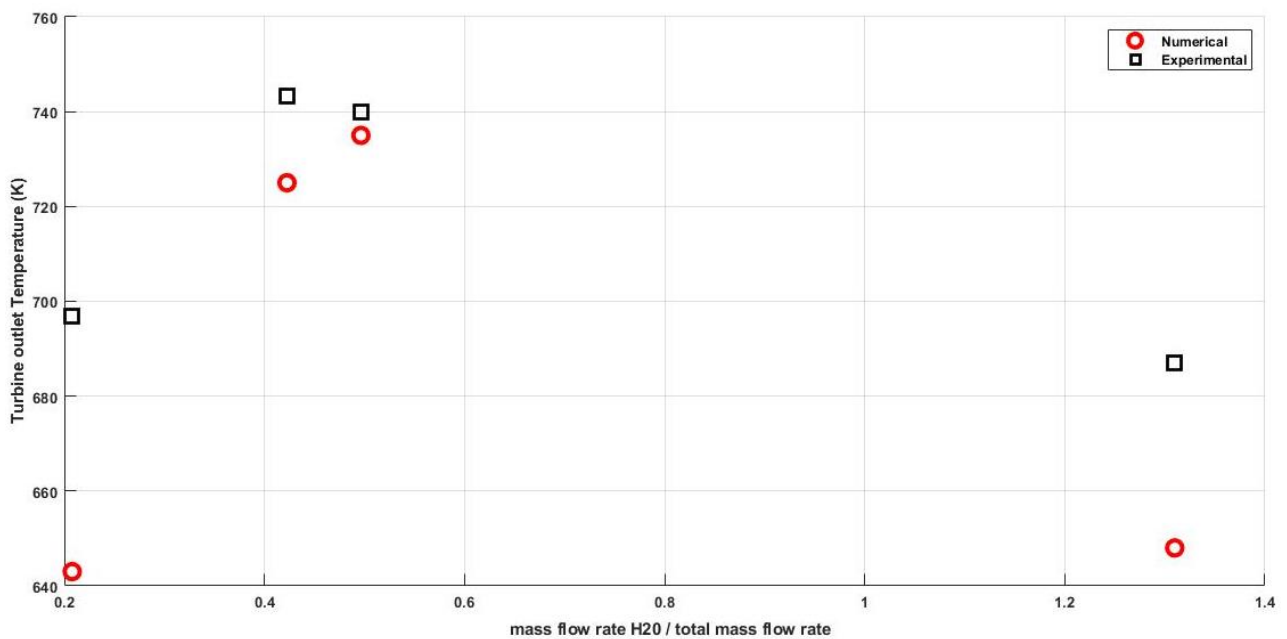


Figure 5.6 – Turbine outlet temperature and water to total mass flow rate ratio comparison between numerical data and experimental results.

Figure 5.7 shows the most important results because there is a comparison between the T3 temperature (turbine inlet temperature) and the water to fuel ratio. As stated before, the turbine inlet temperature is of crucial importance because the higher its value the higher the efficiency of the gas turbine plant. At the same time T3 temperature must be taken under control because there is a threshold for its value that must be never trespassed otherwise the first row of turbine blades could be seriously damaged. Also, in this case there is quite a good match between numerical results and experimental data.

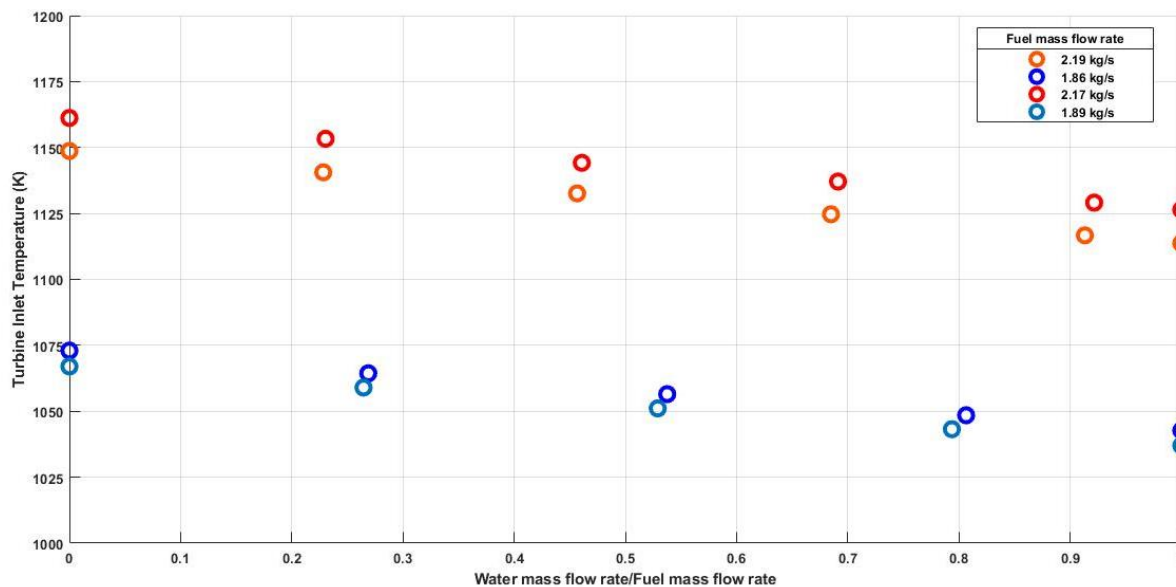


Figure 5.7 – Turbine inlet temperature and water to fuel ratio comparison between numerical results and the experimental data provided by EthosEnergy.

The linear decrease of temperature in function of the water mass flow rate can also be found in literature [29] and [30]. Figure 5.8 shows such trend

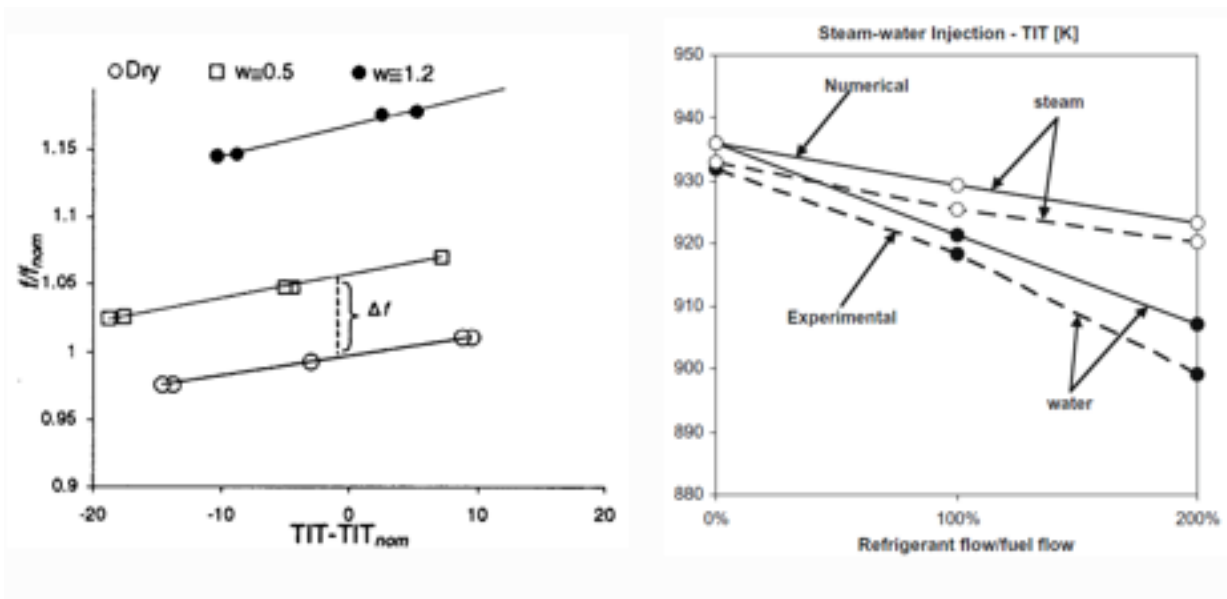


Figure 5.8 - The same linear decrease of the temperature in function of the water mass flow rate can be also found in literature, as shown in these two graphs.

6. TG-20 combustor CFD simulation and results

6.1. Converge CFD Software

CONVERGE CFD software is a multi-purpose computational fluid dynamics code for modelling three-dimensional, reacting or non-reacting, turbulent flows. The software package includes coupled flow and detailed chemical kinetics solvers, the graphical user interface CONVERGE Studio, and a license for a limited version of the post-processing and visualization software Tecplot. CONVERGE features an automated meshing algorithm that generates an orthogonal mesh at runtime and employs Adaptive Mesh Refinement (AMR) to refine the mesh during the simulation in areas with complex phenomena, like moving geometries or fluctuating temperatures or flow velocities. This process is called “autonomous meshing”. The modelling capabilities of CONVERGE include steady-state and transient simulations for incompressible or compressible flows. The software contains a variety of physical models for phenomena including turbulence, spray, conjugate heat transfer, multi-phase flow, fluid-structure interaction, and surface chemistry. Figure 6.1 shows a schematic picture of the Converge Workflow. The starting point for a new simulation is bringing a new geometry in CAD format or in STL format directly into Converge. If there are some problems in the surface of the geometry (like intersections, overlapping triangles, etc) it is possible to fix them directly into Converge. Then the case setup phase can begin, which include:

- Boundary assignment;
- Solver settings;
- Boundary conditions and initial conditions;
- Physical models;
- Output settings;
- Mesh controls.

Now it is possible to export all those information (in ASCII format), which represent the input for the simulation, to the Converge solver. They are made by all the INPUT files (*.in, *.dat) and by the surface geometry files. Now the simulation can run into the Converge solver. During the simulation it is possible to monitor how the run is going. When the simulation ends the post processing can start in order to generate a report.

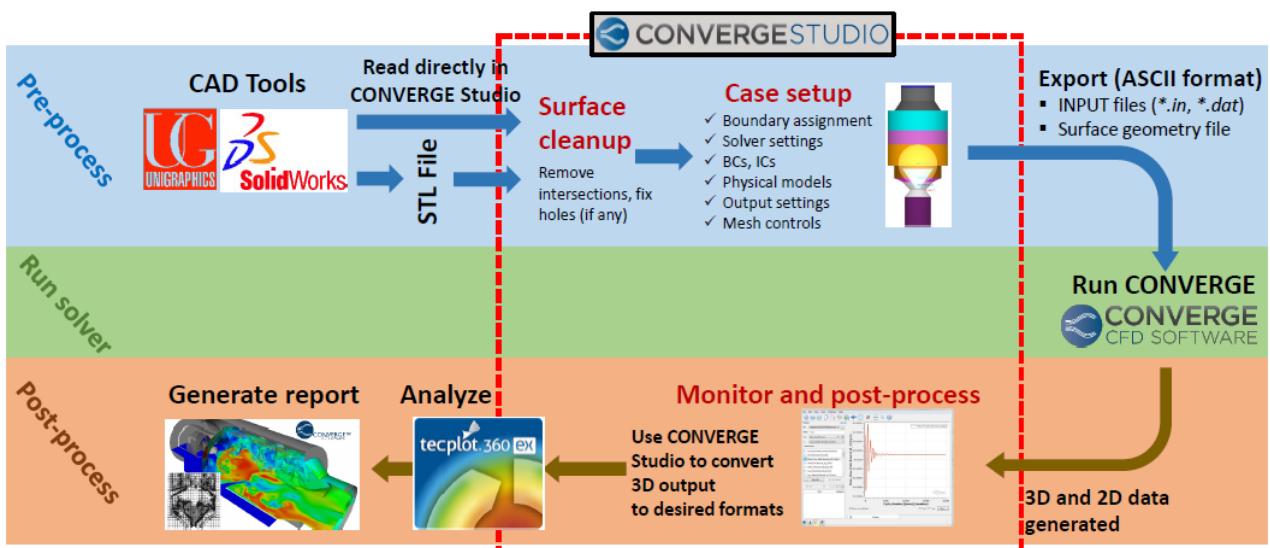


Figure 6.1 - Converge Workflow

6.1.1. Finite Volume method

Finite volume methods can be used to numerically solve the integral form of the conservation equations. This methodology provides some advantages over the other methods, like the possibility to conserve transported quantity for regularly and irregularly shaped cells. In order to understand the inputs for finite volume methodology, a simple three cell computational domain is shown in Figure 6.2.

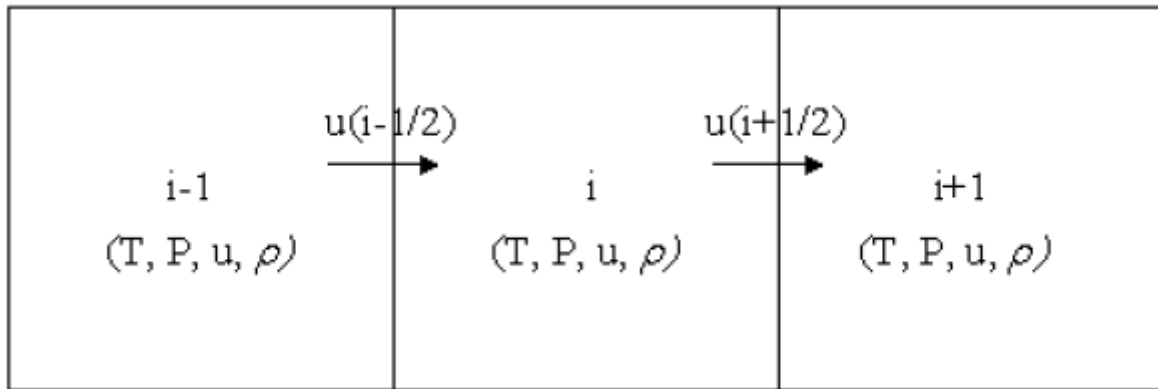


Figure 6.2 - Sample three-cell, one dimensional spatial domain

Consider the simple transport equation applied to a quantity ϕ :

$$\frac{\partial \phi}{\partial t} + \frac{\partial (u\phi)}{\partial x} = 0 \quad (6.1)$$

The above equation can be written in integral form as:

$$\frac{d}{dt} \int \phi dV + \int u \cdot n \phi dS = 0 \quad (6.2)$$

Where:

- V is the cell volume;
- S is the surface area;
- n is the surface normal.

The finite volume methods solve the integral form of the conservation equations instead of the differential form. The integral form of the equation is solved by summing fluxes on the faces of the cells. In CONVERGE, all values are collocated and stored at the centre of the cells as shown in Figure 6.2. So, in order to solve the integral form of the equation, the velocity and ϕ must be interpolated to the cell surface. There are several options for obtaining the cell surface value. One option is to average the two adjacent cell values and place them on the surface, which results in a surface ϕ given as:

$$\phi_{i+1/2} = \frac{1}{2}\phi_i + \frac{1}{2}\phi_{i+1} \quad (6.3)$$

And

$$\phi_{i-1/2} = \frac{1}{2}\phi_i + \frac{1}{2}\phi_{i-1} \quad (6.4)$$

Figure 6.3 below summarizes the order in which CONVERGE solves the transport equations

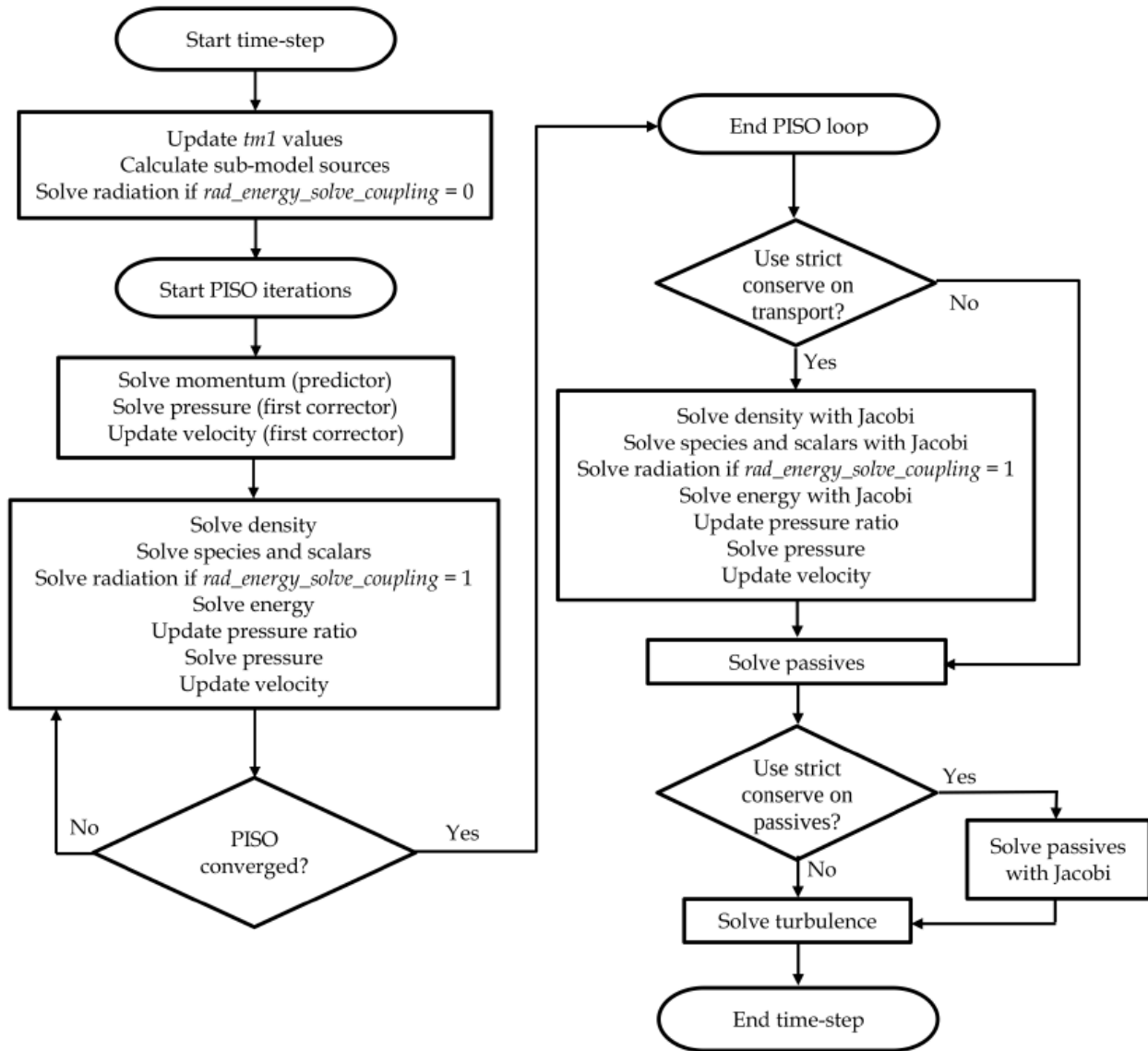


Figure 6.3 - Solution order of the transport equations. the turbulence equations are outside of the PISO loop for efficiency reasons.

At the start of each time-step, the previous values are stored for all transported quantities. Next, explicit sources are calculated for each sub-model that is currently activated and radiation is solved if energy and radiation are decoupled. At the beginning of the PISO loop, CONVERGE solves for momentum and pressures, which sets the velocity for the transport equations. After each PISO iteration, it is necessary

to check for PISO loop convergence. For compressible cases, CONVERGE considers the PISO loop to be converged if

$$\Delta\rho < tol_piso \quad (6.5)$$

Where $\Delta\rho$ is the density correction error. For incompressible cases, CONVERGE considers the PISO loop to be converged if

$$\Delta P < tol_piso \quad (6.6)$$

Where ΔP is the pressure correction error. Note that, if the PISO iteration has converged but the PISO iteration number is less than `piso_itmin`, the PISO iterations will continue until the minimum number of PISO iterations has been exceeded. If the PISO iteration did not converge, CONVERGE executes an additional PISO iteration.

6.1.2. Mesh generation

In order to have a proper CFD simulation, it is necessary that calculations be made over a collection of discrete grid points. The arrangement of these discrete grid points throughout the flow field is simply called a grid, while the way such grid is determined is called grid generation. The determination of a proper grid for any CFD simulations is a serious matter: the type of chosen grid for a given problem can make or break the numerical solution.

Grid scaling

Grid scaling refers to changing the base grid size at specified times during a simulation. This technique is used to reduce runtimes by coarsening the grid during non-critical simulation times, while refining the grid whenever critical flow phenomena happens. Once the original base grid size has been assigned, the `grid_scale` parameter is used to change the base grid size according to the following formula

$$\text{scaled grid} = \frac{dx_{\text{base}}}{2^{\text{grid_scale}}} \quad (6.7)$$

Where `grid_scale` is the scaling factor (must be an integer) and scaled grid is the new base grid size. A `grid_scale` value of 0 will leave the base cells unchanged, a negative value will coarsen the base grid and a positive value will refine the base grid. It is possible to determine the grid sensitivity for any case, by running multiple simulations with different values of `grid_scale`.

Fixed embedding

Fixed embedding is a technique used to refine the grid size at specific locations in the domain where a finer resolution is needed for the accuracy of the solution. Fixed embedding allows the rest of the grid to remain coarse to minimize simulation time. It is also possible to define a specific time period for each fixed embedding, which can further reduce your computational time by refining the grid only for a portion of the simulation. For each fixed embedding, it is necessary to specify an embedding scale that indicates how CONVERGE will refine the grid in that location. The `embed_scale` parameter, which must be a positive integer, scales the base grid sizes (`dx_base`, `dy_base` and `dz_base`) according to the following formula:

$$dx_{\text{embed}} = \frac{dx_{\text{base}}}{2^{\text{embed_scale}}} \quad (6.8)$$

Adaptive Mesh Refinement (AMR)

Adaptive mesh refinement is used to automatically refine the grid based on fluctuating and moving conditions such as temperature or velocity. This option is useful for using a highly refined grid to accurately simulate complex phenomena such as flame propagation or high-velocity flow without unnecessarily slowing the simulation with a globally refined grid. A good algorithm will add high resolution (embedding) where the flow field is most under-resolved or where the sub-grid field is largest (where the gradient of a specified field variable is the highest). The AMR method is CONVERGE estimates the magnitude of the sub-grid field to determine where CONVERGE will add embedding.

For a scalar, the sub-grid field is defined as the difference between the actual field and the resolved field:

$$\phi' = \phi - \bar{\phi} \quad (6.9)$$

Where ϕ is the actual scalar field, $\bar{\phi}$ is the resolved scalar field and ϕ' is the sub-grid scalar field. The sub-grid for any scalar can be expressed as an infinite series given by:

$$\phi' = -\alpha_{[k]} \frac{\partial^2 \bar{\phi}}{\partial x_k \partial x_k} + \frac{1}{2!} \alpha_{[k]} \alpha_{[l]} \frac{\partial^4 \bar{\phi}}{\partial x_k \partial x_k \partial x_l \partial x_l} - \frac{1}{3!} \alpha_{[k]} \alpha_{[1]} \alpha_{[m]} \frac{\partial^6 \bar{\phi}}{\partial x_k \partial x_k \partial x_l \partial x_l \partial x_m \partial x_m} + \dots \quad (6.10)$$

Where $\alpha_{[k]}$ is $dx_k^2/24$ for a rectangular cell and the squared brackets indicates no summation.

6.2. Introduction to CFD TG-20 combustor model

When dealing with CFD 3D simulation, it is necessary to provide a CAD model of the Software in order to start any simulation. In this case the CAD model comes from a pre-existing model that was developed inside EthosEnergy company. Because of the high complexity in the real combustor design, it was necessary to introduce some simplification. In this case the software CONVERGE is able to manage this combustor model without giving any error message. It is important to mention the real TG-20 gas turbine is composed of eight different combustors arranged in a tuboannular way. Thanks to this configuration, it is possible to study and consider just one of the eight combustors assuming that all the combustors behave in the same way. As mentioned before, this is one of the benefits which come when a tuboannular configuration is chosen in the design of a gas turbine combustor. Figure 6.4 shows a view of the TG-20 combustor:

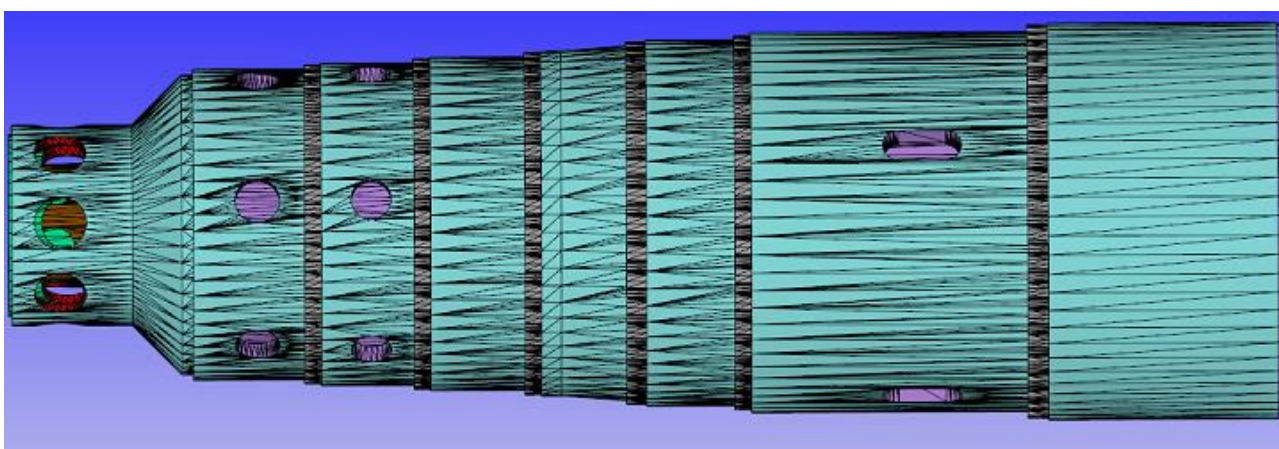


Figure 6.4 – Side view of TG-20 combustor model. It is possible to see the cold liner (outer one, in green) and the hot liner (inner one, in purple).

Figure 6.4 shows the combustor without the external casing. Indeed, because of the tuboannular configuration, the eight combustors are inserted inside a single case which collects the compressed air coming from the compressor. So, another simplification is here introduced and consists of considering a small case which surrounds the combustor. This solution allows to simulate the real geometry as close as possible. The TG-20 combustor model is characterized by the presence of two liners: the inner one, which

is called the hot liner and the outer liner which is called the cold liner. The liners function is to hold the combustion process in a well-defined space and to avoid that the burning mixture fall out of it. In order to fulfil this duty, the liners materials are capable to withstand very high temperatures and a cooling system is provided. The gap between the two liners is used for cooling purposes, indeed, a film of air pass through it. Figure 6.5 shows the cooling slots, which creates the gap between the two liners.

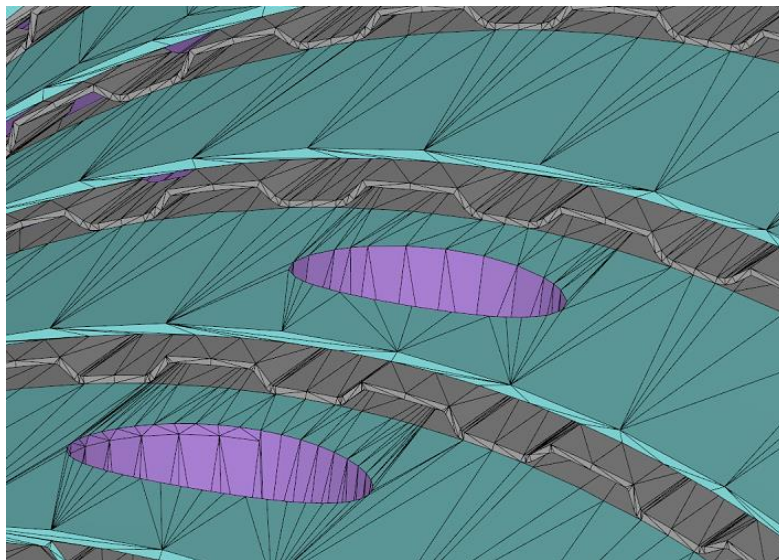


Figure 6.5 – Particular of cold liner. It is possible to notice the cooling slots (in grey) which allows the cooling air to enter in the gap between the two liners.

The combustor is 99.2 cm long and the maximum diameter is 33 cm. There are 7 rings of cooling slots, which form a trapezoidal section and allows a passage for the air creating an air film in the gap between the two liners. Three rows of holes for the primary, secondary and dilution zone are present. While the holes for primary and secondary zones are circular and composed of six holes for primary zone and six holes for secondary zone, in the dilution zone there are four air passages with a different shape (designed to maximize air flow). The air which enters the casing will recirculate and flows inside the holes according to holes diameter and internal pressure. Primary and secondary holes have the function to give a proper mix with the fuel, while the dilution holes have the function to lower the temperature avoiding any damage to the turbine first row of blade.

The fuel is provided in the combustor by the fuel injector, showed in Figure 6.6.

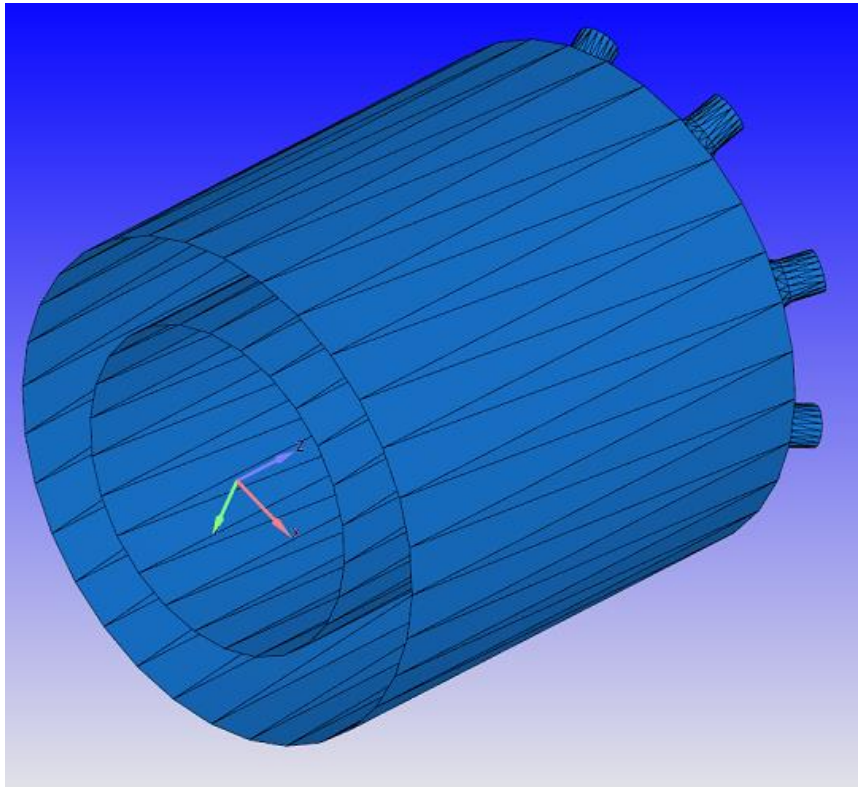


Figure 6.6 – TG-20 fuel injector

The TG-20 fuel injector is characterized by eight holes through which the natural gas (mainly composed of methane) flows inside the combustor primary region. The natural gas flowing from the fuel injector is being hit by the air coming from the air swirler in order to guarantee a proper mixing between air and fuel.

Figure 6.7 shows a crucial component for the TG-20 combustor, the air swirler. In the figure, in purple, it is possible to notice the 26 inclined blades that give the air the correct orientation. The function of this component is to create in the air flowing in the primary zone a proper recirculation shape. Indeed, in this region, air is required to have good mixing properties and, since the combustor is a diffusive flame combustor, the flame must be stable and capable of sustaining itself. In order to keep the flame continuously alive, hot and already burned gas is recirculated towards the fuel injector in a backward motion which is promoted by the air swirler and the primary holes. In this way the combustor can operate continuously and flame ignition is only required at the starting phase.

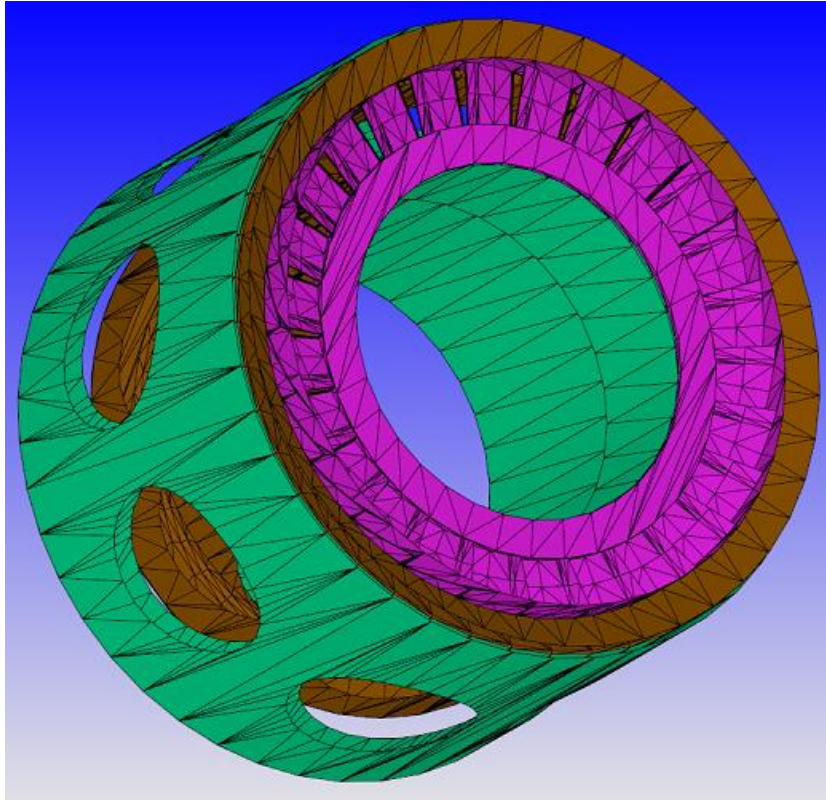


Figure 6.7 – TG-20 air swirler (in purple) together with other air passages components

6.3.Dry case

Two different dry case setups were simulated and the results are here proposed. The difference between these two cases lie on the different reaction mechanism: the GRI-mech and the CRECK mechanism. The former considers 53 species and 325 reactions while the latter considers 159 species and 2459 reactions. From CRECK mechanism is expected a higher level of precision than the GRI-mech. The two simulations settings come from experimental data given directly from EthosEnergy for the Duino plant and are here summarized in Table 6.8

	GRI-mech	CRECK mechanism
Air mass flow rate [kg/s]	17.46	17.46
Fuel mass flow rate [kg/s]	0.27	0.27
Base grid size [mm]	4x4x4	4x4x4
Minimum grid size [mm]	0.625 by AMR	0.625 by AMR
Solver	Steady-state PISO	Steady-state PISO MUSCL
Combustion model	FGM GRI-mech	FGM CRECK mech
Turbulence model	RNG k- ϵ with standard wall function, $C_{\epsilon 1}=1.5$	RNG k- ϵ with non-equilibrium wall function, $C_{\epsilon 1}=1.5$

Table 6.8 – Main parameters for the two TG-20 dry cases simulations

The second order scheme called MUSCL is used to improve the simulation accuracy and it is used only for the simulation with the CRECK mechanism.

A picture of the mesh size and distribution is showed in Figure 6.9. This mesh is used for both the two simulations.

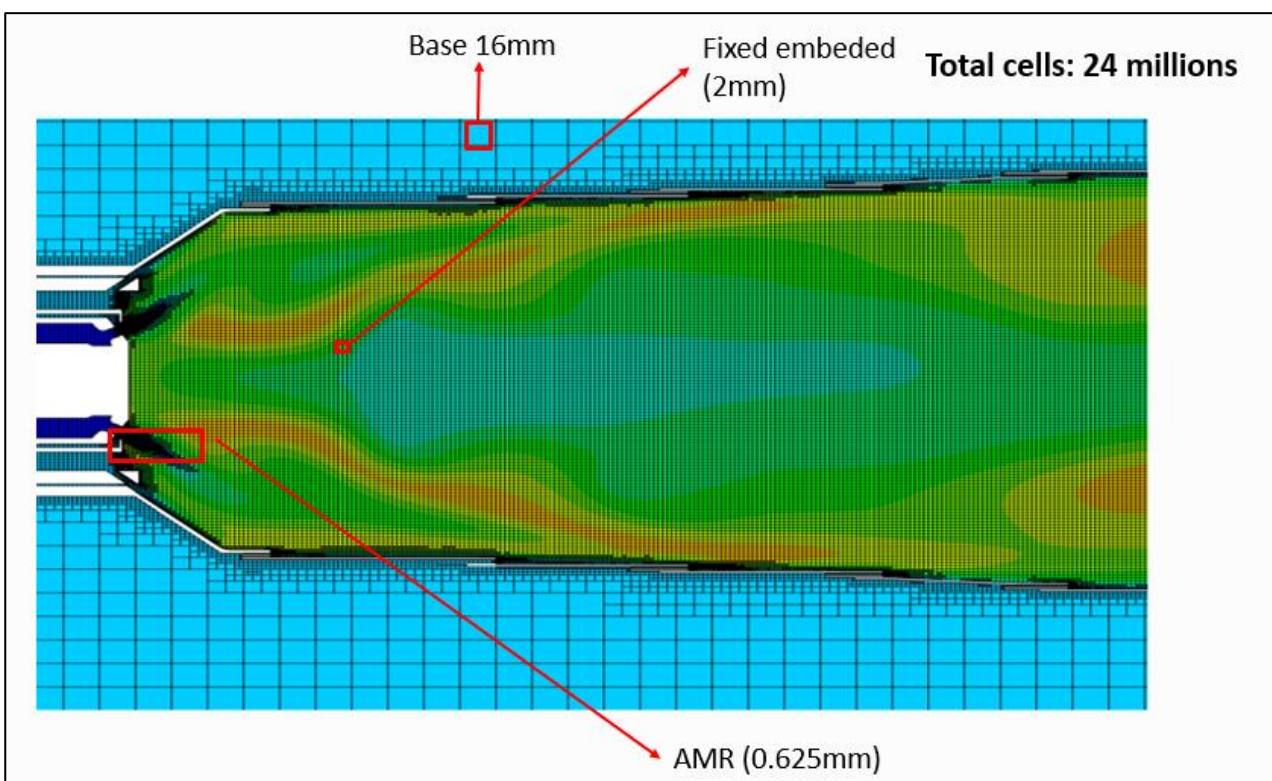


Figure 6.9 - TG-20 mesh size and distribution for dry cases

Figure 6.10 shows the mean temperature for the combustor and air casing for different cycles. Since the simulation is steady-state, only the temperature at very high number of cycles is of relevance. Indeed, at the beginning (for low number of cycle) the temperature is low because the combustion is not yet developed. Then the combustion happens but it is needed a certain amount of time for the temperature to settle at the steady-state value.

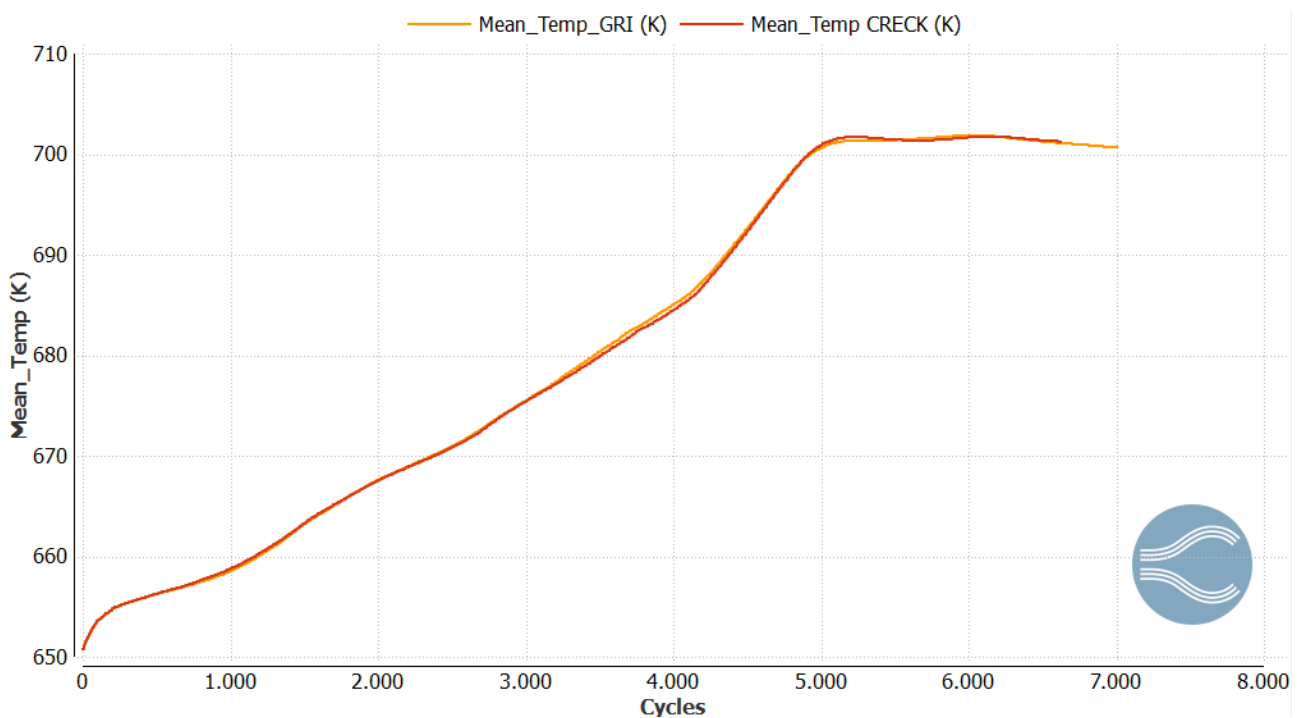


Figure 6.10 – Mean temperature between GRI-mech (yellow) and CRECK mechanism (red)

Figure 6.11 shows the temperature at turbine inlet, which corresponds to the temperature at the combustor outlet. It is possible to notice that only at simulation cycle number 4700 the temperature starts to rise, then there are some temperature oscillations which ends into the steady-state value for very high number of cycles.

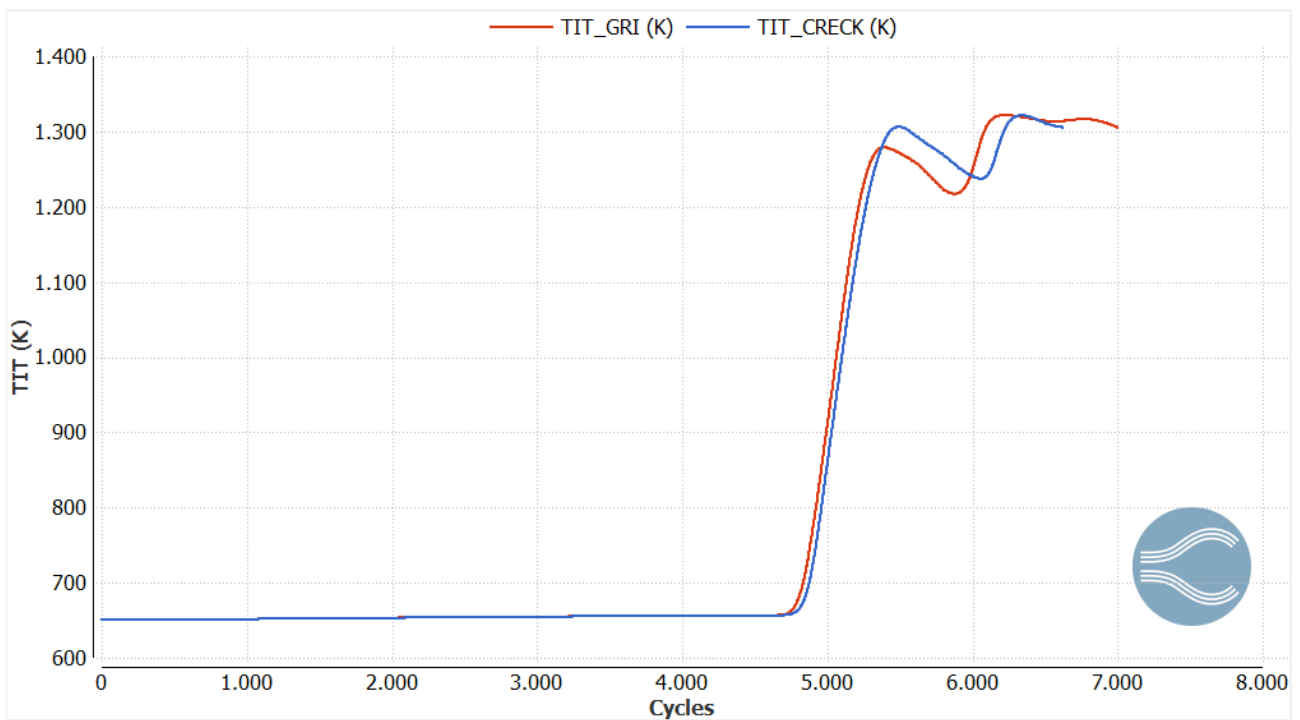


Figure 6.11 – Temperature at turbine inlet between GRI-mech (red) and CRECK mechanism (blue)

Figure 6.12 shows the turbulent kinetic energy between the two cases, while Figure 6.13 shows the turbulent dissipation source. It is very important to have high turbulent flows because this ensure good mixing properties.

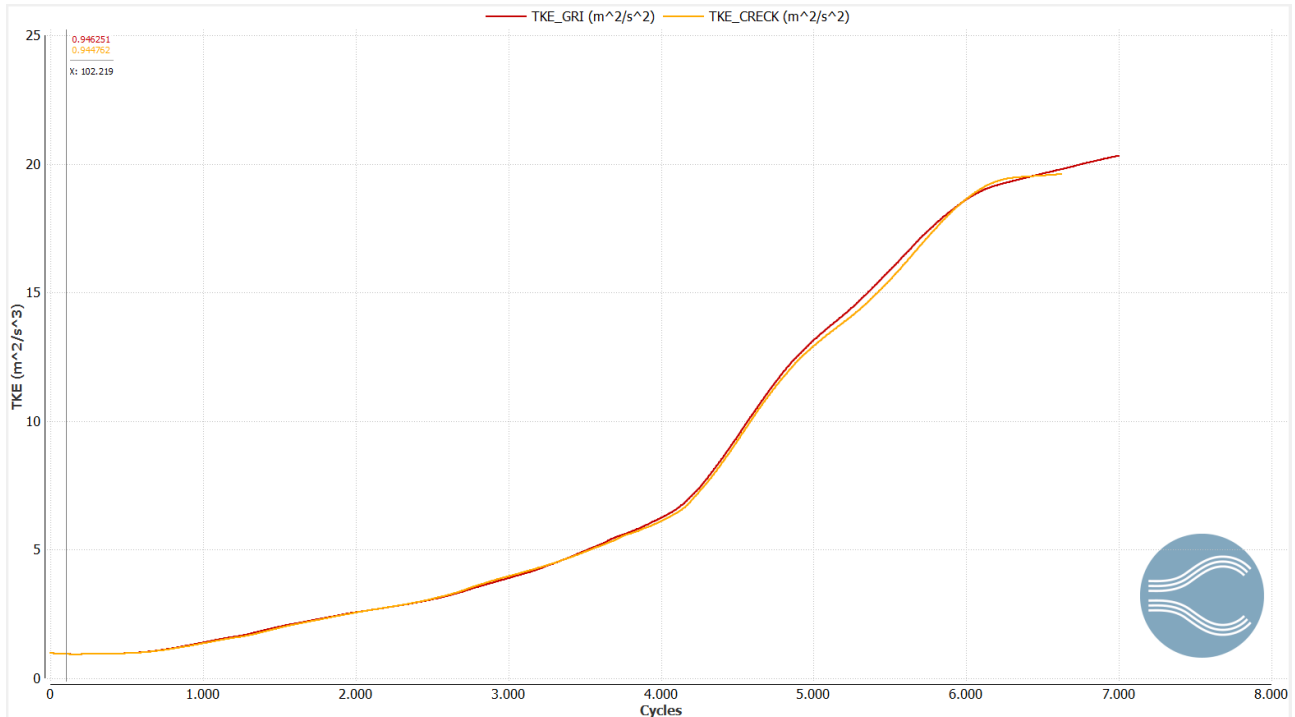


Figure 6.12 - Turbulent kinetic energy between GRI-mech (red) and CRECK mechanism (yellow)

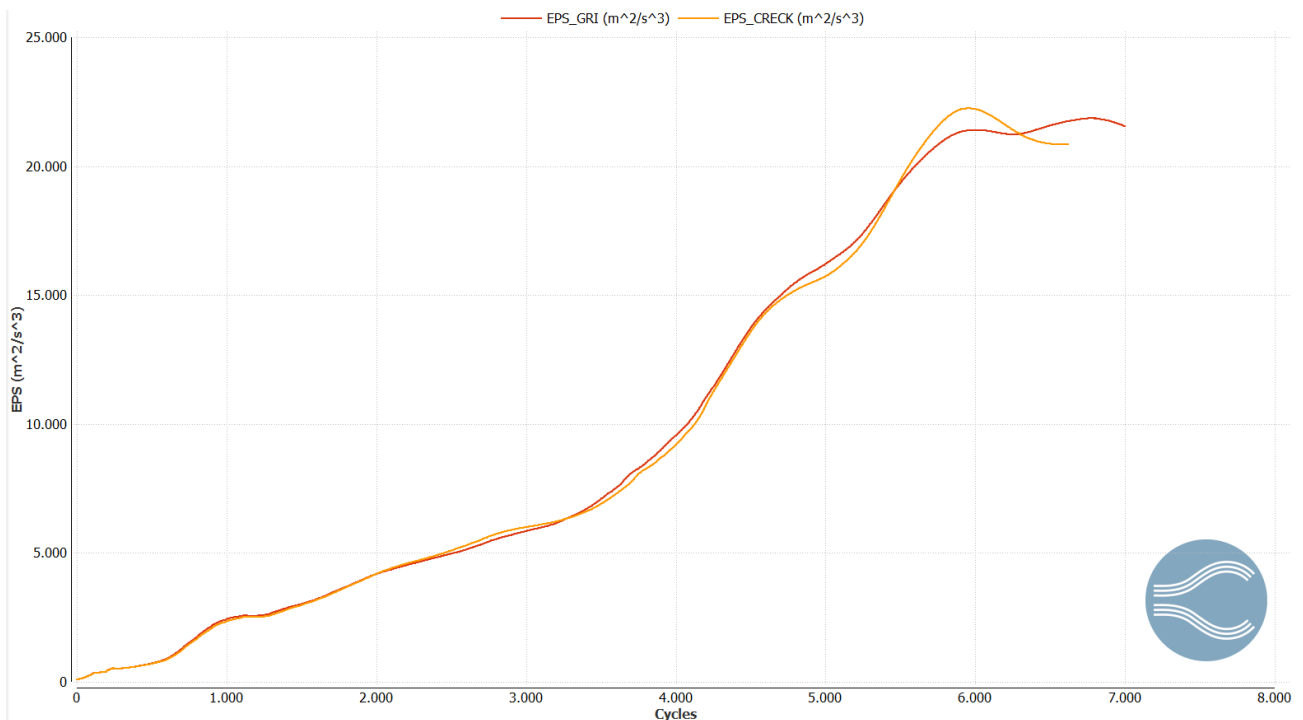


Figure 6.13 – Turbulent dissipation source between GRI-mech (red) and CRECK mechanism (yellow)

Figure 6.14 shows the comparison of NO_x rate between the two dry cases. This is the most important comparison here proposed because the thesis aims to evaluate the NO_x emission reduction between the dry case and the wet case (proposed later).

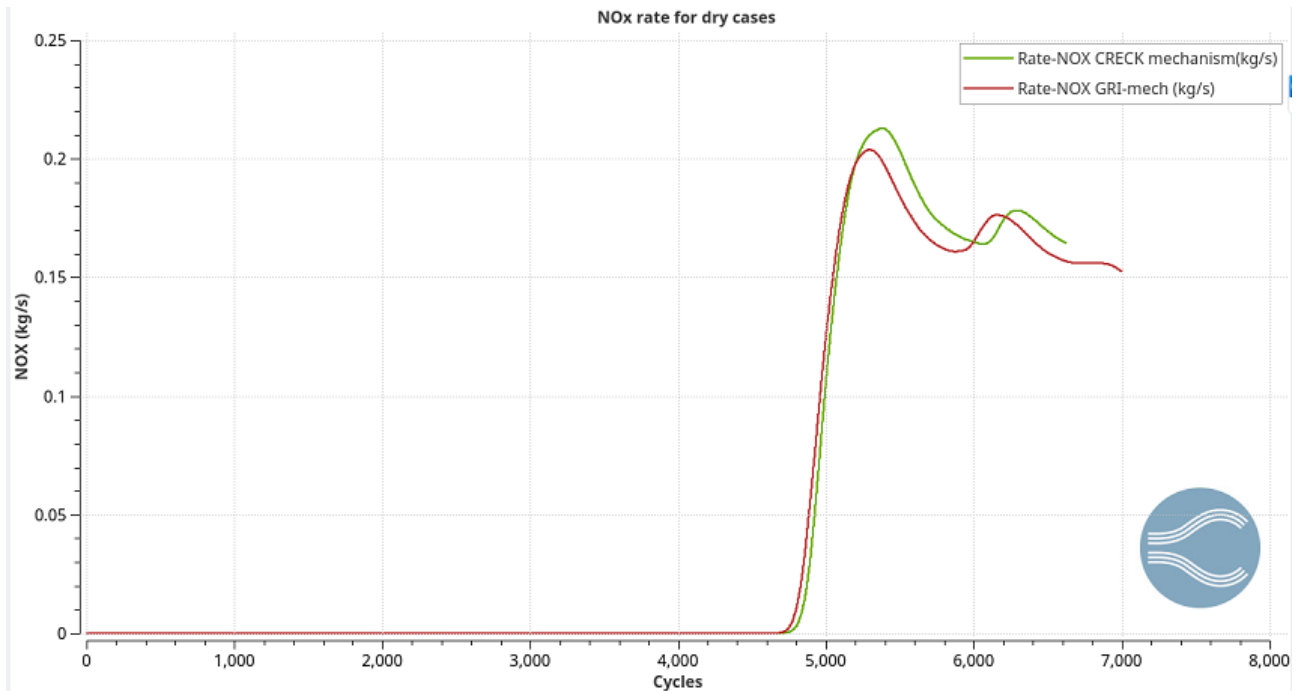


Figure 6.14 – NO_x rate comparison between GRI-mech (red) and CRECK mechanism (green)

From Figure 6.14 it is possible to state that for the CRECK mechanism the NO_x rate reaches the steady state at 0.17 kg/s, while for the GRI-mech the NO_x rate reaches the steady state at 0.15 kg/s.

Figure 6.15 and 6.15 show the temperature distribution in two different planes (the former in plane ZY while the latter in plane ZX). In the CRECK mechanism case it is possible to notice a more symmetric temperature distribution with respect to the GRI-mech case.

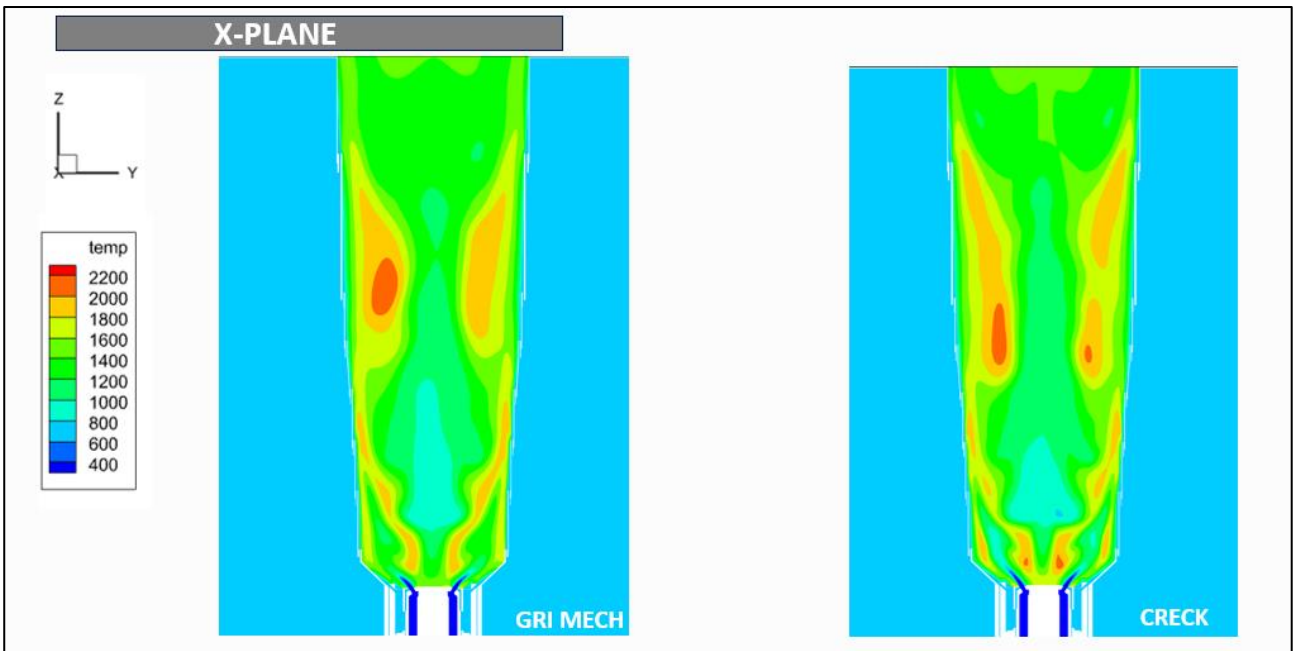


Figure 6.15 – Plane ZY temperature distribution: GRI-mech (left) and CRECK mechanism (right)

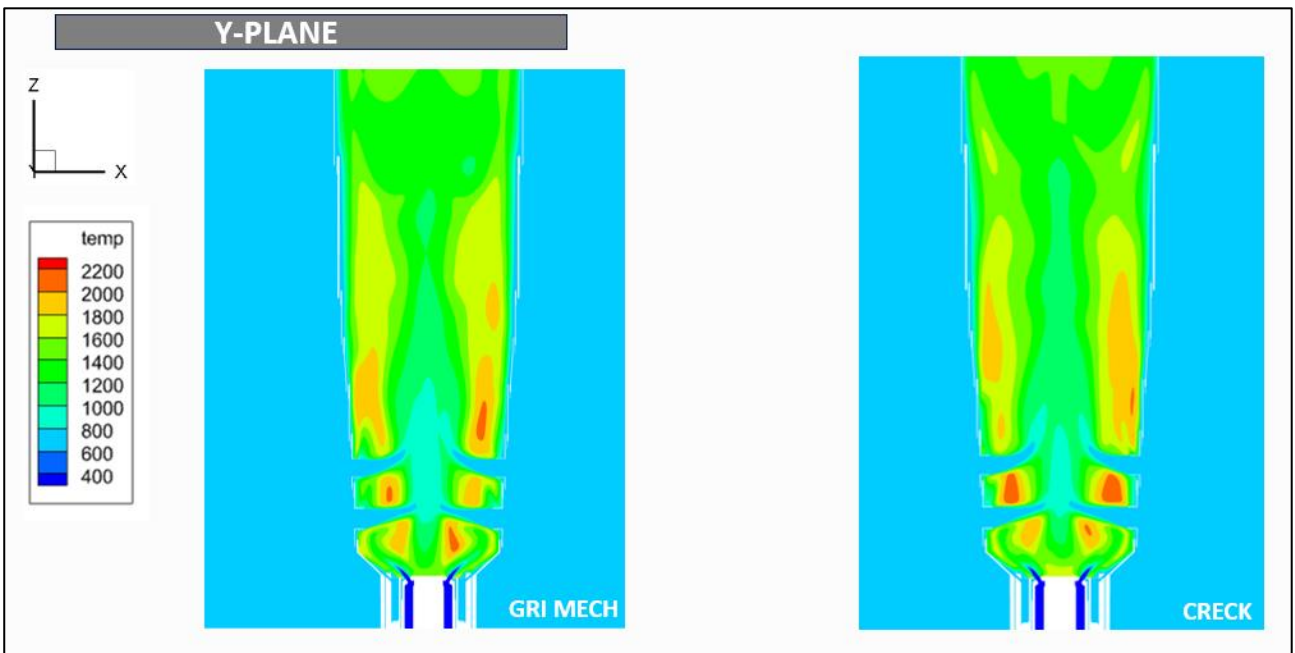


Figure 6.16 – Plane ZX temperature distribution: GRI-mech (left) and CRECK mechanism (right)

Figure 6.17 and Figure 6.18 show the velocity magnitude with vectors in the primary recirculation zone in plane ZY and in plane ZX respectively. It is of crucial importance

that in the primary zone there is a strong recirculation in order to enhance the mixing between air and methane in order to improve flame stability.

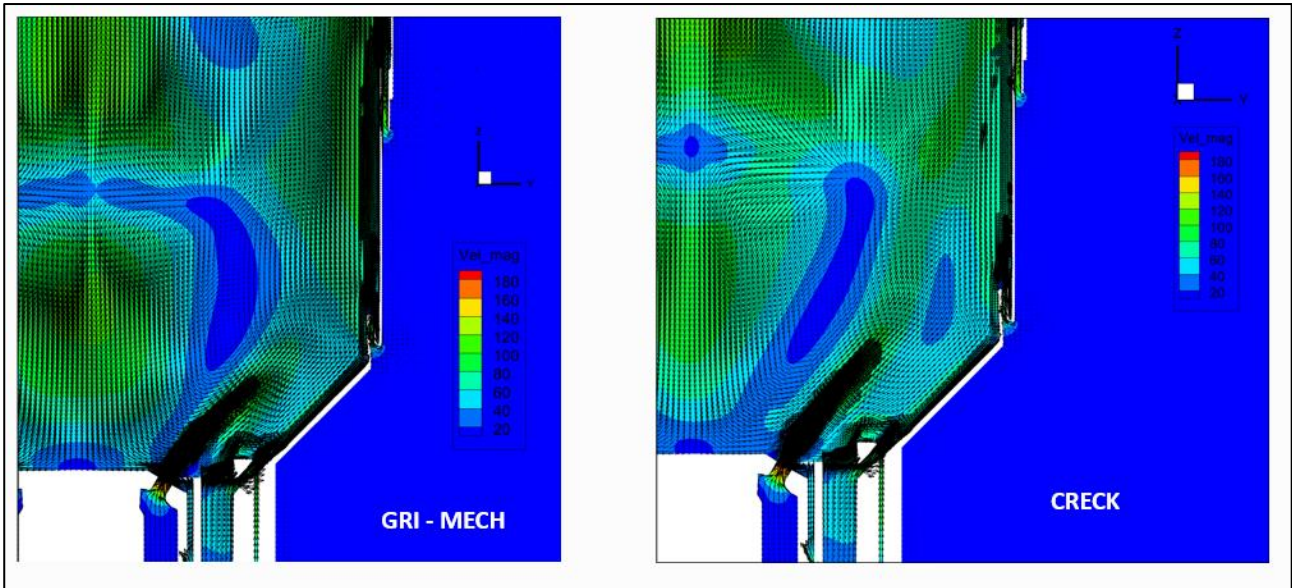


Figure 6.17 – Velocity magnitude in the primary recirculation zone in ZY plane: GRI-mech (left) and CRECK mechanism (right)

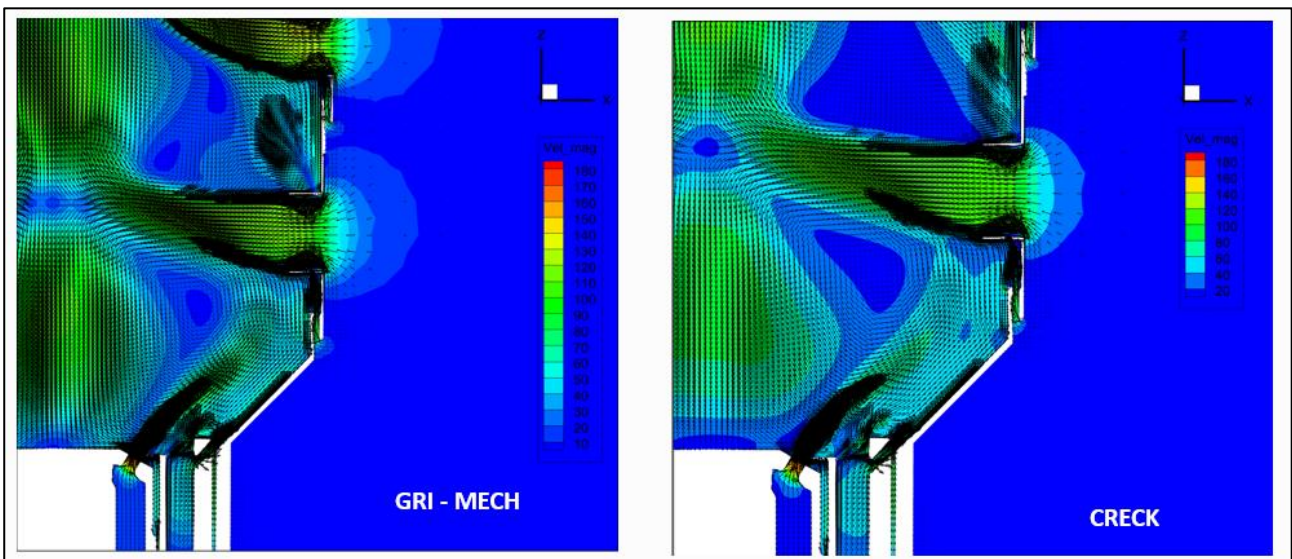


Figure 6.18 - Velocity magnitude in the primary recirculation zone in ZX plane: GRI-mech (left) and CRECK mechanism (right)

Figure 6.19 and Figure 6.20 show CO emission for GRI-mech case and for CRECK mechanism both in plane ZY and ZX. CO emissions are linked with the equivalence ratio, which is present in Figure 6.21 and 6.22. Since CO formation is due to

combustion inefficiencies, its formation is located in the same region where there is a higher equivalence ratio. The reason why CO formation is present mostly in the region close to the injector is because there is no plenty oxygen available for the complete oxidation of CO into CO₂. When CO moves towards the end of combustor, there is sufficient available oxygen for the complete reaction of CO into CO₂.

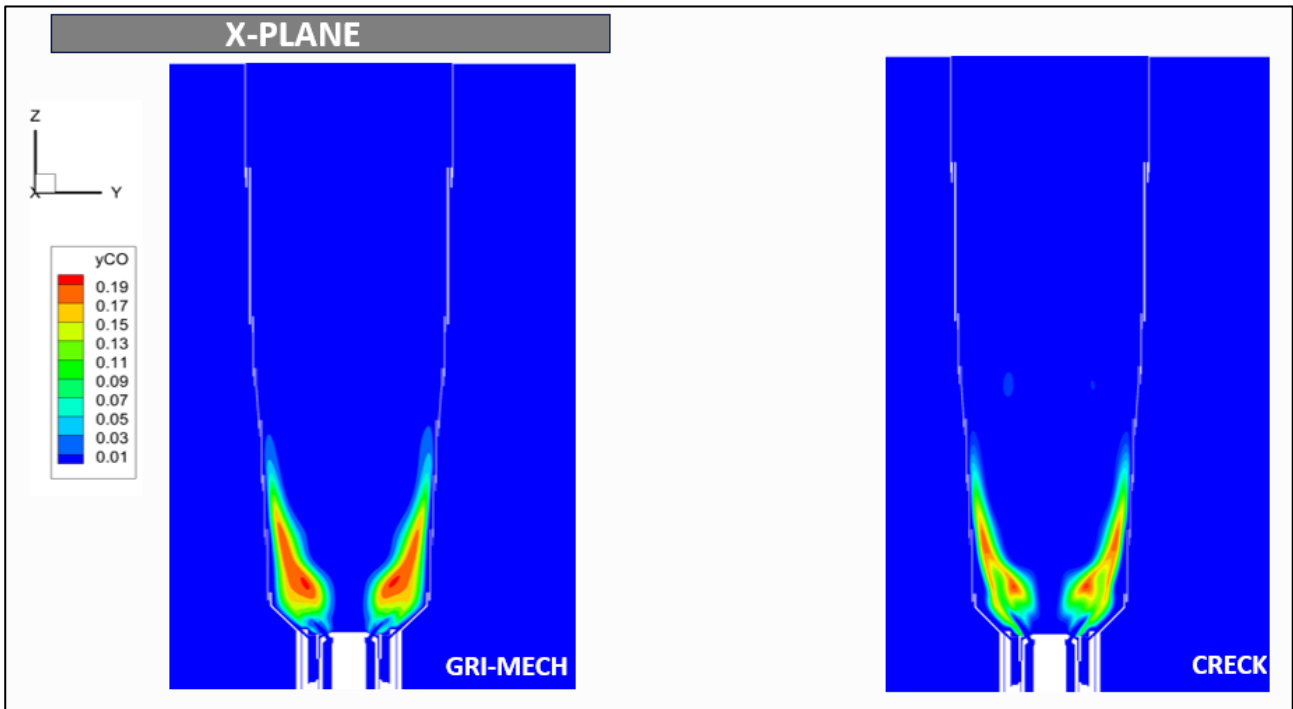


Figure 6.19 – CO emission in ZY plane between GRI-mech (left) and CRECK mechanism (right)

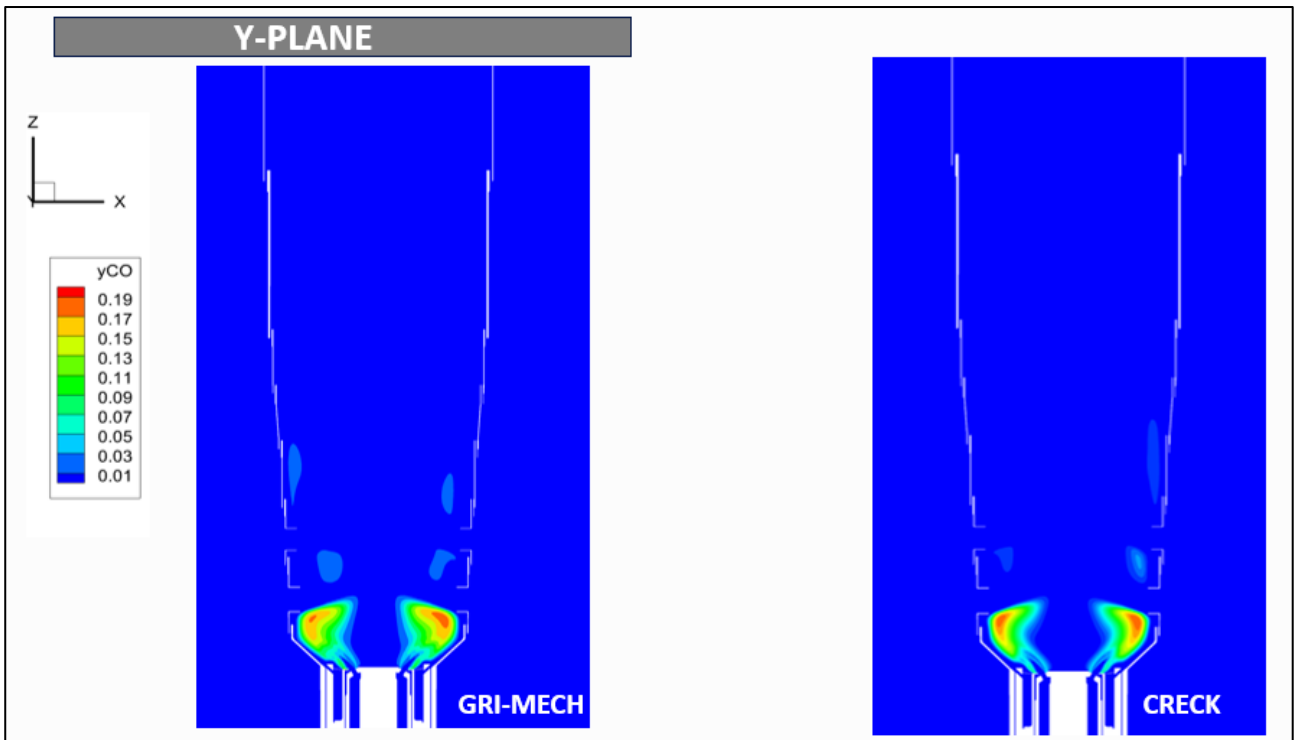


Figure 6.20 - CO emission in ZX plane between GRI-mech (left) and CRECK mechanism (right)

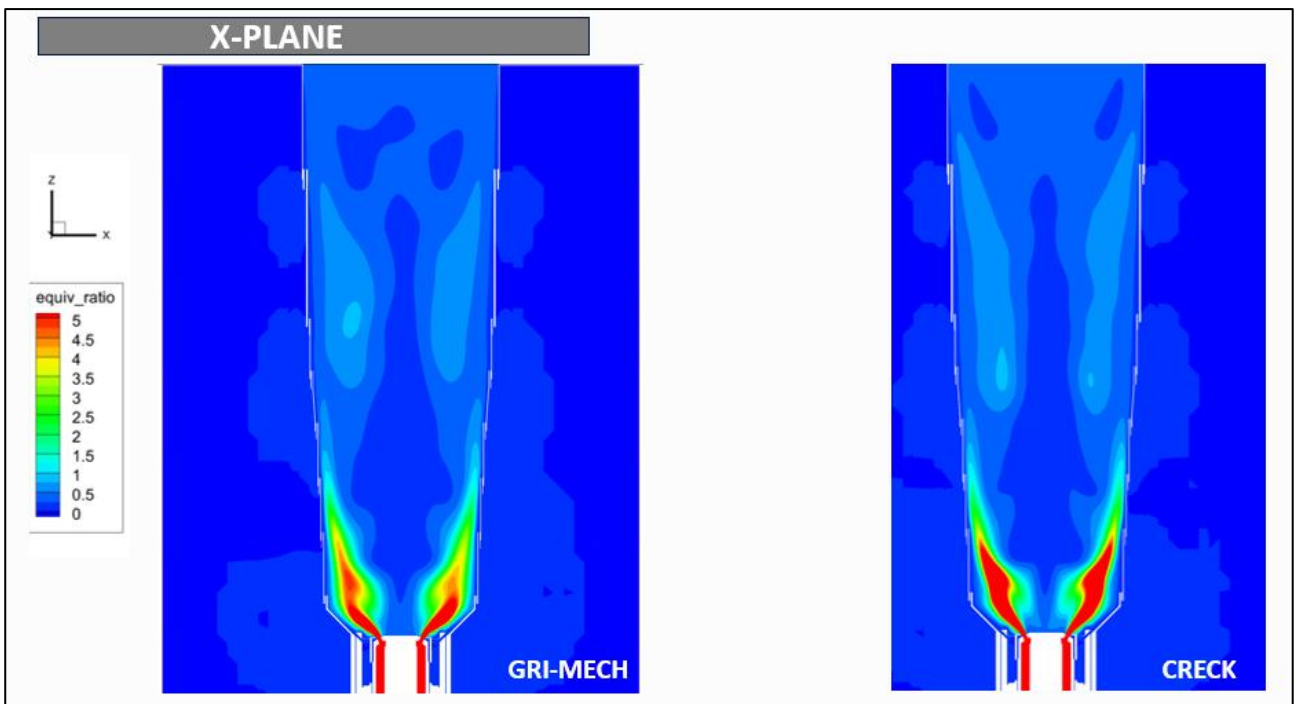


Figure 6.21 – Equivalence ratio in ZY plane between GRI-mech (left) and CRECK mechanism (right)

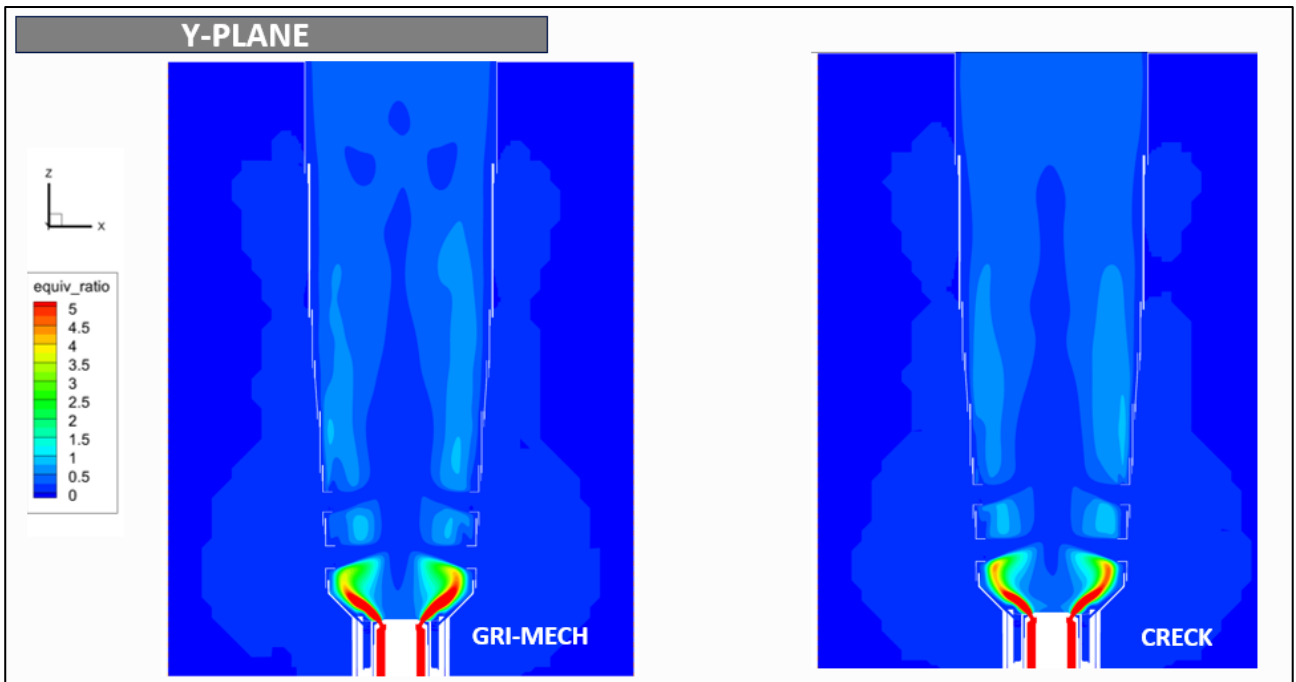


Figure 6.22 - Equivalence ratio in ZX plane between GRI-mech (left) and CRECK mechanism (right)

Figure 6.23 and Figure 6.24 shows the NO_x emission distribution for GRI-mech case and for CRECK mechanism case in both ZX plane and ZY plane. Since the major contribution for NO_x formation come from thermal mechanism, it is possible to notice that in the hotter regions there are the major NO_x formation.

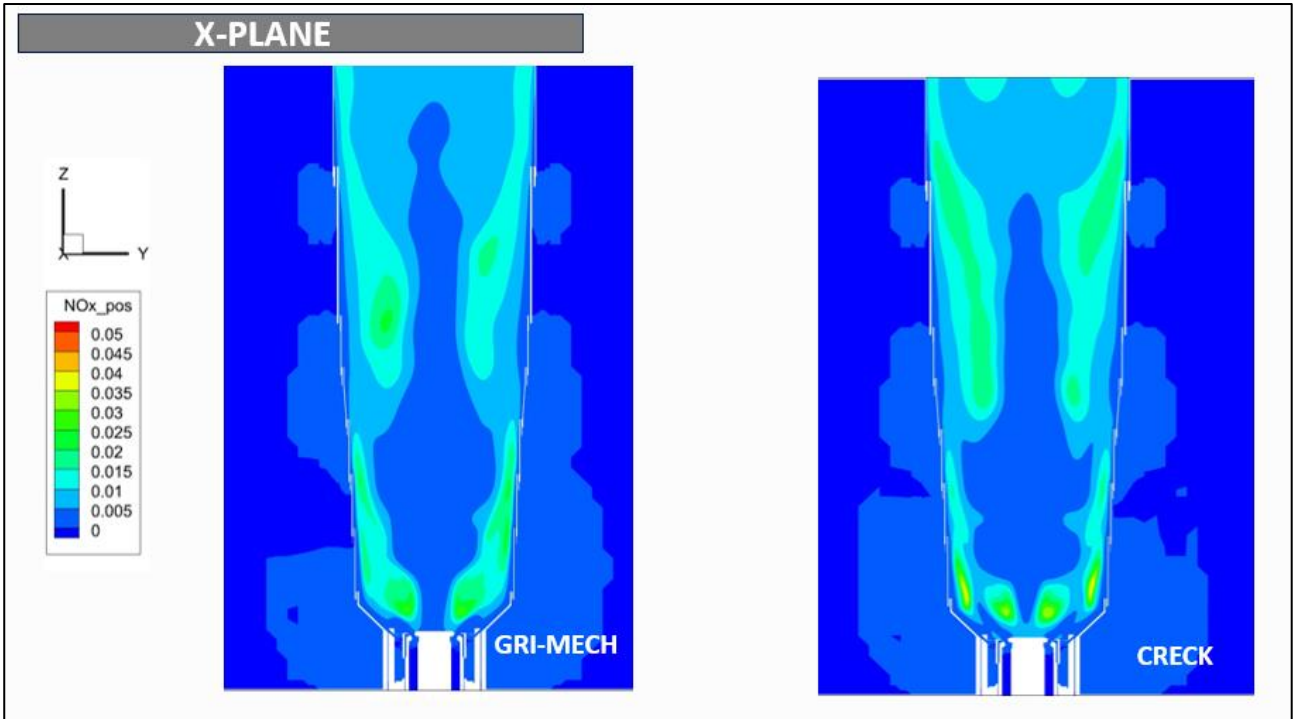


Figure 6.23 - NOx emission in ZY plane between GRI-mech (left) and CRECK mechanism (right)

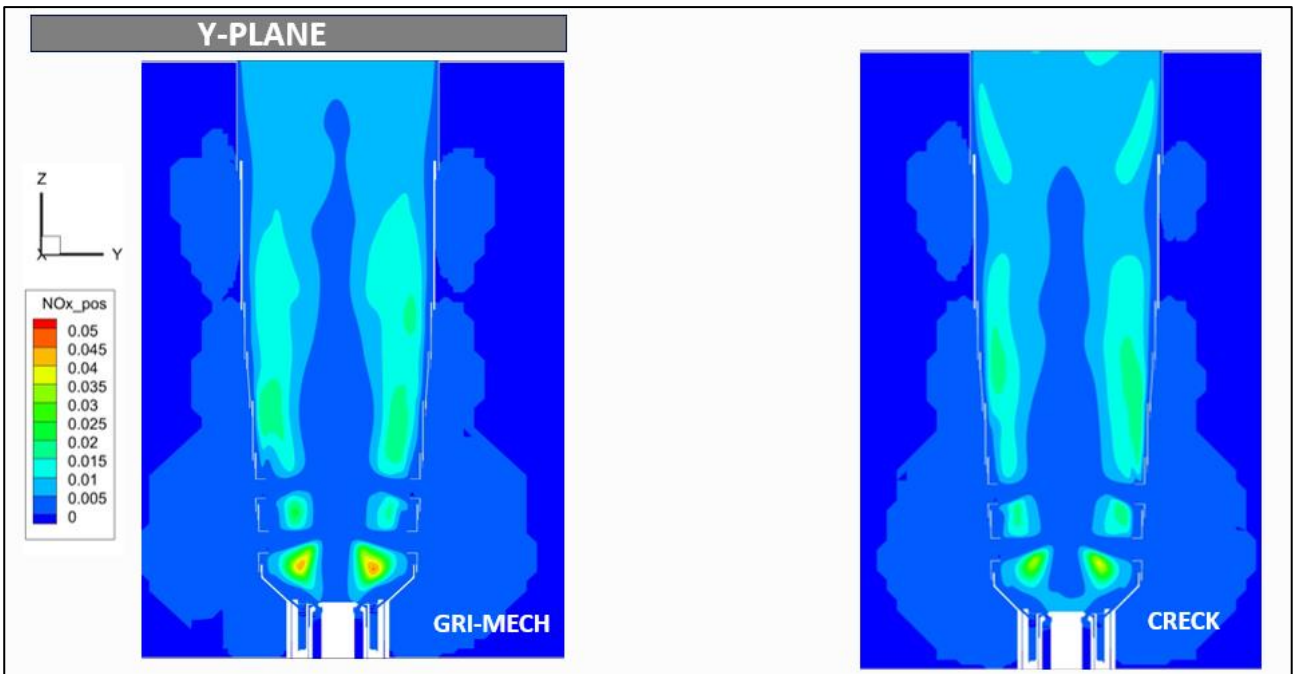


Figure 6.24 – NOx emission in ZX plane between GRI-mech (left) and CRECK mechanism (right)

6.4. Wet case

The objective of the wet case setup on TG-20 gas turbine combustor is to evaluate the effect of water injection into the NO_x emission rate reduction. In order to consider water injection, it is possible to apply a Volume of Fluid (VOF) approach. Since in the TG-20 gas turbine combustor the water is first mixed together with methane and then injected together in the combustor, the VOF should be applied to the whole injector geometry. This cause a simulation which is quite computationally expensive. Moreover, no detailed information is given on the water injection parameters and there is a lack of experimental data which could validate the computed results. For these reasons, a simplified approach is chosen in order to describe the water injection and evaporation in a simpler way but still preserving the model accuracy. This approach considers each injector as a pipe and the water injection as a sink. For this reason, the simplified model is called “sink model”. The first issue to solve is to decide the shape of the sink, because this has to replicate as close as possible the shape the water spray assume when water is injected in the real gas turbine. From Figure 6.25 it is possible to notice that the gas which pass through the injector has a velocity which is greater than 10 m/s.

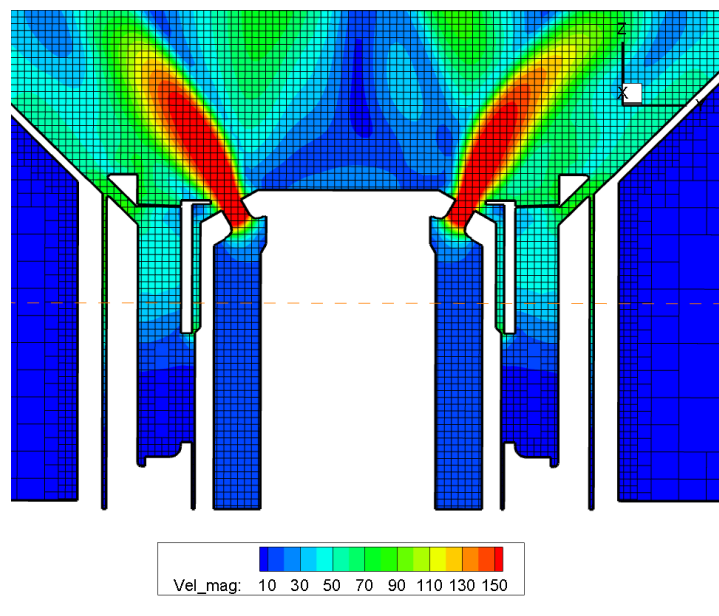


Figure 6.25 – Gas velocity in TG-20 injector (dry case)

This indicates that the flow regime will assume an annular shape, where the liquid phase is pushed towards the injector wall while the gas flows at the pipe centre. This kind of behaviour can be found in literature [31]. This study examines the different flow regimes when a liquid-gas two-phase flows inside a pipe with different velocities. Figure 6.26 shows different flow pattern that are found when two-phase liquid-gas flows in a horizontal duct depending on its velocity

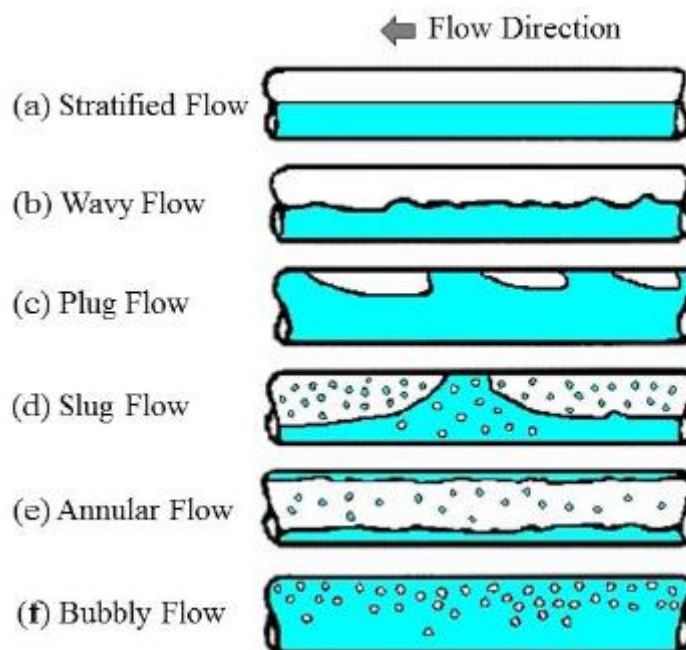


Figure 6.26 - Two-phase flow patterns in a horizontal pipe.

The different possible patterns are ruled by the fluid velocity. Since in the TG-20 gas turbine injector the speed is higher than 10 m/s, from Figure 6.27 it is possible to see that the fluid pattern is the annular flow

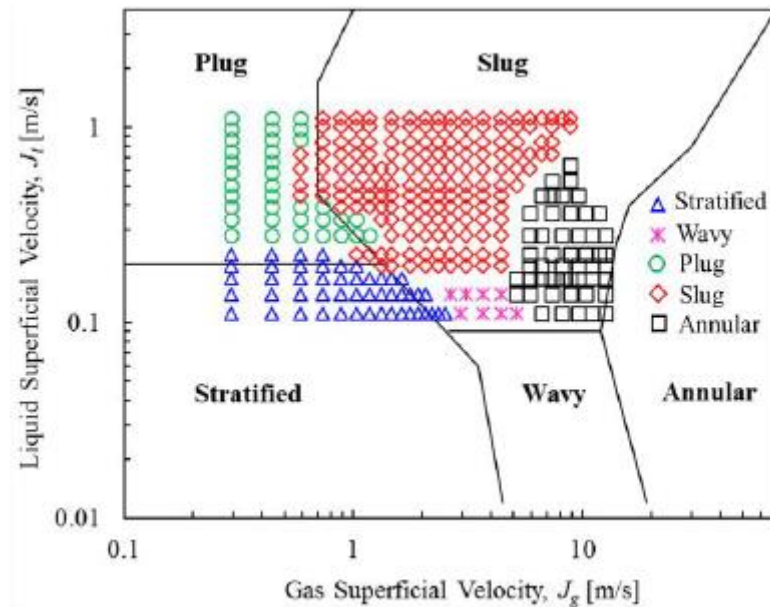


Figure 6.27 – Different possible flow pattern depending on gas superficial velocity

From the previous considerations, it comes out that the water is injected and vaporized in a hollow-conical region. Since the water is injected in its liquid phase (initial temperature is about 300 K for both fuel and water), the water droplets are injected from a circular crown section of the injector hole. When the water is injected, it suddenly evaporates because of the high steady state temperature, so it can mix with the fuel and the air entering the primary holes. Because of water evaporation, a uniform temperature will result and it will be lower with respect to the wet case setup. In this way the energy equation is modified in order to consider the heat subtraction due to water evaporation. Indeed, it is possible to state that

$$\text{Rate of increase of energy of fluid particle} = \text{Net rate of heat added to fluid particle} + \text{Net rate of work done on fluid particle} - S_{\text{evaporation}}$$

Where the work done on fluid particle is made by surface forces while the heat added to fluid particle is the one coming from energy flux due to conduction. $S_{evaporation}$ is the heat subtracted by the water droplet evaporation. The energy equation is modified accordingly:

$$\frac{\partial(\rho e)}{\partial t} = -\nabla \cdot ((\rho e)\mathbf{u}) - \nabla \cdot \mathbf{q} - \nabla \cdot (p\mathbf{u}) - \nabla \cdot (\boldsymbol{\tau} \cdot \mathbf{u}) + \rho \mathbf{g} \cdot \mathbf{u} - S_{evap}. \quad (6.11)$$

The simplified sink model assumes that all the water that enters the TG-20 combustor is in vapour form at the ambient temperature and a pressure equal to the one present in the combustor. The water is mixed with the fuel before the fuel injector. Eight cone shape heat sinks are positioned just downstream of the eight injector holes in order to subtract the same amount of heat that water evaporation would have been extracted. Figure 6.28 shows the eight cone sinks which are positioned right downstream of the eight pipes of the injector

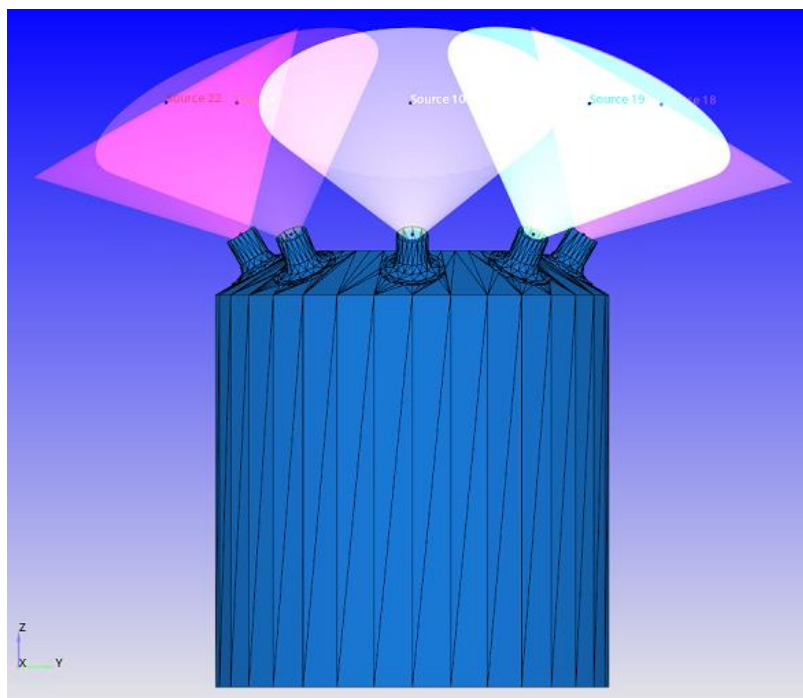


Figure 6.28 – Side view of TG-20 gas turbine injector with the heat sink cone shape

The amount of heat to be subtracted depends on the particular pressure and temperature that water possesses when injected into the combustor. It is possible to establish the enthalpy of vaporization directly from Mollier diagram for water steam. Since water is injected at the pressure of 11.4 bar (the same pressure present inside the combustor) and at the temperature of 300 K, it is necessary to:

- pre-heat water from 300 K to the saturation temperature at 11.4 bar (which is 458.85 K). This gives an enthalpy contribution of $h_L = 112.49$ kJ/kg
- Evaporate at constant pressure and temperature from liquid saturation line (lsl) to the vapour saturation line (vsl). This gives a contribution of $h_N = 2782.53$ kJ/kg

The heat of vaporization that water subtracts from the hot gas stream inside the combustor is:

$$H_{\text{vap}} = h_N - h_L = 2670.04 \frac{\text{kJ}}{\text{kg}} \quad (6.12)$$

It is necessary to multiply the enthalpy of vaporization H_{vap} to water mass flow rate in order to obtain a thermal power which is the one the sink model has to subtract. CONVERGE software gives the possibility to insert a heat source which can be negative in order to simulate the heat sink. In the TG-20 gas turbine there are eight combustors and each combustor has a fuel injector with eight holes. Since in the sink model there are eight sink cones downstream from each of the eight pipes of the fuel injector, it is necessary to divide by 64 the thermal power. The thermal power to be subtracted from each sink is obtained multiplying the total water mass flow rate (0.7 kg/s coming from the Duino trial number 2) to the enthalpy of vaporization ($H_{\text{vap}} = 2670.04$ kJ/kg):

$$\dot{Q}_{\text{vap}} = \frac{\dot{m}_{\text{water}} * H_{\text{vap}}}{64} = \frac{0.7 * 2670.04 * 1000}{64} = 29203 \frac{\text{J}}{\text{s}} \quad (6.13)$$

Figure 6.29 shows the CONVERGE settings window where it is possible to set the sink value for each of the eight sinks. Its value must be negative because this thermal power has to be subtracted from the hot gas stream. Source 1 is the one responsible for flame ignition, while the others are the one which extracts the heat of vaporization for the sink model. All of them have the same amount of thermal power.

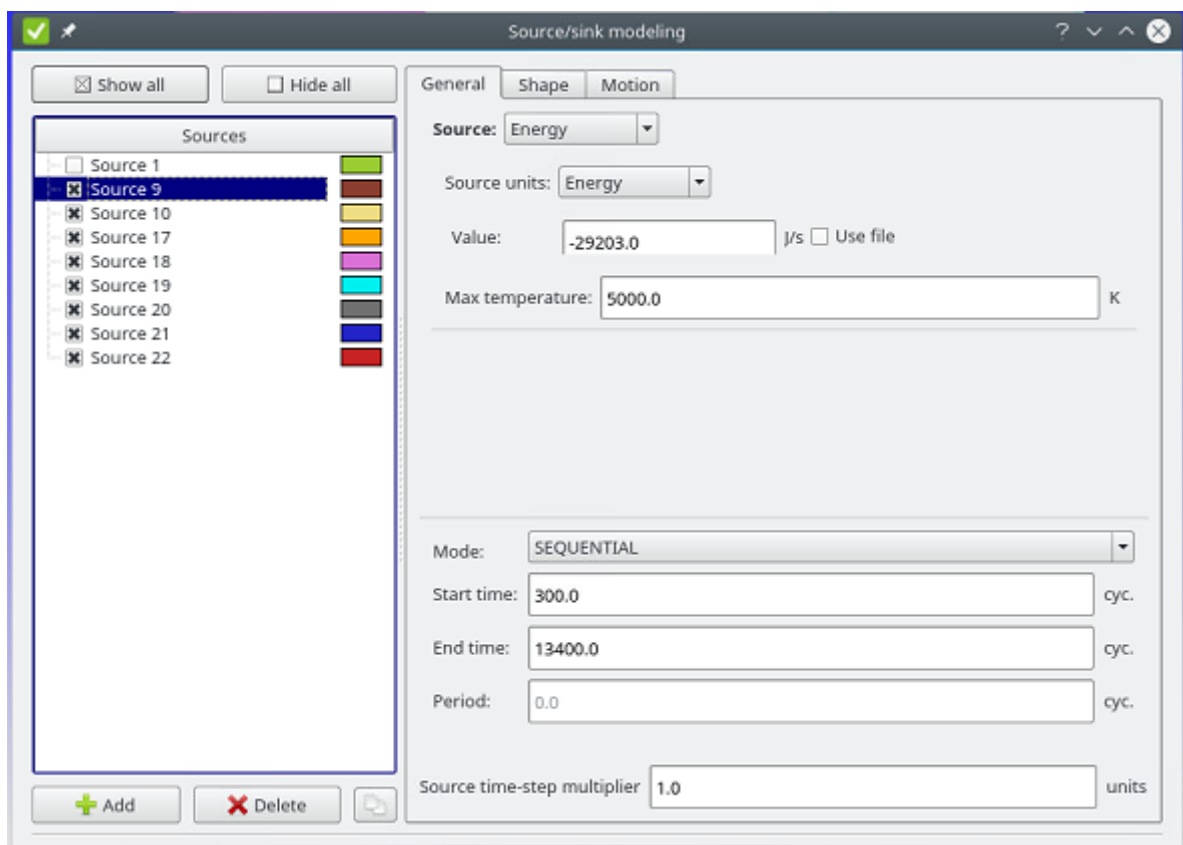


Figure 6.29 – CONVERGE settings window for Source/sink modelling

Table 6.30 collects the main parameters for the TG-20 wet case. The amount of water is the one coming from Duino dataset trial number two and it has been divided into

eight because the simulation considers only one of the eight combustors of the TG-20 gas turbine.

	Wet case
Air mass flow rate [kg/s]	17.46
Water mass flow rate [kg/s]	0.0875
Fuel mass flow rate [kg/s]	0.27
Base grid size [mm]	4x4x4
Minimum grid size [mm]	0.625 by AMR
Solver	Steady-state PISO
Combustion model	FGM GRI-mech
Turbulence model	RNG k- ϵ with standard wall function, $C_{\epsilon 1}=1.5$

Table 6.30 - Main parameters for the TG-20 wet case simulation

The same mesh size and distribution used for dry case is used also for the wet case. It is here showed again, in Figure 6.31

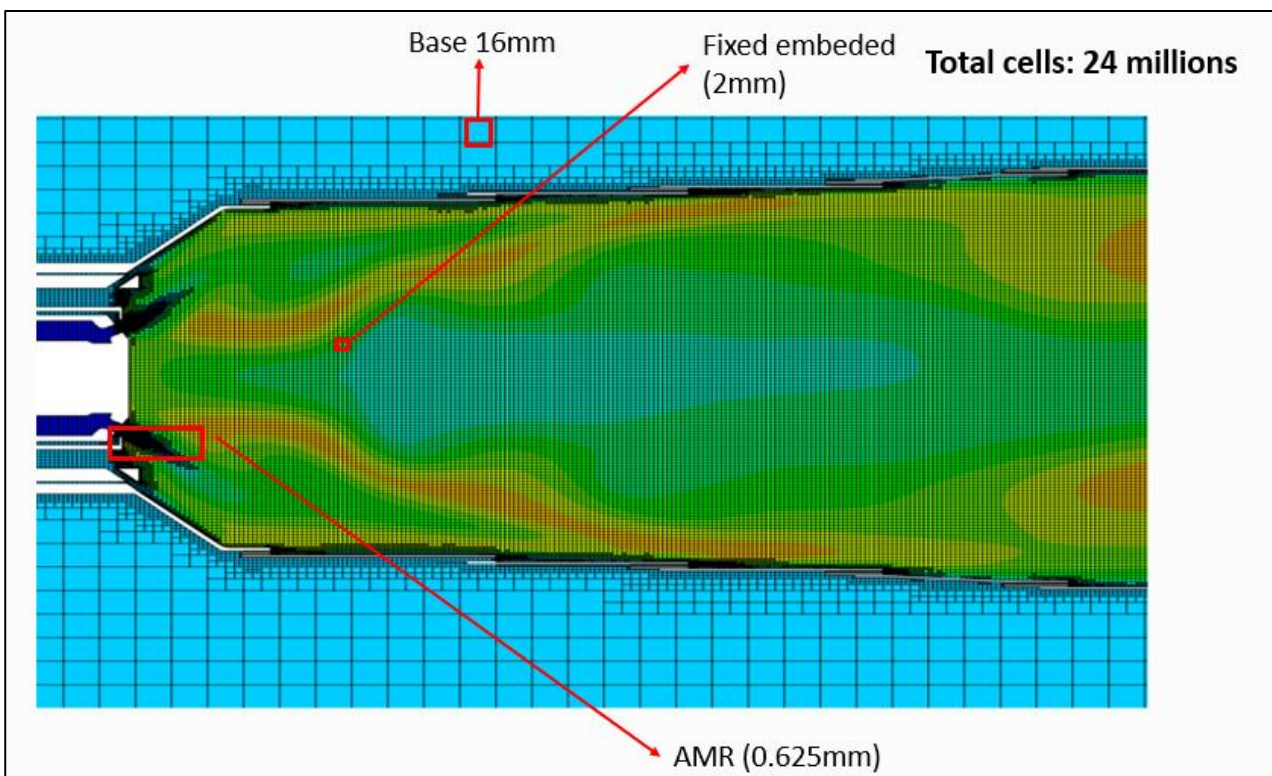


Figure 6.31 - TG-20 mesh size and distribution for wet case

Figure 6.32 shows the mean temperature for the entire wet model. It possible to notice that the steady state value is reached at about cycle number 4000. There are no major differences I with respect to the same chart obtained for the dry cases.

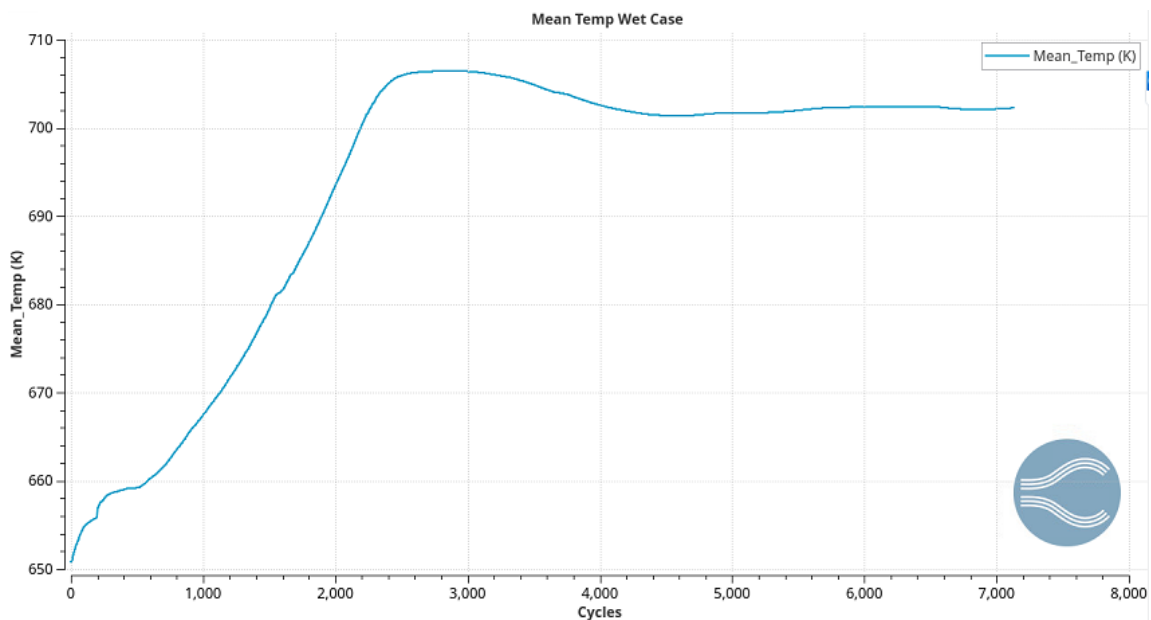


Figure 6.32 – Mean temperature for the wet case

Figure 6.33 shows the turbine inlet temperature, which is the one present at combustor exit section. It is possible to notice that there are no major differences with respect to the two dry cases.

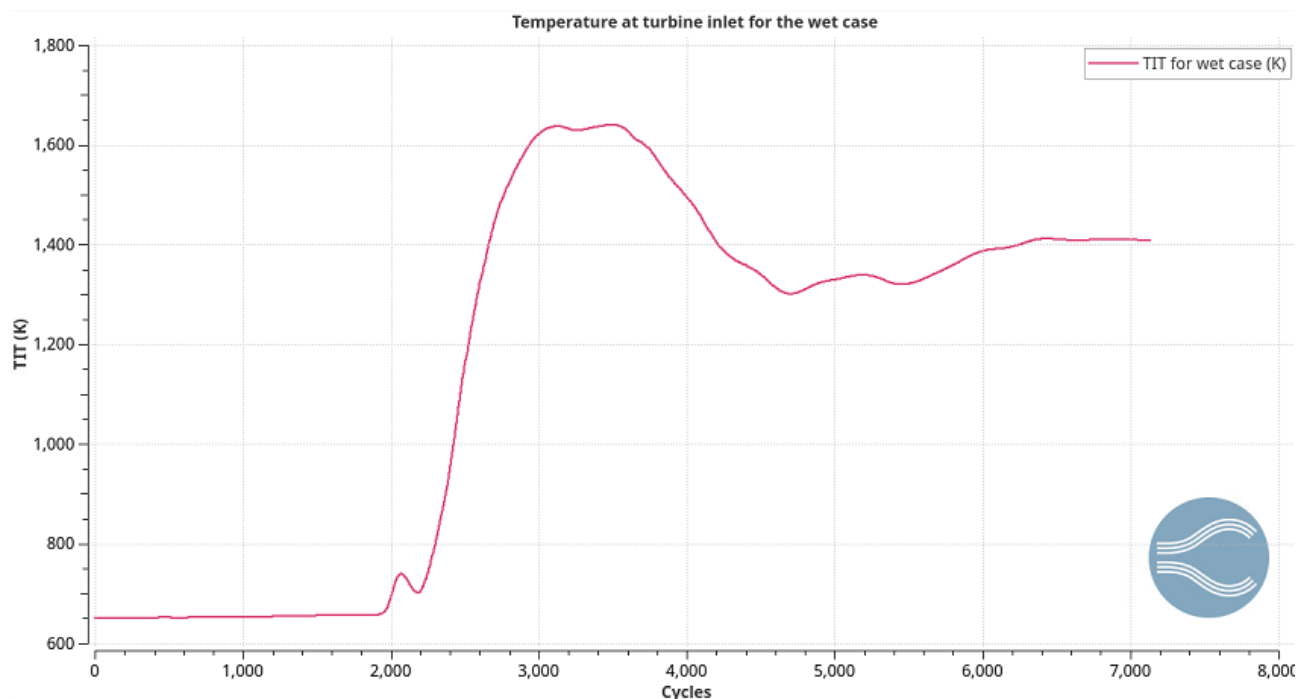


Figure 6.33 – Turbine inlet temperature for the wet case

Figure 6.34 and 6.35 propose the same quantities used for the dry cases to describe the turbulence inside the combustor.

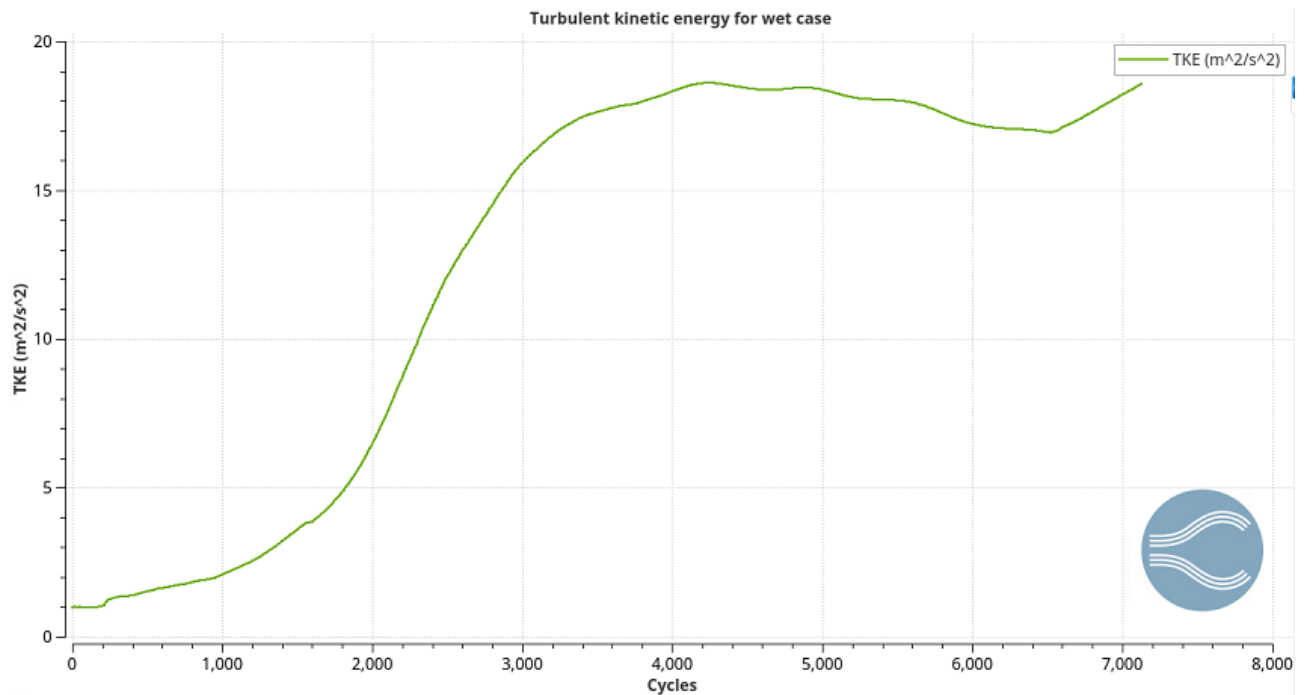


Figure 6.34 – Turbulent kinetic energy for wet case

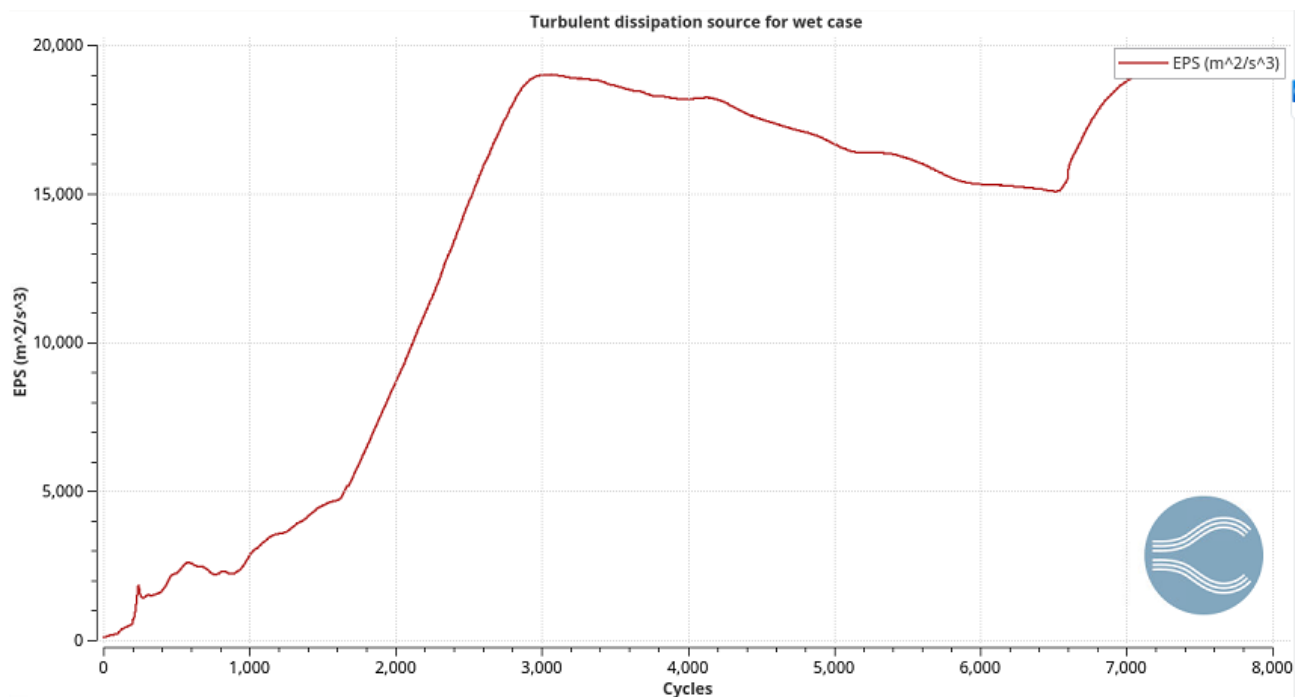


Figure 6.35 – Turbulence dissipation source for wet case

From Figure 6.36 it is possible to notice that the simulation reaches the steady state for the NOx rate at about cycle number 7000 at a value of 0.15 kg/s.

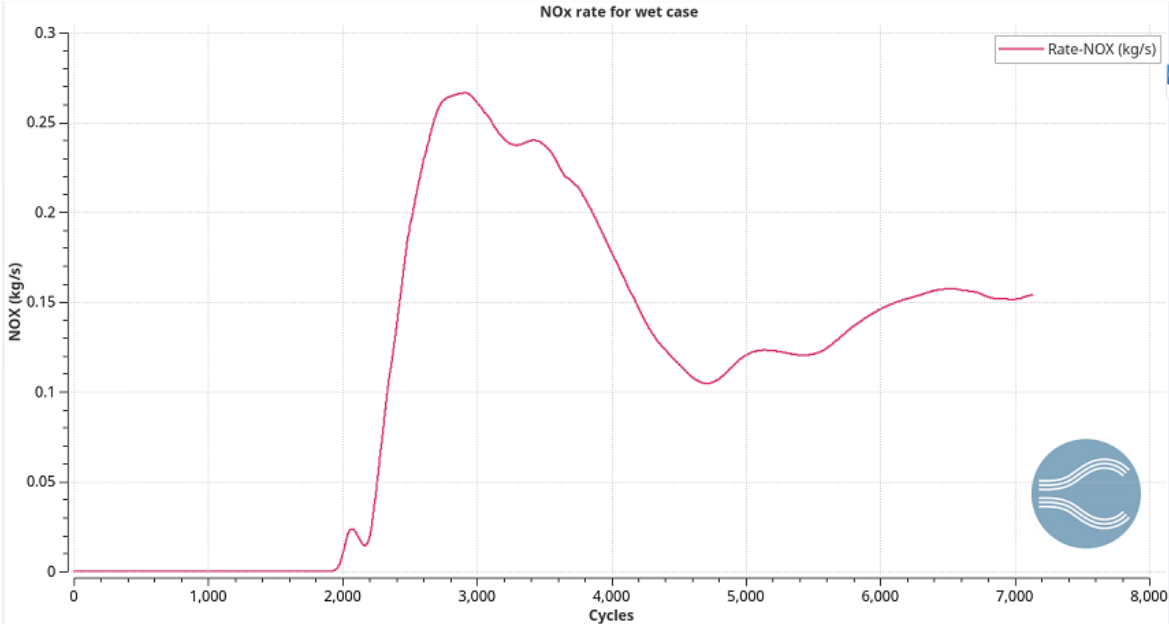


Figure 6.36 – NOx emission rate for wet case

Figure 6.37 show the temperature distribution comparison between plane ZY and ZX for the wet case. It is possible to notice a temperature reduction in the area downstream from the fuel injector in correspondence of the presence of the sink model cones

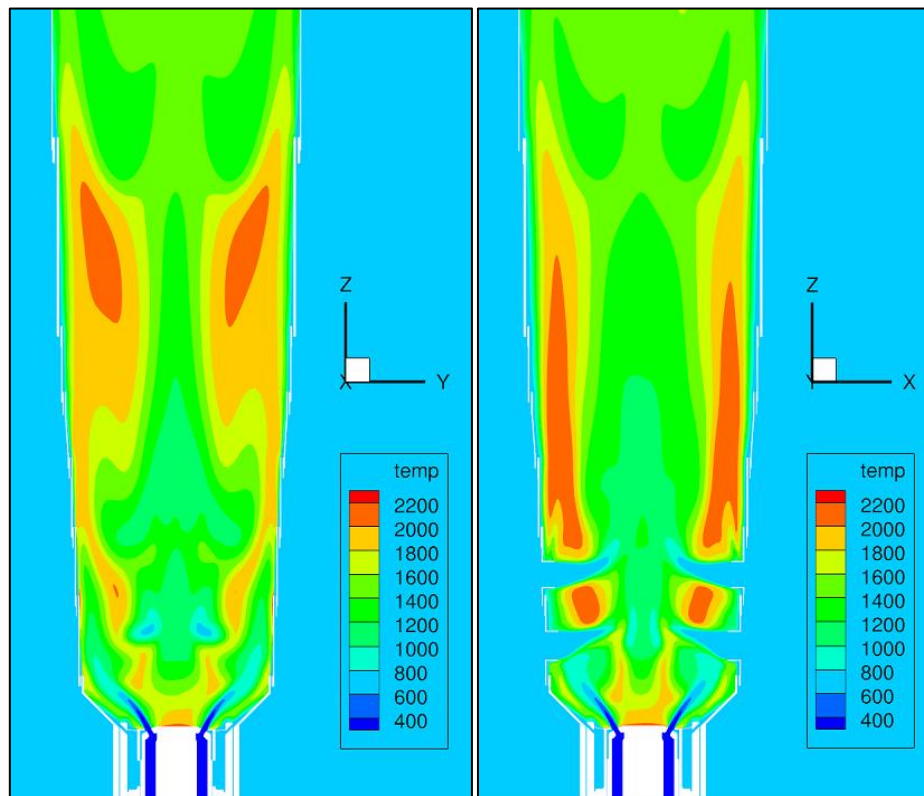


Figure 6.37 – Wet case temperature distribution plane ZY (left) and plane ZX (right)

Figure 6.38 and Figure 6.39 show the velocity magnitude for the wet case in the primary recirculation zone. The sink modelling allows to keep the same turbulence and recirculation pattern of the dry cases.

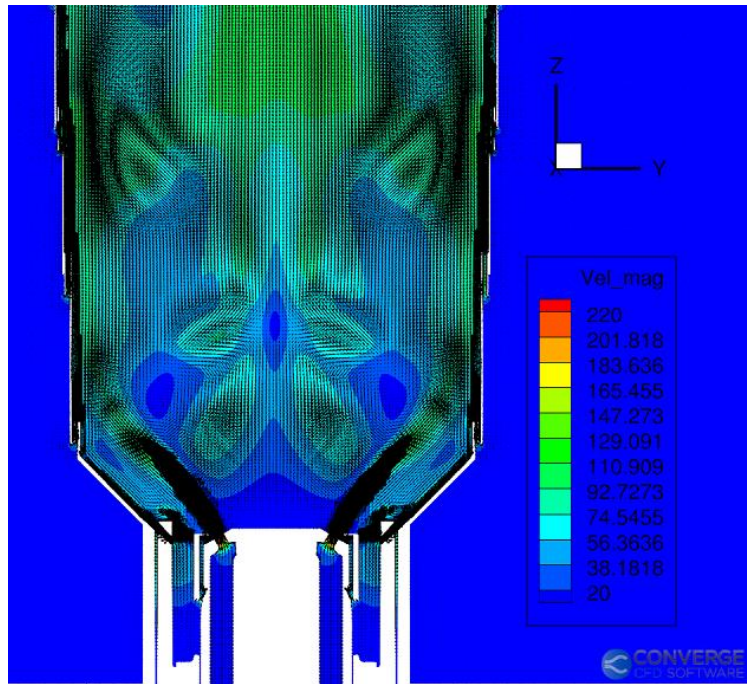


Figure 6.38 – Velocity magnitude in the primary recirculation zone for wet case in plane ZY

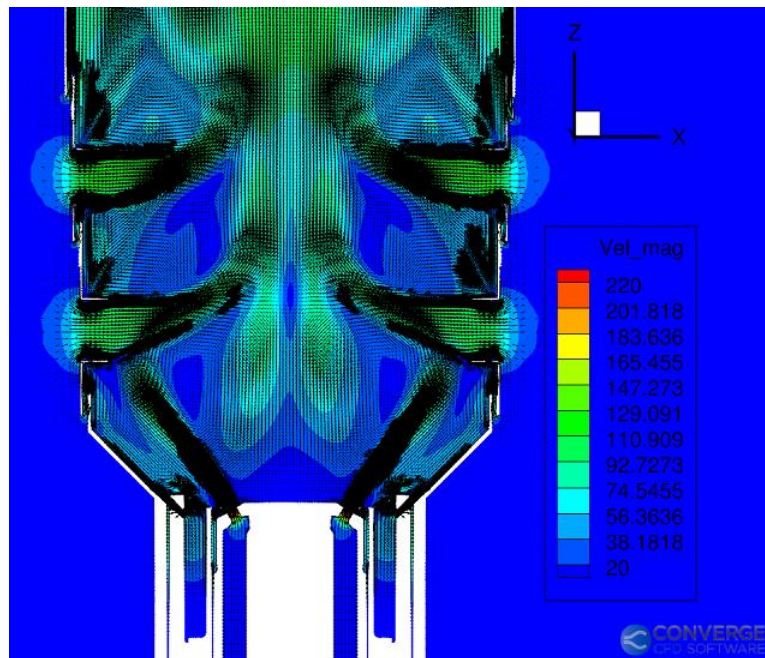


Figure 6.39 - Velocity magnitude in the primary recirculation zone for wet case in plane ZX

Figure 6.40 show the NOx emission distribution for the wet case and foe plane ZY and ZX.

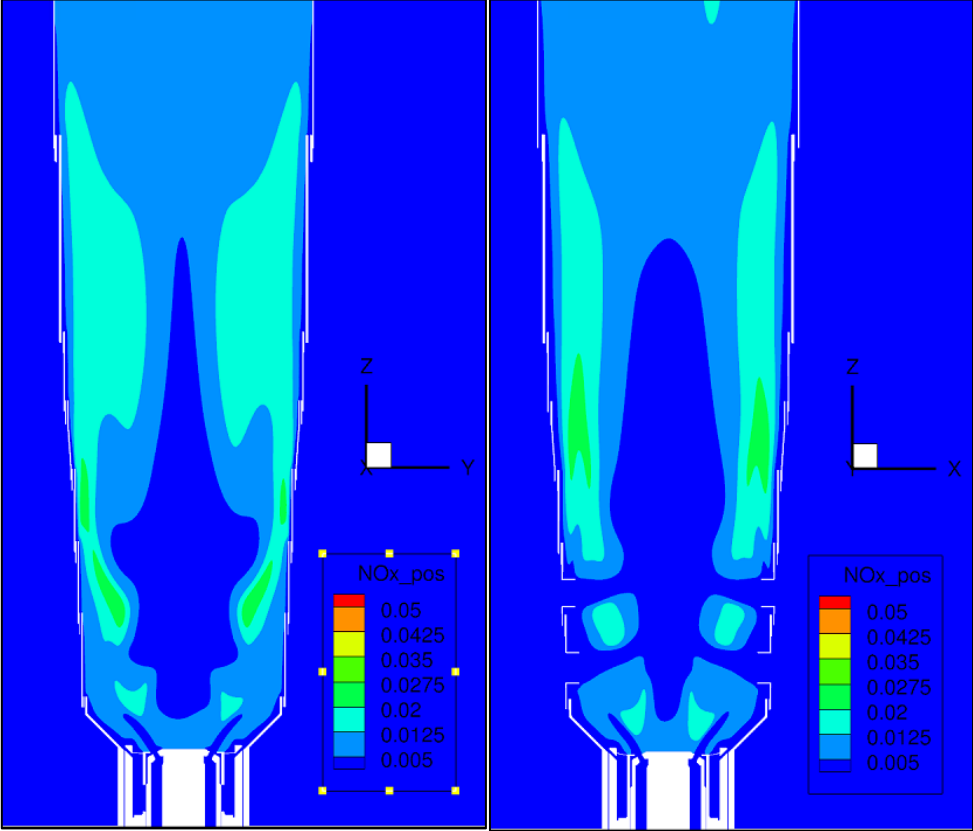


Figure 6.40 – NOx distribution for wet case in plane ZY (left) and in plane ZX (right)

7. Conclusion and future developments

In this project, different CFD 3D simulations both for dry case and wet case have been set and run. The objective is to evaluate if the sink model works properly on NO_x emission reduction. In order to understand if this target is reached, a multiple comparison of charts, slices, figures have been proposed.

From the temperature comparison between figures 6.10, 6.11, 6.15, 6.16 (for the dry cases) and figures 6.32, 6.33, 6.37 (for the wet case), it is possible to notice the absence of major differences between the dry case temperatures and the wet case temperatures both for slice distributions and for steady state charts. This may be due to a not satisfactory sink model setup or improper calibration.

Because of that, from a comparison between the NO_x emission charts of figure 6.14 (for dry cases) and figure 6.36 (for wet case), it is possible to recognize that the steady state value for NO_x rate is quite the same for dry cases and wet case. This could be due to the absence of major differences in temperature between dry cases and wet case, as stated before. Another possible reason could lie on the improper set and calibration of the NO_x modelling in CONVERGE CFD software. Which means that the way CONVERGE models the NO_x production is not properly optimized.

Future steps for reducing NO_x emission include a new combustor shape in order to get a more efficient combustion, a new study on swirler shape which allows a better mixing and recirculation zone and the use of hydrogen as a fuel.

8. Bibliography

- [1] - A. M. Y. Razak, – “Industrial Gas Turbines”, 2007
- [2] - A. Donini, - “Advanced Turbulent Combustion Modeling for Gas Turbine Application”, 2014
- [3] - Law, C.K – “Combustion Physics”, Cambridge University Press, 2006
- [4] - Bird, R.B., W.E. Stewart, and E.N. Lightfoot, - “Transport Phenomena”, Wiley, 2007
- [5] - Wilke, C.R. - “A Viscosity Equation for Gas Mixtures”, Chemical Physics, 1950
- [6] - Kee, R.J., M.E. Coltrin, and P. Glarborg - “Chemically Reacting Flow: Theory and Practice”, Wiley, 2003
- [7] - Williams, F.A. - “Combustion Theory”, Westview Press, 1994
- [8] - J. Ferziger and M. Peric, - “Computational methods for fluid dynamics”, 3rd ed. Springer, 2002
- [9] - J. Bardina, J. Ferziger, and W. Reynolds, - “Improved subgrid-scale models for large-eddy simulation,” 2013
- [10] - A. Leonard, - “Energy cascade in large-eddy simulations of turbulent fluid flows,” Adv. Geophys., vol. 18, no. PA, pp. 237–248, 1975.
- [11] – H.I.H. Saravanamuttoo, G.F.C. Rogers, H. Cohen, P.V. Straznicky, A.C. Nix, - “Gas Turbine Theory”, Seventh Edition, Pearson
- [12] - Arthur H. Lefebvre, Dilip R. Ballal, - “Gas Turbine Combustion Alternative Fuels and Emissions”, Third Edition, CRC Press
- [13] - Goodger, E. M., - “Transport Fuels Technology”, Landfall Press, Norwich, UK, 2000
- [14] - Goodger, E. M., - “Aerospace Fuels”, Landfall Press, Norwich, UK, 2007
- [15] - Edwards, J. T., - “Liquid Fuels and Propellants for Aerospace Propulsion”, 1903–2003, AIAA Journal of Propulsion and Power, Vol. 19, pp. 1089–107, 2003
- [16] – “Aviation Fuels Technical Review”, Chevron Products Company, San Ramon, CA, 2000
- [17] - Blazowski, W. S., and Maggitti, L., “Future Fuels in Gas Turbine Engines,” Progress in Astronautics and Aeronautics, Vol. 62, pp. 21–73, 1978

- [18] - Giammar, R. D., Krause, H. H., and Locklin, D. W., “The Effect of Additives in Reducing Particulate Emissions from Residual Oil Combustion,” ASME Paper 75-WA/CD-7, 1975
- [19] - Heneghan, S. P., Ballal, D. R., and Harrison, W. E. III, “JP-8 + 100: The Development of High Thermal Stability Jet Fuel,” Transactions of ASME, Journal of Energy Resources Technology, Vol. 118, pp. 170–9, 1996.
- [20] - Lewis, A., “Fuels for Aircraft Gas Turbine Engines,” in E. R. Norster, ed., Cranfield International Symposium Series, pp. 309–25, Pergamon, Oxford, 1971
- [21] - Rowling, H., “Ash Deposition—Petroleum Fuels,” Chap. 19 in Sir Harold Roxbee Cox, ed., Gas Turbine Principles and Practice, Newnes, London, 1955
- [22] - Foster, A. D., “Gas Turbine Fuels,” Combustion and Flame, Vol. 44, No. 10, pp. 4–14, 1973.
- [23] - Szetela, E. J., and Chiapetta, L., “External Fuel Vaporization Study, Phase 1 Report,” NASA CR 159850, 1980
- [24] - Naegeli, D. W., and Moses, C. A., “Effect of Fuel Molecular Structure on Soot Formation in Gas Turbine Engines,” ASME Paper 80-GT-62, Gas Turbine Conference, New Orleans, LA, 1980
- [25] - Lewis, A., “Fuels for Aircraft Gas Turbine Engines,” in E. R. Norster, ed., Cranfield International Symposium Series, pp. 309–25, Pergamon, Oxford, 1971
- [26] - White, A. O., “20 Years’ Experience Burning Heavy Fuels in Heavy Duty Gas Turbines,” ASME Paper 73-GT-22, 1973.
- [27] – B. G. Kyle, “Chemical and Process Thermodynamics”, Englewood Cliffs, NJ
- [28] – John B. Heywood, “Internal combustion engine fundamentals”, McGraw-Hill series in mechanical engineering.
- [29] - K. Mathioudakis, “Analysis of the Effects of Water Injection on the Performance of a Gas Turbine”, Journal of Engineering for Gas Turbines and Power, vol. 124, n. 3, pagg. 489–495, lug. 2002
- [30] - E. Benini, S. Pandolfo, e S. Zoppellari, “Reduction of NO emissions in a turbojet combustor by direct water/steam injection: Numerical and experimental assessment”, Applied Thermal Engineering, vol. 29, n. 17–18, pagg. 3506–3510, dic. 2009
- [31] – Milad Darzi, Chanwoo Park, “Experimental Visualization and Numerical Simulation of Liquid-Gas Two-Phase Flows in a Horizontal Pipe” Conference Paper, 2017